

D2.2 – Conventional and advanced models of the EVEREST research reactors

Version 0.2

August/2026

Szabolcs Czifrus[1], András Szabolcs Ványi[1.2], Jozsef Janik[3], Tamás Belgya[3], Yann Perin[4], Silvia lo Muzio[4], Jonathan Zert[4], Ludovic Jantzen[5], Cesare Barbera[5], Mathieu Hursin[5], Anže Pungerčič[7,8], Klemen Ambrožič[7.8], Alexander Vasiliev[6], Flavio de Martino[6], Riku Tuominen[9], Erkki Laurila[9]

Funded by the European Union

[1]Department of Nuclear Energy, Budapest University of Technology and Economics, Hungary

[2]Fuel and Reactor Materials Department, Institute for Atomic Energy Research, HUN-REN Centre for Energy Research, Hungary

[3]Budapest Neutron Centre. Institute for Energy Security and Environmental Safety, HUN-REN Centre for Energy Research, Hungary

[4]Gesellschaft für Anlagen- und Reaktorsicherheit (GRS) gGmbH, Germany

[5]Laboratory for Reactor Physics and Systems Behavior, EPFL - Swiss Federal Technology Institute of Lausanne, Switzerland

[6]Laboratory for Reactor Physics and Thermal-Hydraulics, Paul Scherrer Institute, Switzerland

[7]Reactor Physics Division, Jožef Stefan Institute, Slovenia

[8]Faculty of Mathematics and Physics, University of Ljubljana, Slovenia

[9]VTT Technical Research Centre of Finland, Finland

Disclaimer

Funded by the European Union. Views and opinions expressed are however those of the author(s) only and do not necessarily reflect those of the European Union or the European Atomic Energy Community ('EC-Euratom'). Neither the European Union nor the granting authority can be held responsible for them.

Document information

Grant Agreement	n°101163288
Project Title	Experiments for Validation and Enhancement of the REactor preSsure vessel fluence assessmenT
Project Acronym	EVEREST
Project Coordinator	Yann Perin – GRS
Project Duration	01.09.2024 – 30.08.2028 (48)
Related Work Package	WP2
Related Task(s)	T 2.2, T 2.4
Lead Organisation	EPFL
Contributing Partner(s)	BME, HUN-REN, JSI, GRS, EPFL, PSI, VTT
Due Date	August 31st, 2026
Submission Date	28.08.2026
Dissemination level	PU

History

Date	Version	Submitted by	Reviewed by	Comments
26/08/26	0.1	M. Hursin	Y. Perin	Initial version
28/08/26	0.2	Karine Lavoisier	Mathieu Hursin	Final version

Funded by the European Union

Funded by the European Union. Views and opinions expressed are however those of the author(s) only and do not necessarily reflect those of the European Union or the European Atomic Energy Community ('EC-Euratom'). Neither the European Union nor the granting authority can be held responsible for them.

Table of contents

1. Introduction 12
1.1. Objectives 12
1.2. Scope 13
2. Budapest Research Reactor 14
2.1. Facility overview 14
2.2. Conventional model 15
2.2.1. KIKO3D 15
2.2.1.1. Neutron-Kinetics Model 16
2.2.1.2. Delayed Neutrons and Decay Heat 16
2.2.1.3. Control rods 16
2.2.1.4. Coupling with ATHLET 16
2.2.2. BREKI model of the BRR 17
2.3. Advanced models 17
2.3.1. foamForNuclear 17
2.3.1.1. Serpent Full-Core Simulation 18
2.3.1.2. Single assembly advanced thermal-hydraulic model with FFN 22
2.3.1.3. Single assembly FFN model using a porous media approach 24
2.3.1.4. High-Fidelity Coupled Serpent–foamForNuclear Simulation 26
2.3.1.5. Low-Fidelity Coupled Serpent–foamForNuclear Simulation 28
2.3.1.6. Outlook 31
2.3.2. nTRACER/CTF 31
3. BME Training Reactor 33
3.1. Facility overview 33
3.2. Conventional model 33
3.2.1. PARCS model 33
3.2.2. TRACE model 36
3.2.3. Coupling 38
3.3. Advanced models 38
3.3.1. FENNECS/CTF 38
3.3.1.1. Description of the neutronics model with FENNECS 39
3.3.1.2. Description of the thermal-hydraulics subchannel model with CTF 43
3.3.1.3. Coupling FENNECS/CTF 43
3.3.2. foamForNuclear 44
3.3.2.1. Thermal-Hydraulic Model and Mesh Topology 45
3.3.2.2. Neutronic Model 47

Funded by the European Union

Funded by the European Union. Views and opinions expressed are however those of the author(s) only and do not necessarily reflect those of the European Union or the European Atomic Energy Community ('EC-Euratom'). Neither the European Union nor the granting authority can be held responsible for them.

3.3.2.3. Coupling strategy 49
3.3.2.4. Application to the modelling of the FB#2 Transient Case 50
4. JSI TRIGA reactor 53
4.1. Facility overview 53
4.2. Conventional model 53
4.3. Advanced models 54
4.3.1. Serpent/OpenFOAM 54
4.3.1.1. OpenFOAM model 54
4.3.1.2. Serpent model 55
4.3.1.3. Coupled simulation 57
4.3.1.4. Steady-state demonstration and development needs 57
4.3.2. FENNECS/CTF 58
4.3.2.1. Description of the neutronics model using FENNECS 58
4.3.2.2. Description of the thermal-hydraulics subchannel model with CTF 60
4.3.2.3. Coupling FENNECS/CTF 61
5. Conclusions and future work 63
5.1.1. Outlook 63

Funded by the European Union

Funded by the European Union. Views and opinions expressed are however those of the author(s) only and do not necessarily reflect those of the European Union or the European Atomic Energy Community ('EC-Euratom'). Neither the European Union nor the granting authority can be held responsible for them.

List of figures

Figure 1: BRR core loading map (start of campaign, March 2022). Each hexagonal position is colour-coded by assembly type: fresh and irradiated fuel elements of different burnup levels, beryllium displacers, control rods, and irradiation channels. 15
Figure 2: Example radial power map obtained with BREKI for BRR at the beginning of cycle 40..... 17
Figure 3: Illustration of the BRR geometry obtained via the Serpent code 19
Figure 4: Assembly-wise fission power distribution. Only the 190 fuel assemblies are colored. 20
Figure 5: BRR flux maps obtained with Serpent2 without feedbacks. 21
Figure 6: Axial flux profiles for selected assembly positions, normalized by the assembly volume..... 22
Figure 7: Explicit chtMultiRegionFoam simulation of the VVR-M2 fuel assembly. Left: horizontal cross-section showing the three fuel plates, the cladding and the coolant channels. Centre: mesh details at a plate corner. Right: steady-state temperature results at the outlet (color scale 318 K - 341 K). 24
Figure 8: FFN tetrahedral mesh of a single assembly showing three different zones. Each zone encompasses a fuel plate. 25
Figure 9: Radial temperature profile from the explicit chtMultiRegionFoam simulation (solid blue) compared with the FFN homogeneous model temperatures (dashed lines): mean coolant (322.9 K, red), average cladding (340.8 K, orange), and maximum fuel temperature (341.2 K, green). 25
Figure 10: Full-core FFN porous-media mesh. Each hexagonal assembly is discretised with 6 radial cells and 20 axial layers. The colour coding reflects the two main types of assemblies (in—core assemblies in magenta and reflector assemblies in yellow)..... 26
Figure 11: Convergence of the Serpent–FFN coupling. (a) Effective multiplication factor keff with 1σ Monte Carlo uncertainty band. (b) Mean relative change in the coolant, cladding, and fuel temperature fields between successive iterations; shaded bands represent the standard deviation over all fuel cells. Both quantities converge after a single iteration..... 27
Figure 12: ParaView visualisation of the converged coupled fields on the full-core FFN mesh. Left: volumetric power density ($W.m^{-3}$). Centre: coolant temperature (K), rising from the inlet (318 K) to the outlet. Right: fuel temperature (K). 27
Figure 13: Axial temperature profiles in the hottest assembly at each coupling iteration (color scale from dark to light = iteration 0 to 11). (a) Coolant temperature. (b) Fuel temperature. 28
Figure 14: Impact of Serpent–FFN coupling on the assembly power distribution. (a) Relative power change (coupled minus isothermal, normalised to isothermal) as a function of isothermal assembly power. (b) Histogram of per-assembly power changes over the 190 fuelled positions. 28
Figure 15: *gmsh* neutronics mesh used for the FFN diffusion calculation: structured hexagonal core region (6 radial cells per assembly, 20 axial layers) surrounded by an extruded tetrahedral mesh of the water reflector..... 29
Figure 16: Assembly-wise power distribution from the FFN diffusion solver (left) and the Serpent reference (centre), and the corresponding relative difference (right). 30
Figure 17: Outlet coolant temperature fields obtained with the LF (FFN-driven) coupled simulation. 30
Figure 18: Homogenised fuel regions (1: position B3, 2: position F3, 3: regular fuel assembly, 4: irregular fuel around rod AUT, 5: position D4, 6: irregular fuel around rod MAN, 7: position D5, 8: irregular fuel around the safety rods, 9: position E5) 34
Figure 19: Homogenised reflector regions (10: neutron source, 11: graphite with irradiation channel, 12-13: double layer of graphite blocks, 14: vertical irradiation channel in water, 15: thermal sample-delivery rabbit system, 16: vertical irradiation channel in)..... 35
Figure 20: Radial cross-section of the PARCS model in core height. The numbers in the nodes refer to the homogenised regions of Figure 18 and Figure 19..... 36
Figure 21: TRACE model of BME TR..... 37

Funded by the European Union

Funded by the European Union. Views and opinions expressed are however those of the author(s) only and do not necessarily reflect those of the European Union or the European Atomic Energy Community ('EC-Euratom'). Neither the European Union nor the granting authority can be held responsible for them.

Figure 22: Computational workflow of FENNECS pin-wise modelling: conventional two-step deterministic scheme using a SERPENT reference calculation. 39
Figure 23: BME TR core midplane layout with the six FA types, showing the distorted pin arrangements near the control-rod positions. 40
Figure 24: Mesh generation for FA Type 6: (a) algebraic construction of the pin-cell, shroud and FA boundaries; (b) the HELIOS structure representation with internal mesh refinement; (c) the FENNECS triangulation derived from the same boundaries. 41
Figure 25: Spatial distribution of relative pin-power error of HELIOS model (left), normalised SERPENT pin-power distribution (right)..... 41
Figure 26: Spatial distribution of relative pin-power error (left) and relative linear power density (right), FENNECS against SERPENT, with the normalised SERPENT pin-power distribution alongside..... 42
Figure 27: Channel-centered modelling with CTF of two fuel bundle types..... 43
Figure 28: Probability distribution of the relative difference of the pin power between (FENNECS/CTF - FENNECS) / FENNECS..... 44
Figure 29: Global mesh topology, featuring a vertically truncated side view (right) within the pool region to highlight the core and diffuser discretization while preserving the full pool volume in the computational domain. 46
Figure 30: Core–pool interface: (top) the non-conformal mesh layout at the block boundary; (bottom) the resulting velocity field obtained through the ACMI coupling. 46
Figure 31: FFN vs. Serpent 2 relative error in radial power distribution..... 48
Figure 32: Axial power density profiles: FFN vs. Serpent 2, for the assemblies surrounding the AUT control rod..... 49
Figure 33: Development of the vertical velocity component uz in a core cross- section at successive instants, illustrating the establishment of natural circulation in the reactor pool 51
Figure 34: Comparison of measured and simulated temperature profiles for four fuel assemblies (E3, B3, C7, F7) under the forced power history. Data are extracted from the FFN solution at the top of the active fuel length. 51
Figure 35: On left: Different geometric zones of the TRIGA CFD model. The colours indicate steel support structures (blue and yellow), graphite reflectors (green), and fuel (red). The outer boundary of the fluid domain is shown with opaque grey, while the cladding is not shown. On right: Cross-section of different solid structures including cladding (cyan), fuel (red), and zirconium rods (blue). The control rod/special channels are not included in the current CFD model..... 55
Figure 36: YZ plot of the Serpent model for core configuration 190. 56
Figure 37: XY plot of the Serpent model for core configuration 190. 56
Figure 38: Results from a stand-alone CFD simulation of the TRIGA core. On left: Vertical component of the velocity in the fluid region. On right: Temperature distribution in both the fluid and solid regions. 58
Figure 39 FENNECS mesh for the TRIGA Mark II model. 60
Figure 40: Representation of CTF thermal-hydraulics channels in the TRIGA core 60
Figure 41: Axial distribution of coolant temperature in CTF a core central channel (#1) – Comparison of Stand-Alone and Coupled simulations 62
Figure 42: Axial distribution of coolant temperature in CTF a core channel in the third ring of pins (#61) – Comparison of Stand-Alone and Coupled simulations..... 62

Funded by the European Union

Funded by the European Union. Views and opinions expressed are however those of the author(s) only and do not necessarily reflect those of the European Union or the European Atomic Energy Community ('EC-Euratom'). Neither the European Union nor the granting authority can be held responsible for them.

List of tables

Table 1. State variables for the KIKO3D model of BRR. 16
Table 2. Serpent simulation parameters. 19
Table 3. Statistical power distribution of the fuelled assemblies. 20
Table 4. Water thermophysical properties at $T = 318\ K$ and $P = 1\ atm$. 23
Table 5. Solid material properties at $T = 355\ K$ (representative fuel/cladding operating temperature) 23
Table 6. Perturbed states used for the two-group cross-section generation, in addition to the isothermal 318 K reference state. 29
Table 7: Branches used for the parameterised group constant library 35
Table 8: BME TR core TH boundary conditions 43
Table 9: TRIGA core TH boundary conditions 60
Table 10: Axial nodalization of the TRIGA core in CTF 61

Funded by the European Union

Funded by the European Union. Views and opinions expressed are however those of the author(s) only and do not necessarily reflect those of the European Union or the European Atomic Energy Community ('EC-Euratom'). Neither the European Union nor the granting authority can be held responsible for them.

Summary

This deliverable (D2.2) documents the conventional and advanced multi-physics models developed within Work Package 2 of the EVEREST project for three research reactors: the Budapest Research Reactor (BRR), the BME Training Reactor (TR), and the JSI TRIGA Mark II reactor. For each facility, an established conventional model (KIKO3D/ATHLET for the BRR, PARCS/TRACE for the BME TR, and TRIGLAV/MCNP-based schemes for the JSI TRIGA) is presented alongside at least one advanced, higher-resolution multi-physics coupling combining continuous-energy Monte Carlo neutronics (Serpent 2) or deterministic pin-resolved transport (HELIOS-2/FENNECS) with CFD or subchannel thermal-hydraulics (foamForNuclear, CTF or OpenFOAM).

For the BRR, a Serpent/foamForNuclear coupling demonstrates that a full-core, geometry-faithful Monte Carlo neutronics model can be coupled to an efficient porous-media thermal-hydraulic representation, reaching a converged steady state after a single fixed-point iteration and reproducing explicit CFD reference temperatures to within a fraction of a kelvin. A lower-fidelity foamForNuclear diffusion variant reproduces the Serpent power distribution to within about four percent at a fraction of the computational cost. A deterministic nTRACER/CTF route was assessed but found impractical within the project timeline.

For the BME Training Reactor, a FENNECS/CTF pin-wise deterministic scheme built on an algebraic mesh-generation methodology preserving the distorted-pin topology of the EK-10 assemblies approximately halves the mean and RMS assembly-power error relative to a conventional assembly-homogenised model. In parallel, a foamForNuclear model combining a porous-medium core with a two-group diffusion solver and point-kinetics/thermal-hydraulics coupling performed qualitatively well against the FB#2 natural-circulation transient, correctly reproducing the observed heating onset, system inertia, and relaxation behaviour.

For the JSI TRIGA Mark II reactor, two complementary advanced routes were established: a Serpent 2/OpenFOAM coupling using the Cerberus/Kraken multi-physics driver, demonstrated in a simplified core-only configuration reproducing the expected buoyancy-driven flow pattern (full two-way coupling pending resolution of non-convex mesh cells in Serpent's temperature/density search); and a FENNECS/CTF deterministic scheme with a dedicated pin-slot mesh generator.

Together, these models establish the computational basis needed to interpret the experimental data reported in D2.1 and to inform the design of high-resolution experiments planned in WP3. Remaining work includes resolving the non-convex mesh limitation in the Serpent/OpenFOAM toolchain, extending the coupled schemes to transient and pulse conditions, and applying the models to a validation exercise against the D2.1 experimental data using the uncertainty quantification estimates reported in D2.3.

Keywords

Research reactors; Multi-physics modelling; Monte Carlo neutron transport; Deterministic neutron transport; Serpent 2; foamForNuclear (FFN); OpenFOAM; FENNECS; CTF; KIKO3D / ATHLET; PARCS / TRACE; Porous-media thermal-hydraulics; Conjugate heat transfer; Pin-wise homogenisation; Cross-section generation; Reactor pressure vessel (RPV) fluence; Long-term operation (LTO); Budapest Research Reactor (BRR); BME Training Reactor; JSI TRIGA Mark II reactor.

Funded by the European Union

Funded by the European Union. Views and opinions expressed are however those of the author(s) only and do not necessarily reflect those of the European Union or the European Atomic Energy Community ('EC-Euratom'). Neither the European Union nor the granting authority can be held responsible for them.

Abbreviations and acronyms

Acronym	Description
WP	Work Package
TRIGA	Training Research Isotope production by General Atomics
LTO	Long-Term Operation
RPV	Reactor Pressure Vessel
MP	Multi-Physics
TR	Training Reactor
NPP	Nuclear Power Plant
PWR	Pressurized Water Reactor
FFN	foamForNuclear (multi-physics simulation platform)
CFD	Computational Fluid Dynamics
RANS	Reynolds-Averaged Navier–Stokes
CP	Collision Probabilities (transport method)
MoC	Method of Characteristics
CMFD	Coarse-Mesh Finite Difference
SP3	Simplified P3 (transport approximation)
Sn	Discrete Ordinates (transport approximation)
RBF	Radial Basis Functions
ACMI	Arbitrary Coupled Mesh Interface
TMS	Target Motion Sampling
FSP	Fission Source Propagation
MARE	Mean Absolute Relative Error
RMS	Root Mean Square
ENDF	Evaluated Nuclear Data File
ACE	A Compact ENDF (cross-section data format)
OMP	OpenMP (Open Multi-Processing)
SNU	Seoul National University
LEU	Low-Enriched Uranium
HEU	Highly-Enriched Uranium
KFKI	Central Research Institute for Physics (Hungary)
PEMTY	Python External Meshing Tool for YAML input

Funded by the European Union

Funded by the European Union. Views and opinions expressed are however those of the author(s) only and do not necessarily reflect those of the European Union or the European Atomic Energy Community ('EC-Euratom'). Neither the European Union nor the granting authority can be held responsible for them.

NEMTAB	Nodal Expansion Method cross-section table format
NRC	(U.S.) Nuclear Regulatory Commission
OpenFOAM	Open Field Operation And Manipulation
CAD	Computer-Aided Design
JEFF	Joint Evaluated Fission and Fusion (nuclear data library)
AUT	Automatic (control rod, BME TR)
MAN	Manual (control rod, BME TR)
SZAV-1	Russian Al-Mg-Si structural alloy (cladding material)
VVR-M2	Fuel assembly type (BRR)
EK-10	Fuel assembly type (BME TR)
IC	Irradiation Chamber/Channel
CFUL08	Fission-chamber detector chain designation (BME TR)
pcm	per cent mille (10^{-5}, unit of reactivity)

Funded by the European Union

Funded by the European Union. Views and opinions expressed are however those of the author(s) only and do not necessarily reflect those of the European Union or the European Atomic Energy Community ('EC-Euratom'). Neither the European Union nor the granting authority can be held responsible for them.

1. Introduction

The safety of nuclear reactors relies heavily on computational modelling, and the accuracy of those models is only as reliable as the experimental data used to validate them. Over the past two decades, advanced multi-physics (MP) simulation platforms have been developed to reduce the level of conservatism inherent in conventional reactor modelling approaches. Unlike the traditional two-step, assembly-level methods that rely on pin-power reconstruction schemes, these advanced tools apply a first-principles approach and deliver solutions at a much finer spatial resolution without the need for intermediate reconstruction. Despite this improved capability, advanced MP codes remain seldom used in practice, in part because dedicated, high-resolution experimental data for their validation are scarce.

The EVEREST project (Experiments for Validation and Enhancement of the REactor preSsure vessel fluence assessmenT, Grant Agreement n°101163288) was established under the Euratom Research and Training Programme to address this gap. The project focuses on three complementary objectives: quantifying the added value of advanced MP models for long-term operation (LTO) applications and reactor pressure vessel (RPV) fluence assessment; demonstrating the trustworthiness of these models through the production of dedicated experimental data; and promoting their adoption among key stakeholders in the nuclear engineering community, including utilities, regulators, and students.

To generate the experimental data required for model validation, the project makes use of four research facilities operated by consortium partners: the Budapest Research Reactor (BRR) at HUN-REN EK, the Training Reactor (TR) at the Budapest University of Technology and Economics (BME), the TRIGA Mark II reactor at the Jožef Stefan Institute (JSI), and the zero-power CROCUS facility at EPFL, which is used for instrumentation testing. The first three reactors mentioned above produce a significant amount of thermal power, enabling the observation of genuine multi-physics behaviour, the coupled interaction of neutron flux, coolant and fuel temperature, and flow velocity, which is essential for meaningful model validation.

Work Package 2 (WP2) of the EVEREST project is specifically dedicated to the production of validated high-resolution multi-physics models of these research reactors, with EPFL as work package leader. The present document, Deliverable D2.2, reports on the conventional and advanced computational models developed for each of the three research reactors involved in WP2.

1.1. Objectives

The primary objective of WP2 is to produce validated advanced multi-physics computational models for the research reactors involved in the project: the BRR at HUN-REN EK, the TR at BME, and the TRIGA Mark II at JSI. This deliverable focuses specifically on describing the conventional and advanced modelling approaches developed for each facility.

The modelling approaches adopted in WP2 are deliberately chosen to be as consistent as possible, in terms of codes, nuclear data libraries, and level of spatial discretisation with the approaches used for the nuclear power plant (NPP) modelling carried out in Work Package 1 (WP1). This consistency is essential for the subsequent representativity analysis, which assesses the degree to which the neutronic conditions in the research reactors are representative of those encountered at the periphery of an operating pressurized water reactor (PWR) core.

More specifically, the objectives of this deliverable are to document the conventional and advanced computational schemes developed for each research reactor, including the codes, nuclear data, and discretisation choices adopted.

Funded by the European Union

Funded by the European Union. Views and opinions expressed are however those of the author(s) only and do not necessarily reflect those of the European Union or the European Atomic Energy Community ('EC-Euratom'). Neither the European Union nor the granting authority can be held responsible for them.

1.2. Scope

This report covers the conventional and advanced multi-physics models developed for the three research reactors involved in WP2: the Budapest Research Reactor (BRR), the BME Training Reactor (TR), and the JSI TRIGA Mark II reactor. For each facility, the modelling work encompasses both the neutronics and the thermal-hydraulics components of the coupled multi-physics problem. On the neutronics side, both deterministic solvers and Monte Carlo approaches are used. On the thermal-hydraulics side, models based on computational fluid dynamics (CFD) and subchannel codes are used, depending on the reactor geometry and code systems available at the participating institution.

The research reactors covered in this report span a range of power levels, geometries, fuel types, and coolant configurations, providing diversity in the experimental and modelling basis for the EVEREST project. The BRR is a light water-cooled and moderated reactor of 10 MW nominal thermal power; the BME TR is a light water-cooled and moderated reactor of 100 kW nominal power; and the JSI TRIGA Mark II is a pool-type reactor of 250 kW nominal power. This diversity is an intentional design feature of the EVEREST consortium, providing redundancy in the production of experimental data and broadening the range of neutronic conditions that can hopefully be compared to those prevailing at the periphery of a PWR core.

Funded by the European Union

Funded by the European Union. Views and opinions expressed are however those of the author(s) only and do not necessarily reflect those of the European Union or the European Atomic Energy Community ('EC-Euratom'). Neither the European Union nor the granting authority can be held responsible for them.

2. Budapest Research Reactor

This chapter presents the conventional and advanced multi-physics models developed for the Budapest Research Reactor (BRR), the first of the three research reactors covered by this deliverable. Section 2.1 introduces the BRR facility, its core configuration and fuel design, and summarises the experimental campaign against which the models presented in this chapter are ultimately intended to be validated. Section 2.2 describes the conventional modelling scheme, based on the nodal code KIKO3D (including its BREKI variant for the BRR) coupled to the ATHLET thermal-hydraulics code. Section 2.3 then presents the advanced multi-physics approaches investigated within EVEREST, comparing a Serpent–foamForNuclear coupling developed at EPFL against an initial feasibility assessment of the nTRACER/CTF system at PSI. Together, these models establish the computational basis needed to interpret the BRR measurements reported in D2.1.

2.1. Facility overview

The Budapest Research Reactor (BRR) is a 10MW pool-type research reactor of the VVR-M2 type, operated by HUN-REN in Budapest, Hungary. Light water serves simultaneously as moderator and primary coolant; the active core is surrounded radially by a solid beryllium reflector, and axially by water. The fuel elements are VVRM2 hexagonal assemblies, each consisting of three concentric aluminium--magnesium-clad fuel tubes containing a uranium--aluminium alloy meat enriched to approximately 20% U-235. The assemblies are arranged in a compact hexagonal lattice with a pitch of 3.5 cm and a total of 190 fuelled positions in the current loading.

The core also houses several types of non-fuel elements: beryllium displacers, control and safety rods (boron-based absorbers), irradiation rigs, and measurement channels. A set of ten horizontal beam tubes penetrates the reflector and biological shielding, providing cold, thermal, and epithermal neutron beams for a broad experimental programme including neutron scattering, activation analysis, and radioisotope production. Figure 1 shows the core loading map at the start of the campaign modelled in the project.

Funded by the European Union

Funded by the European Union. Views and opinions expressed are however those of the author(s) only and do not necessarily reflect those of the European Union or the European Atomic Energy Community ('EC-Euratom'). Neither the European Union nor the granting authority can be held responsible for them.

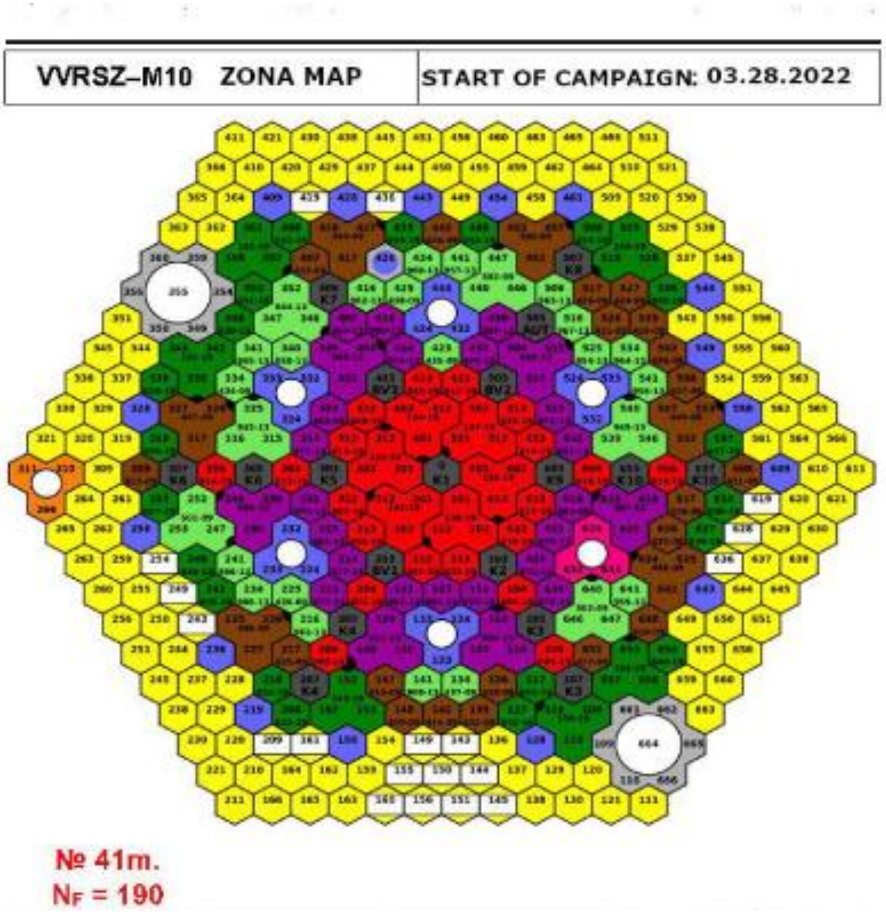


Figure 1: BRR core loading map (start of campaign, March 2022). Each hexagonal position is colour-coded by assembly type: fresh and irradiated fuel elements of different burnup levels, beryllium displacers, control rods, and irradiation channels.

The measurements involved in the project consist in an axial neutron-flux mapping experiment carried out in the fast irradiation channel 426 of the BRR [1]. Three sets of high-purity Fe and AlAu(110 ppm) activation wires were irradiated for 58–62 minutes. Following a decay period, the axial profiles of the $^{54}Fe(n,p)^{54}Mn$ and $^{58}Fe(n,\gamma)^{59}Fe$ reaction rates (fast and epithermal/thermal flux indicators, respectively) and of the $^{197}Au(n,\gamma)^{198}Au$ reaction rate (thermal flux indicator) were obtained. These daughter-activity profiles constitute the primary experimental reference for the axial flux shapes produced by the models of channel 426 presented in Sections 2.2 and 2.3.

2.2. Conventional model

The conventional model of the BRR reactor used in EVEREST is based on the KIKO3D program. A brief summary of the physical model, the input/output data chain, and the coupling with the ATHLET thermal-hydraulics code is provided in this section. More information on the models as well as their validation can be found in literature [2]–[4]. Two families of BRR fuel are covered by the model: the historical U-Al elements at 36% enrichment (VVRSZM) and the low-enriched UO_2-Al elements at 19.75% (VVRM2), consistent with the HEU-to-LEU core-conversion context of the reactor. The low-enriched version of the fuel is the focus of this work as it is the fuel loaded in the reactor during the EVEREST project.

2.2.1. KIKO3D

KIKO3D is a three-dimensional, nodal reactor-dynamics code originally developed at the KFKI Atomic Energy Research Institute for VVER-type power reactors and later adapted to the Budapest Research Reactor (BREKI3D code). It is used for two related purposes: (i) campaign-planning, i.e. following the core through successive fuel cycles as burnup accumulates and fuel is reshuffled, and (ii) reactor-

Funded by the European Union

Funded by the European Union. Views and opinions expressed are however those of the author(s) only and do not necessarily reflect those of the European Union or the European Atomic Energy Community ('EC-Euratom'). Neither the European Union nor the granting authority can be held responsible for them.

kinetics / safety-analysis calculations, i.e. simulating fast reactivity-induced transients such as control-rod ejection or drop events.

2.2.1.1. Neutron-Kinetics Model

KIKO3D solves the time-dependent, two-group neutron diffusion equation in three dimensions using a nodal method. Each node corresponds to one fuel or non-fuel position (hexagonal cross-section) subdivided into a fixed number of axial layers.

The time-dependent nodal equations are solved using a standard Improved Quasi-Static method: the solution is factorized into a slowly time-varying, position-dependent shape function and a rapidly varying, position-independent amplitude function, the latter obeying the point-kinetics equations.

For computational efficiency, the response matrices of the nodal scheme are not recomputed from first principles at every state point. Instead, in the KIKO3D-RM variant used for the BRR, they are pre-tabulated as a function of a small set of feedback parameters (see Table 1) and evaluated by interpolation at run time.

To determine the evolution of the fuel composition with time, a burnup routine is available which uses a closed-form (non-iterative) solution of the local burnup, iodine/xenon and promethium/samarium balance equations over each time step, assuming the nodal flux is constant during the step.

Table 1. State variables for the KIKO3D model of BRR.

Symbol	Physical quantity	Reference value	Unit
RMOD	Moderator density	0.9834	g/cm³
TMOD	Moderator temperature	3.330 (×100)	K
SRTF	Square root of fuel temperature	18.63	K^0.5
CXE5	Xe-135 concentration	0.1255	$\times 10^{16}$ /cm³
CSM9	Sm-149 concentration	1.004	$\times 10^{16}$ /cm³

2.2.1.2. Delayed Neutrons and Decay Heat

Point-kinetics feedback uses 10 delayed-neutron groups with best-estimate decay constants ranging from about 1.3×10^{-3} s^{-1} to 2.9 s^{-1}. Decay heat is represented by a 4-group model whose relative contributions and decay constants are fitted to the ANS decay-heat curve; this feeds a fuel-element heat-conduction model that converts nodal-average nuclear power into thermal power and, ultimately, into fuel and coolant temperatures.

2.2.1.3. Control rods

Control and safety absorber rods are handled through an intermediate-position scheme: because the absorber boundary rarely coincides with a fixed axial node boundary, a node may contain a mixture of absorber and absorber-free medium. The BRR model currently distinguishes two rod types, the manually/automatically driven regulating groups and the automatic (fine-control) rod, with up to 12 independently movable absorber groups in total.

2.2.1.4. Coupling with ATHLET

For the BRR, thermal-hydraulic feedback (coolant temperature and density) is normally not computed by KIKO3D's own simplified model but is instead supplied by the ATHLET system thermal-hydraulics code, run jointly with KIKO3D[5]. The radial nodalization of ATHLET is coarser than that of KIKO3D as

Funded by the European Union

Funded by the European Union. Views and opinions expressed are however those of the author(s) only and do not necessarily reflect those of the European Union or the European Atomic Energy Community ('EC-Euratom'). Neither the European Union nor the granting authority can be held responsible for them.

several fuel elements are typically grouped into one ATHLET channel, so the mapping between KIKO3D positions and ATHLET channels (e.g. by initial power ranking) is an explicit modelling choice documented in the companion KIKO3D-ATHLET handbook.

2.2.2. BREKI model of the BRR

The BRR core is represented on a hexagonal lattice of up to 397 positions (lattice pitch 3.5 cm), each subdivided into 8 axial nodes of 7.5 cm. Radial and axial boundary conditions are imposed through pseudo-nodes carrying Monte-Carlo-derived albedo matrices for the top, bottom and (up to three types of) radial reflector.

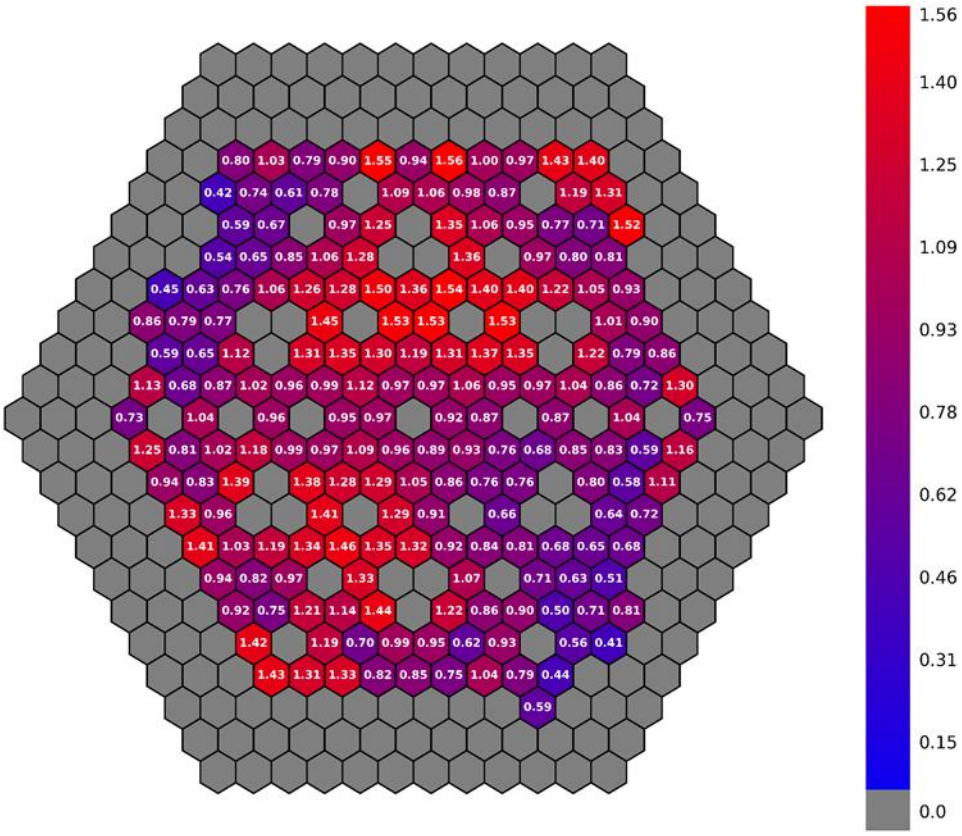


Figure 2: Example radial power map obtained with BREKI for BRR at the beginning of cycle 40.

For each core position, KIKO3D reports the axial burnup and two-group flux at the 8 axial nodes, together with a radial (kq) and an axial peaking indicator. These axial profiles are the primary diagnostic for hot-channel and thermal-margin evaluation, and are also archived (with the inventory file).

2.3. Advanced models

This section presents the advanced multi-physics models developed for the BRR within EVEREST. Two independent routes were investigated. The first, detailed in Section 2.3.1, couples the Serpent 2 Monte Carlo code [6] to the foamForNuclear (FFN) [7] platform developed at EPFL. The second route, described in Section 2.3.2, assessed the applicability of the deterministic nTRACER/CTF system [8] used at PSI. These models provide the assembly-wise and axial neutron flux, power, and temperature distributions required both for comparison with the D2.1 experimental campaign.

2.3.1. foamForNuclear

This section describes the production of a high-fidelity, fully coupled neutronic--thermal-hydraulic (TH) model of the BRR, capable of reproducing the reactor behaviour under realistic operating conditions. Such a model will serve as a reference for the validation of the multi-physics simulation platform foamForNuclear [7] against experimental measurements available at the BRR: in-core neutron flux

Funded by the European Union

Funded by the European Union. Views and opinions expressed are however those of the author(s) only and do not necessarily reflect those of the European Union or the European Atomic Energy Community ('EC-Euratom'). Neither the European Union nor the granting authority can be held responsible for them.

measurements from fission chambers and activation foils, and temperature measurements from thermocouples. Achieving quantitative agreement with these measurements requires a geometry-faithful neutronics model and a realistic TH representation of the assembly-level heat transfer.

First, the existing MCNP model of the BRR is translated into a Serpent 2 input, followed by a full-core Monte Carlo criticality calculation at isothermal conditions. The resulting assembly power and flux distributions constitute the neutronics reference state. Second, a thermal-hydraulic model of a representative VVR-M2 fuel assembly is developed: an explicit multi-region finite-volume simulation using chtMultiRegionFoam is used to resolve the actual temperature field in the three-plate geometry, and its results are compared against a homogeneous porous-media model implemented in FFN with a lumped power structure. The good agreement between the two approaches support the use of the FFN porous media approach, which is then extended to the full core. Finally, Serpent and FFN are coupled, leveraging the compatibility of their hexagonal meshes and the low computational cost of the porous-media TH representation, to produce a high-fidelity steady-state multiphysics solution for validation against in-core measurements.

Two coupled neutronics--TH schemes are presented and compared. The first relies on Serpent2 to provide the neutron flux and power distribution at each coupling iteration through an explicit Monte Carlo solve, while TH module of FFN provides the temperature and density fields. The second solver is a lower fidelity scheme, in which the Monte Carlo solve is replaced by FFN's own steady-state diffusion neutronics module, driven by assembly-wise cross-section libraries pre-generated with Serpent. FFN's diffusion solver supports an arbitrary number of energy groups; a two-group structure was chosen here as sufficient for this comparison. The LF scheme reuses the same validated FFN thermal-hydraulic model as the HF scheme, at a much lower per-iteration computational cost, making it a candidate for future transient and parametric studies; its accuracy is assessed here by direct comparison against the reference Serpent2/FFN.

2.3.1.1. Serpent Full-Core Simulation

The BRR geometry was originally encoded as an MCNP input deck. Because the subsequent multiphysics workflow relies on Serpent 2 for cross-section generation, a complete translation of the model was required. Rather than rebuilding the geometry from scratch, a set of Python parsers was developed to read the four structural blocks of the MCNP deck and emit the corresponding Serpent 2 cards into four include files (`surfaces_s.i`, `cells_s.i`, `materials_s.i`, `transformations_s.i`), assembled by a master input `main_s.i`.

Surfaces. Both codes use a surface-based constructive solid geometry, but with different mnemonics and parameterisations. Most mappings are straightforward (planes, cylinders, spheres, macrobodies). The non-trivial cases are: (i) axial cones (`kx/ky/kz`), which have no native Serpent 2 equivalent and are converted analytically to the general `quadratic` surface; (ii) MCNP's shifted quadric (`sq`), whose origin-offset form is expanded algebraically to the Serpent standard quadric; and (iii) surface transformations (TR cards), where the MCNP rotation matrix is decomposed into ZYX Euler angles via `scipy.spatial.transform` and emitted as Serpent `trans s` cards.

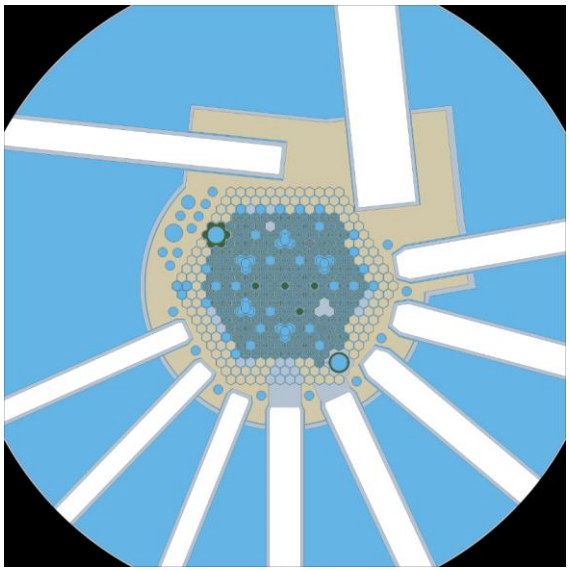
Cells and materials. Cell geometry expressions use an identical Boolean syntax in both codes; keyword parameters (`u=`, `fill=`, `imp:n=`) are extracted and remapped to their Serpent equivalents. The one structural difference is the treatment of the hexagonal fill cell: MCNP combines the lattice definition and the fill in a single card, whereas Serpent 2 requires them to be declared separately (`lat` card plus `CELL fill` card). This was handled as the single manual step in the otherwise automated translation. For materials, densities are recovered from the cell block, all cross-section library suffixes are set to `.03c` (ENDF/B-VII.1 at 300 K), and a `moder` thermal-scattering card (`lwtr.30t`) is automatically appended to water-containing materials. A total of 197 materials were translated.

Funded by the European Union

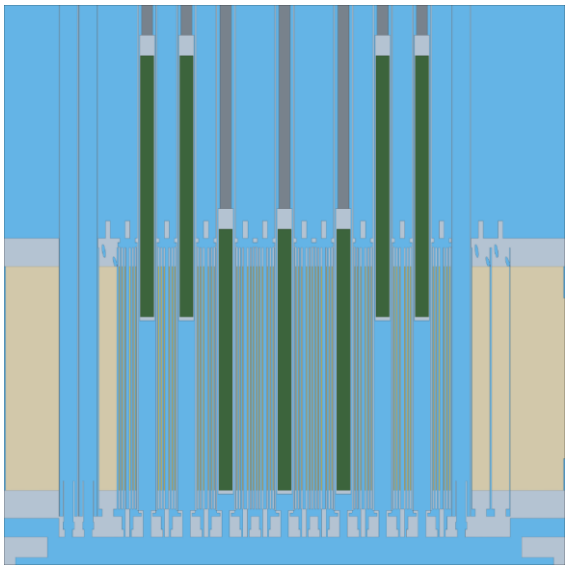
Funded by the European Union. Views and opinions expressed are however those of the author(s) only and do not necessarily reflect those of the European Union or the European Atomic Energy Community ('EC-Euratom'). Neither the European Union nor the granting authority can be held responsible for them.

The full-core geometry model of Serpent2 is composed of:

- **Active core**: a flat-top hexagonal lattice (universe 10001) with pitch p=3.5 cm, enclosed in a cylindrical volume of radius 114 cm and height 200 cm (Figure 3).
- **Fuel assemblies** (190 assemblies): each assembly contains three VVR-M2 fuel plates with aluminium–magnesium cladding, separated by water channels. A total of 190 fuel positions are active (i.e. carry a non-zero power). The MCNP provides the burnup level and corresponding isotopic fuel composition for each assembly at the time of the experiment.
- **Control and safety rods** (18 assemblies): absorber assemblies enriched in ^{10}B, located at fixed positions, with adjustable penetration height.
- **Beryllium reflector**: surrounding the fuel zone; clearly visible in Figure 3 as the beige annular region.
- **Beam tubes**: ten horizontal channels penetrating the reflector and shielding, used for experimental purposes. They appear as white rectangular cuts in the top view (Figure 3).
- **Irradiation channels** (17 assemblies): at the periphery of the fuel region, including one fast irradiation channel located within the fuel region.



Horizontal cross-section at midplane (z=0)



Vertical cross-section highlighting the control rod position

Figure 3: Illustration of the BRR geometry obtained via the Serpent code

All nuclide cross sections are taken from the ENDF/B-VII.1 library in ACE format, at 300 K Doppler-broadened data. Thermal neutron scattering in light water is treated with the library `lwtr.30t`. The criticality calculation settings are summarised in Table 2. The simulation was run with 20 OpenMP threads on an AMD Ryzen Threadripper PRO 7995WX workstation. The mentioned calculation time corresponds to one steady-state critical calculation. The simulation parameters can be found.

Table 2. Serpent simulation parameters.

Parameter	Value
Neutrons per cycle	500 000
Active cycles	100
Inactive (skip) cycles	20

Funded by the European Union

Funded by the European Union. Views and opinions expressed are however those of the author(s) only and do not necessarily reflect those of the European Union or the European Atomic Energy Community ('EC-Euratom'). Neither the European Union nor the granting authority can be held responsible for them.

Boundary conditions	Vacuum
Isothermal temperature	318 K
Thermal power	10 MW
Cross-section library	ENDF/B-VII.1
Thermal scattering	`lwtr.30t`
Serpent version	2.2.2
OMP threads	20
Wall-clock time	78.3 min

The k_{eff} value obtained with the model is 1.00884 with a statistical uncertainty of 16 pcm. This slight positive reactivity could be an effect of the non-adjusted control rod position. In addition, the temperature effect will be discussed in the next section.

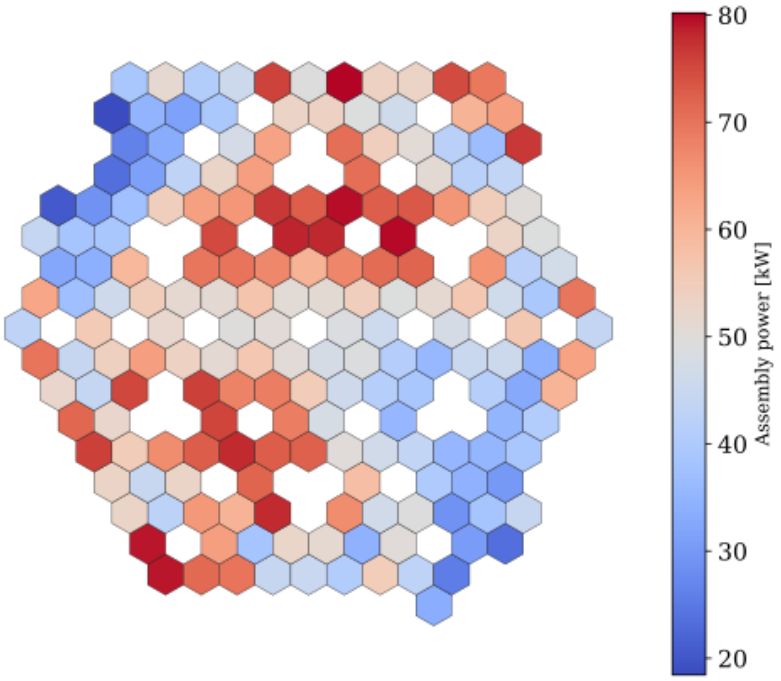


Figure 4: Assembly-wise fission power distribution. Only the 190 fuel assemblies are colored.

Figure 4 shows the assembly-integrated fission power at a nominal thermal power of 10 MW. The statistical properties of the power distribution are summarised in Table 3. The maximum statistical uncertainty on individual assembly power tallies is 0.44%.

Table 3. Statistical power distribution of the fuelled assemblies.

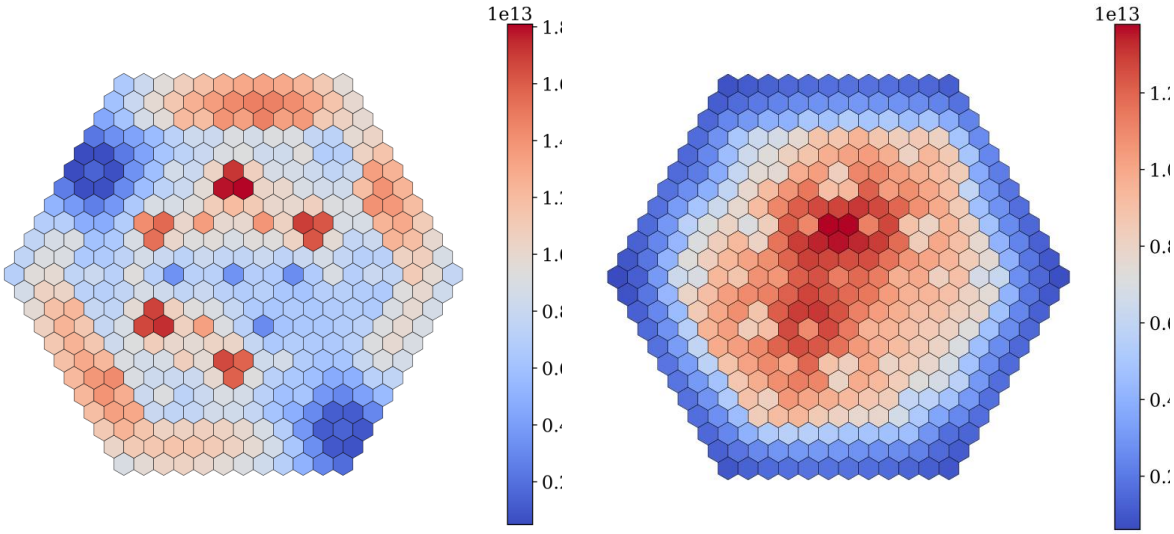
Quantity	Value
Number of fuelled assemblies	190
Mean assembly power	52.6 kW
Standard deviation	14.6 kW
Minimum assembly power	18.5 kW

Funded by the European Union

Funded by the European Union. Views and opinions expressed are however those of the author(s) only and do not necessarily reflect those of the European Union or the European Atomic Energy Community ('EC-Euratom'). Neither the European Union nor the granting authority can be held responsible for them.

Maximum assembly power	80.2 kW
Power peaking factor	1.52
Max. tally statistical uncertainty	0.44%

Figure 5 shows the radial distribution of the thermal (left) and fast (right) scalar flux, normalised to the assembly volume, at a total power of 10 MW. The impact of the absorber rods and the absorber filters is visible on the thermal flux, while the fast flux is quite homogeneous over the core center and drops at the core's boundaries due to leakages.



Thermal flux (E<1.86 eV). Fast flux (E>0.18 MeV)

Figure 5: BRR flux maps obtained with Serpent2 without feedbacks.

In the aim to reproduce the foil irradiation experiments, axial flux in specific assemblies is reported below:

- Universe 225 (*fast IC*): a fast irradiation chamber position near the outer core boundary (used for the experiments of the EVEREST project);
- Universe 1 (*abs_1*): central absorber assembly;
- Universe 138 (*abs_up*): upper absorber assembly;
- Universe 230 (*fuel*): a typical fuel assembly.

The profiles are normalised to the assembly volume and plotted as a function of distance from the bottom of the active zone.

Funded by the European Union

Funded by the European Union. Views and opinions expressed are however those of the author(s) only and do not necessarily reflect those of the European Union or the European Atomic Energy Community ('EC-Euratom'). Neither the European Union nor the granting authority can be held responsible for them.

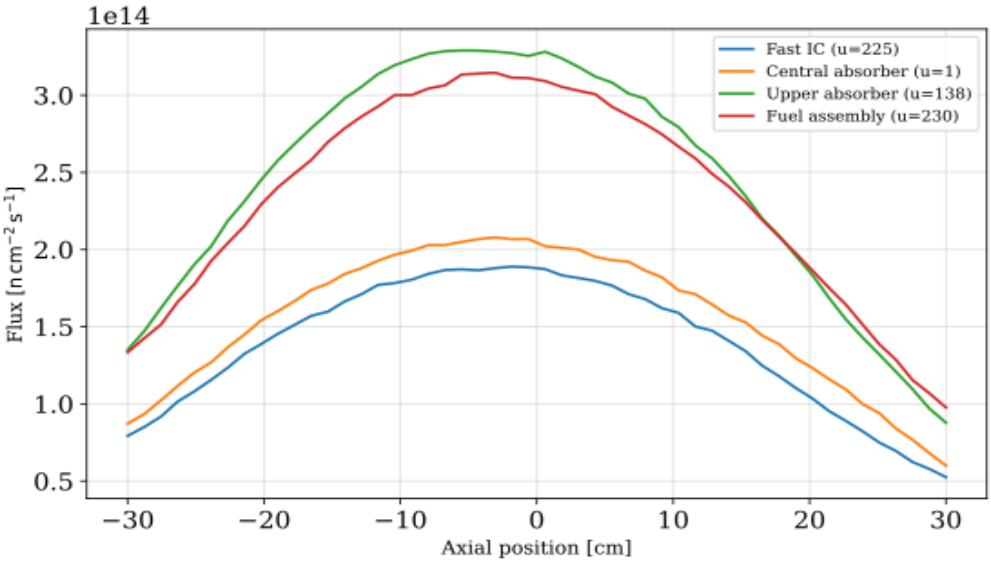


Figure 6: Axial flux profiles for selected assembly positions, normalized by the assembly volume.

2.3.1.2. Single assembly advanced thermal-hydraulic model with FFN

Before coupling the neutronics model with a full-core thermal-hydraulic solver, a unit-cell TH model of a representative VVR-M2 fuel assembly was developed. This geometry is quite unique and requires investigation to fully understand the thermal behavior at the assembly scale. The goal was two-fold: (i) characterise the actual temperature distribution in the three-plate geometry under the isothermal Serpent power distribution, and (ii) validate a homogeneous FFN model against the explicitly resolved calculation. The Serpent power output from the full-core simulation serves as the heat source input; there is no feedback in this uncoupled step.

Geometry and flow parameters

The VVR-M2 fuel assembly comprises three co-axial fuel elements within a hexagonal unit cell. The primary coolant (light water at 1 atm) enters the active zone at $T_{in} = 318\ K$ and flows downward along the fuel plates. The total volumetric flow rate through the core is 1650 t/h ($\approx 458\ kg/s$). Assuming uniform distribution among 397 assemblies, the per-assembly mass flow rate is about $\dot{m} = 1.155\ kg/s$, giving a mean coolant velocity of $U \approx 1.97\ m/s$ through the open cross-section and a core-average bulk temperature rise of $\Delta T_{bulk} = 5.3\ K$ at $P = 10\ MWth$.

The hydraulic diameter of the inter-plate channels is estimated as $D_h \approx 3\ mm$. The Reynolds number at inlet conditions,

$$Re = \frac{\rho_w\, U\, D_h}{\mu_w(T_{\text{in}})} = \frac{990.3 \times 1.97 \times 3 \times 10^{-3}}{5.964 \times 10^{-4}} \approx 9820, \tag{1}$$

confirms fully turbulent flow. The convective heat transfer coefficient is evaluated with the correlation [9]:

$$Nu = \frac{(f/8)\,(Re - 1000)\,Pr}{1 + 12.7\sqrt{f/8}\,(Pr^{2/3} - 1)}, \qquad f = (0.790 \ln Re - 1.64)^{-2} \tag{2}$$

Eq. (2) gives $Nu = 62.6$, yielding $h \approx 13900\ W.m^{-2}.K^{-1}$.

Material properties and correlations

Determining and reporting the thermal properties of the material composing the BRR is key since there is scarce property knowledge for aluminium-based fuel and SZAV-1 cladding. The fuel-meat

Funded by the European Union

Funded by the European Union. Views and opinions expressed are however those of the author(s) only and do not necessarily reflect those of the European Union or the European Atomic Energy Community ('EC-Euratom'). Neither the European Union nor the granting authority can be held responsible for them.

composition is derived from the Serpent material card: the uranium atom densities yield a ^{235}U enrichment of 19.94 at% and, assuming 98% theoretical density for UO_2, a UO_2 volume fraction $V_{f,UO_2} = 23.9\%$, with $V_{f,Al} = 74.1\%$ and a 2% fabrication porosity.

The thermal conductivity of the UO_2 particles are described by the two-term model [10]:

$$k_{UO_2}(T) = \frac{100}{6.548 + 23.533 \times 10^{-3} T} + 5.70 \times 10^{-5} T^2 e^{16361/T} \; [W.m^{-1}.K^{-1}] \quad (3)$$

The effective conductivity of the dispersion is obtained from the Bruggeman modified-Maxwell effective-medium model, treating UO_2 as spherical inclusions in a continuous Al matrix :

$$k_{meat}(T) = k_{Al}(T)\left[1 - \frac{1.5\, V_{f,UO_2}\left(k_{Al}(T) - k_{UO_2}(T)\right)}{k_{Al}(T) + 0.5\, k_{UO_2}(T)}\right], \quad (4)$$

validated for UO_2/Al and U-Mo/Al dispersions up to $V_f = 0.55$. Because $k_{Al} \gg k_{UO_2}$, the Al matrix dominates and the overall meat conductivity remains high. Density and specific heat are computed from volume-weighted and mass-weighted mixture rules, respectively.

SZAV-1 is a Russian Al-Mg-Si structural alloy (approximately Al 6061) used as cladding in VVR-K fuel assemblies. Its thermal conductivity follows a quadratic polynomial fitted to measurements on VVR-K cladding samples over the temperature range 290 to 490 K [11]:

$$k_{clad}(T) = -1.4 \times 10^{-3} T^2 + 1.048 T - 22.8 \; [W.m^{-1}.K^{-1}]. \quad (5)$$

Specific heat and density are from linear correlations for Al-Mg-Si alloy.

All water properties are evaluated from correlations fitted to reference data in the subcooled range 300–373 K at 1 atm: density from [12]; dynamic viscosity from a Vogel-type fit to the IAPWS-2008 formulation[13]; thermal conductivity from the IAPWS-2011 release [14]; and specific heat from a quadratic fit to NIST WebBook tabulated data[15]. Property values at the inlet temperature are given in Table 4, and properties are interpolated by OpenFOAM on the fly through polynomial functions.

Table 4. Water thermophysical properties at $T = 318\ K$ and $P = 1\ atm$.

Property	Symbol	Value	Unit
Density	ρ	990.3	$kg.m^{-3}$
Dynamic viscosity	μ	5.964×10^{-4}	$Pa.s$
Thermal conductivity	λ	0.635	$W.m^{-1}.K^{-1}$
Specific heat	c_p	4178	$J.kg^{-1}.K^{-1}$
Prandtl number	Pr	3.93	—

The constant solid material properties used in both simulations (explicit and homogeneous) are collected in Table 5.

Table 5. Solid material properties at $T = 355\ K$ (representative fuel/cladding operating temperature)

Material	Property	Value	Unit
	Density	4555	$kg.m^{-3}$

Funded by the European Union

Funded by the European Union. Views and opinions expressed are however those of the author(s) only and do not necessarily reflect those of the European Union or the European Atomic Energy Community ('EC-Euratom'). Neither the European Union nor the granting authority can be held responsible for them.

Fuel meat (UO_2-Al)	Specific heat	949	$J.kg^{-1}.K^{-1}$
	Thermal conductivity	142	$W.m^{-1}.K^{-1}$
SZAV-1 cladding	Density	2668	$kg.m^{-3}$
	Specific heat	916.6	$J.kg^{-1}.K^{-1}$
	Thermal conductivity	172.8	$W.m^{-1}.K^{-1}$

Explicit multi-region simulation

The first simulation used `chtMultiRegionFoam`, the OpenFOAM solver for conjugate heat transfer in explicit multi-region geometries. The mesh captures the full cross-sectional geometry of the VVR-M2 assembly: three fuel-plate regions, inner and outer cladding layers for each plate, and four distinct coolant channels. Solid-fluid interfaces are treated with conjugate boundary conditions; the coolant inlet is set to $T_{in} = 318\ K$ with the mass flow rate derived from the core-level hydraulic analysis above.

Figure 7 shows the assembly cross-section, the computational mesh detail at a corner, and the resulting radial temperature field. The temperature spans 318.0 K (inlet coolant) to 341.2 K (peak fuel temperature), and confirms that the assembly operates well below any material or safety limit at the simulated power level.

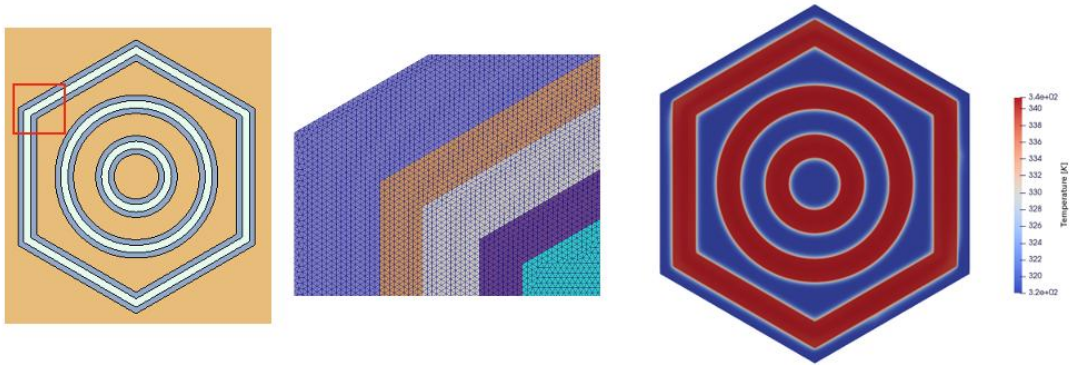


Figure 7: Explicit chtMultiRegionFoam simulation of the VVR-M2 fuel assembly. Left: horizontal cross-section showing the three fuel plates, the cladding and the coolant channels. Centre: mesh details at a plate corner. Right: steady-state temperature results at the outlet (color scale 318 K - 341 K).

As depicted, we can see that the thermal layer is really thin (a few micrometer) between the cladding surface and the bulk flow. This aspect is mainly linked to the relatively high fluid velocity. It requires a really refined mesh to capture this radial coolant temperature profile and properly describe the heat transfer process. In this case, the mesh contained 2 million cells for a single assembly simulation, not suitable for reactor-scale modelling. This led to the homogeneous/porous media approach developed in FFN.

2.3.1.3. Single assembly FFN model using a porous media approach

The second simulation used FFN leveraging its porous-media capabilities. The assembly cross-section is represented as a single fluid region divided into three radial zones, each assigned a distinct power model relying on a lumped structure, combining a series of heat conductances from the surface cladding temperature to the central fuel temperature. Figure 8 shows the hexagonal mesh with the three zones: the inner fuel zone (yellow), an intermediate zone (magenta), and the outer water-channel zone (cyan).

Funded by the European Union

Funded by the European Union. Views and opinions expressed are however those of the author(s) only and do not necessarily reflect those of the European Union or the European Atomic Energy Community ('EC-Euratom'). Neither the European Union nor the granting authority can be held responsible for them.

The fuel temperature is computed via a lumped nuclear structure: a single effective conductance links the fuel "meat" to the coolant, yielding one average cladding temperature $\bar{T}_{\text{clad}}$ and one maximum fuel temperature $T_{\text{max,fuel}}$ per zone. The conductance values are derived from a 1-D heat-transfer model based on the fuel-plate geometry.

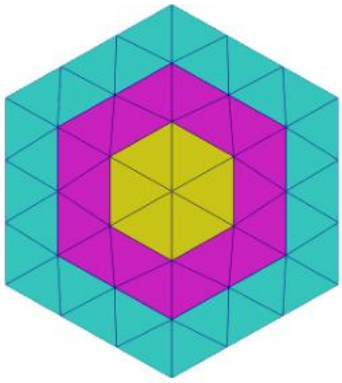


Figure 8: FFN tetrahedral mesh of a single assembly showing three different zones. Each zone encompasses a fuel plate.

Figure 9 overlays the radial temperature profile from the explicit simulation with the three scalar temperatures produced by FFN: mean coolant temperature, average cladding temperature, and maximum fuel temperature from the lumped nuclear structure. These temperatures are all compared at the outlet of the assembly.

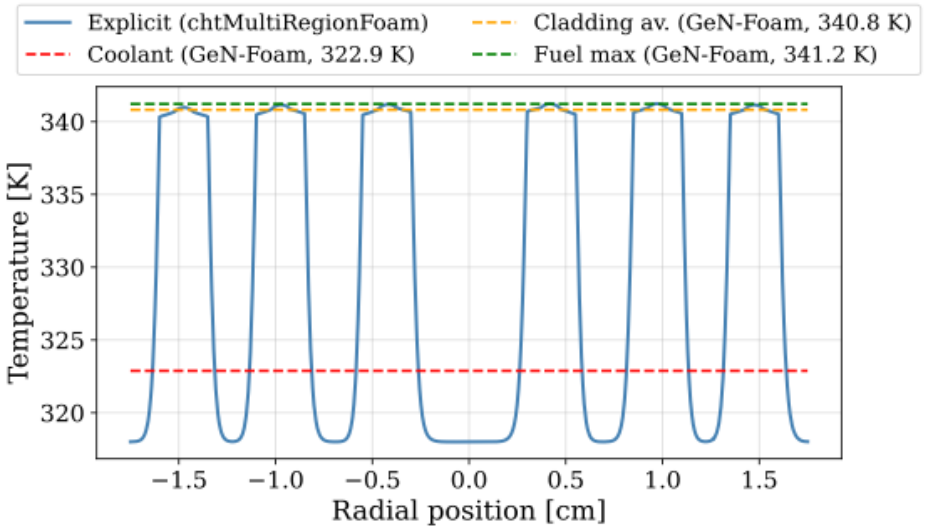


Figure 9: Radial temperature profile from the explicit chtMultiRegionFoam simulation (solid blue) compared with the FFN homogeneous model temperatures (dashed lines): mean coolant (322.9 K, red), average cladding (340.8 K, orange), and maximum fuel temperature (341.2 K, green).

The FFN homogeneous temperatures align well with the corresponding quantities from the explicit simulation: the mean coolant temperature of 322.9 K is consistent with the plateau visible in the fluid channel regions of the explicit profile, and the cladding and fuel temperatures (340.8 K and 341.2 K) reproduce the peak values of the explicit field. This agreement confirms the accuracy of the lumped conductance model and provides confidence that the homogeneous FFN representation captures the thermal behaviour of the assembly to sufficient accuracy for coupled neutronic–TH calculations.

Furthermore, the near-uniform temperature profile across the three radial zones in FFN indicates that the thermal behaviour at the assembly level can be captured with a single power zone rather than three. This simplification is adopted for the full-core model, where each of the 397 assemblies is

Funded by the European Union

Funded by the European Union. Views and opinions expressed are however those of the author(s) only and do not necessarily reflect those of the European Union or the European Atomic Energy Community ('EC-Euratom'). Neither the European Union nor the granting authority can be held responsible for them.

represented by a single hexagonal cell discretised into 6 radial cells and 20 axial layers, yielding a total full-core mesh of approximately 50 000 cells. The resulting geometry preserves the hexagonal lattice structure and is directly compatible with the Serpent 2 lattice universe numbering, enabling straightforward neutronics–TH coupling.

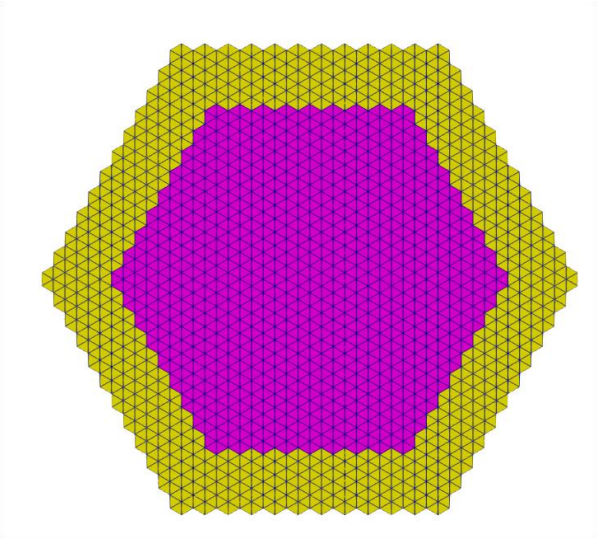


Figure 10: Full-core FFN porous-media mesh. Each hexagonal assembly is discretised with 6 radial cells and 20 axial layers. The colour coding reflects the two main types of assemblies (in—core assemblies in magenta and reflector assemblies in yellow)

2.3.1.4. High-Fidelity Coupled Serpent–foamForNuclear Simulation

The multiphysics coupling between Serpent 2 and FFN is performed through a fixed-point iterative scheme. At each iteration, Serpent computes the neutron flux and assembly power distribution; FFN then solves the porous-media thermal-hydraulics and returns updated temperature and density fields to Serpent for the next neutronics solve. The coupling exploits three key features of the two codes:

- **Shared mesh via `ifc 7`**: Serpent's interface-file format 7 reads the FFN `polyMesh` directly and projects the power density onto the OpenFOAM cells without any intermediate interpolation, ensuring exact geometric consistency between the neutronics and TH meshes.
- **Temperature–material coupling**: at each iteration, the fuel temperature (T_{fuel}), cladding temperature (T_{clad}), coolant temperature (T_{coolant}), and coolant density (ρ_{coolant}) are updated by FFN cell-by-cell in the Serpent material cards, enabling spatially resolved Doppler and moderator-density feedback.
- **TMS on-the-fly Doppler broadening**: the Target Motion Sampling (TMS) method is used to evaluate cross sections at the actual local fuel temperature rather than the nearest tabulated temperature, eliminating the temperature grid discretisation error at negligible computational cost.
- **Fission source propagation (FSP)**: the converged fission source distribution from the previous iteration is passed as the initial source for the next Serpent run, reducing the number of inactive cycles required for source convergence.

The simulation starts from a fully isothermal state at 318 K (the experimentally measured inlet temperature) and iterates until k_{eff} and the temperature fields are stable. Each Serpent run uses the same settings as the isothermal reference calculation (see Table 2).

Funded by the European Union

Funded by the European Union. Views and opinions expressed are however those of the author(s) only and do not necessarily reflect those of the European Union or the European Atomic Energy Community ('EC-Euratom'). Neither the European Union nor the granting authority can be held responsible for them.

Figure 11 shows the evolution of k_{eff} and the mean relative change of the three temperature fields across the 11 coupling iterations. Both quantities converge rapidly: the temperature fields reach their asymptotic values after a single iteration (iteration 1 → 2), as the large first-step change from the isothermal 318 K state to the realistic operating temperatures dominates all subsequent fluctuations, which remain below 0.01% and are indistinguishable from Monte Carlo statistical noise. The multiplication factor drops by 483 pcm from the isothermal value ($k_{\text{eff,iso}} = 1.00884$) to the coupled steady-state value ($k_{\text{eff,coupled}} = 1.00352 \pm 0.00018$), k_{eff}=1.00352+/-0.00018 reflecting the negative temperature and density reactivity feedback associated with the transition from 318 K to realistic fuel and moderator temperatures.

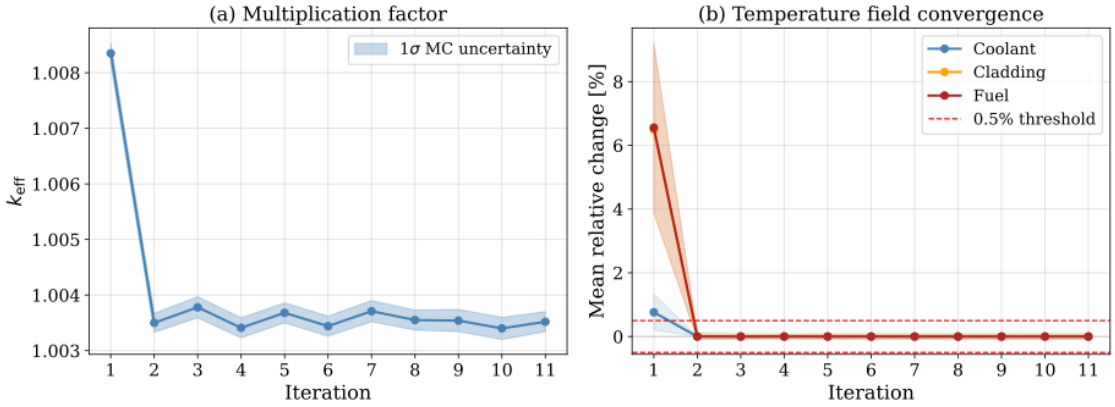


Figure 11: Convergence of the Serpent–FFN coupling. (a) Effective multiplication factor k_{eff} with 1σ Monte Carlo uncertainty band. (b) Mean relative change in the coolant, cladding, and fuel temperature fields between successive iterations; shaded bands represent the standard deviation over all fuel cells. Both quantities converge after a single iteration.

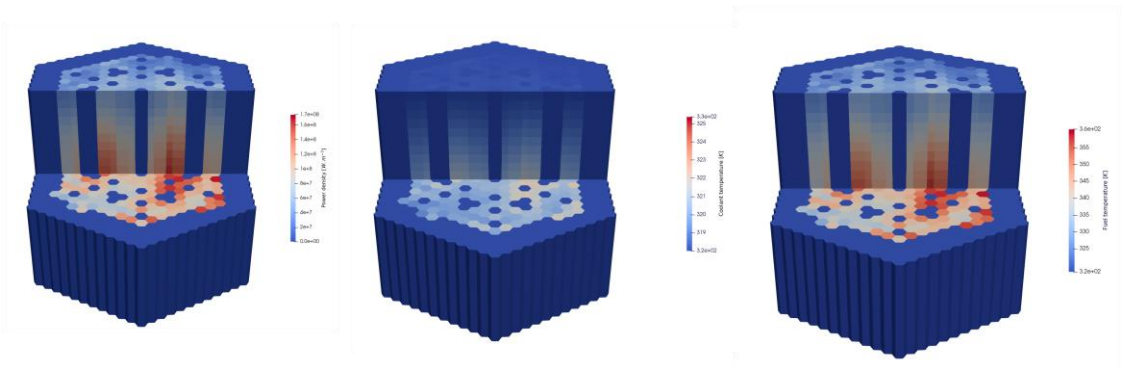


Figure 12: ParaView visualisation of the converged coupled fields on the full-core FFN mesh. Left: volumetric power density (W.m^{-3}). Centre: coolant temperature (K), rising from the inlet (318 K) to the outlet. Right: fuel temperature (K).

The final coupled temperatures for the core are: mean coolant 320.4 K (peak 325.5 K), mean cladding 338.7 K (peak 360.1 K), and mean fuel temperature 338.9 K (peak 360.5 K). The axial evolution of the coolant and fuel temperatures in the hottest assembly across all iterations is shown in Figure 13, confirming that the temperature profiles are established in a single step and subsequently does not fluctuate.

Funded by the European Union

Funded by the European Union. Views and opinions expressed are however those of the author(s) only and do not necessarily reflect those of the European Union or the European Atomic Energy Community ('EC-Euratom'). Neither the European Union nor the granting authority can be held responsible for them.

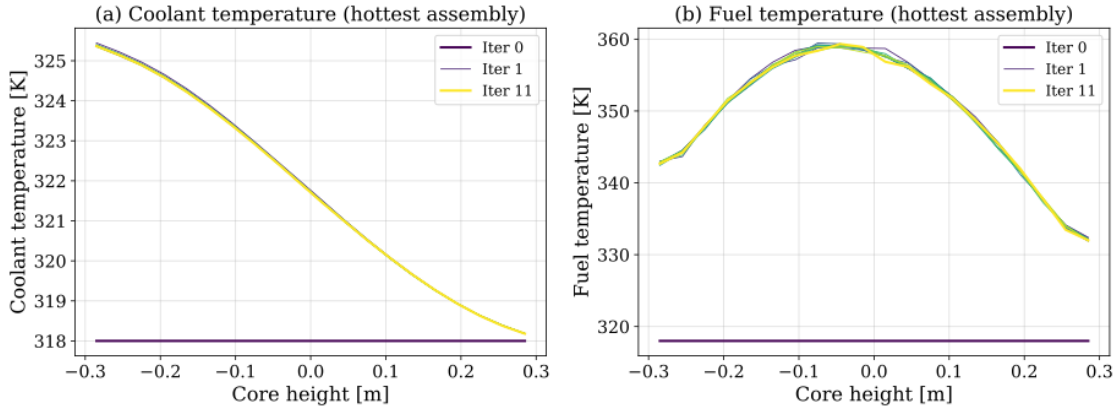


Figure 13: Axial temperature profiles in the hottest assembly at each coupling iteration (color scale from dark to light = iteration 0 to 11). (a) Coolant temperature. (b) Fuel temperature.

Figure 14 shows the effect of the neutronic–TH coupling on the assembly power distribution. The scatter plot (a) shows the relative power change of each assembly as a function of its isothermal power, and the histogram (b) shows the overall distribution of these changes. The coupling induces a modest redistribution: the individual assembly changes range from -1.29% to $+2.29\%$. Overall, the power redistribution is small, confirming that the temperature feedback at this operating point does not significantly reshape the neutron flux distribution. This is supported by the small temperature difference between the inlet and the outlet.

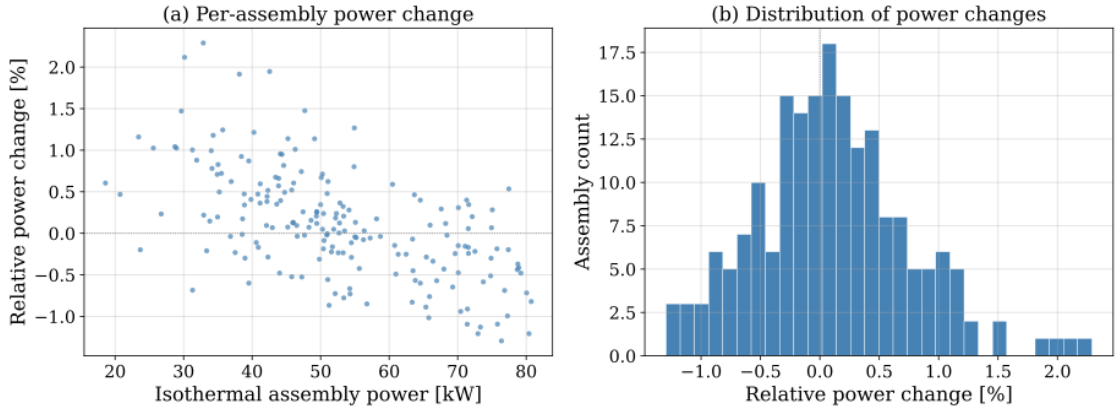


Figure 14: Impact of Serpent–FFN coupling on the assembly power distribution. (a) Relative power change (coupled minus isothermal, normalised to isothermal) as a function of isothermal assembly power. (b) Histogram of per-assembly power changes over the 190 fuelled positions.

2.3.1.5. Low-Fidelity Coupled Serpent–foamForNuclear Simulation

The Monte Carlo-based coupling presented in the previous section provides a coupled solution for the BRR reactor at a high computational cost: a full-core Serpent criticality calculation at every coupling iteration. It makes it impractical for transient or parametric studies. This section presents the development of a lower fidelity alternative in which the porous-media thermal-hydraulic model of FFN is retained unchanged, while the neutronics solve is provided by FFN's diffusion module. Two-group macroscopic cross sections are pre-generated with the same explicit full-core Serpent model described previously, homogenised per assembly and tabulated as a function of the local fuel, cladding, and coolant temperature. The diffusion and TH modules of FFN are then coupled internally, following the same fixed-point iteration philosophy as the reference scheme, but replacing the per-iteration Serpent Monte Carlo solve with FFN's own much faster diffusion solve, driven by interpolated cross sections. FFN provides a serpentToFoam utility that reads Serpent cross-section output directly onto the FFN neutronic case.

Funded by the European Union

Funded by the European Union. Views and opinions expressed are however those of the author(s) only and do not necessarily reflect those of the European Union or the European Atomic Energy Community ('EC-Euratom'). Neither the European Union nor the granting authority can be held responsible for them.

A dedicated mesh was generated with gmsh to serve as the computational support for the FFN diffusion calculation. The mesh covers the active core region and the surrounding water reflector. The core region is discretised on the same basis as the FFN TH mesh, with 6 radial cells per assembly and 20 axial layers, so that the assembly-wise cross sections generated can be mapped directly onto the corresponding mesh volumes. The peripheral region, outside the hexagonal lattice envelope, is meshed with extruded tetrahedral cells to conform to the cylindrical core boundary while remaining compatible with the structured core mesh. Figure 15 shows the resulting mesh.

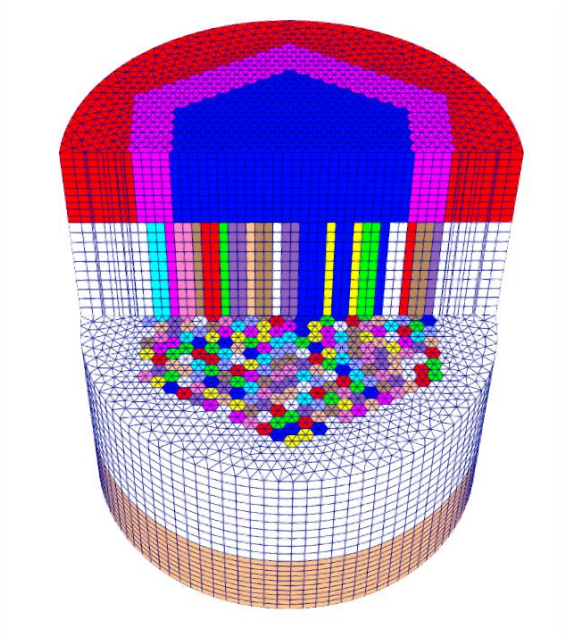


Figure 15: *gmsh* neutronics mesh used for the FFN diffusion calculation: structured hexagonal core region (6 radial cells per assembly, 20 axial layers) surrounded by an extruded tetrahedral mesh of the water reflector.

Two-group (fast/thermal) macroscopic cross sections were generated with the same explicit full-core Serpent model described in Section 2.3.1.1, homogenised over each of the 190 fuel assemblies, the control and safety rods, the beryllium reflector, the irradiation channels, and the surrounding water, for a total of 404 distinct spatial regions. Each cross-section set was generated with a statistical uncertainty of approximately 20 pcm on k_{eff}.

A reference cross-section set was generated at the isothermal state used for the Serpent full-core calculation ($T = 318\ K$). In addition, a set of perturbed states was generated by independently varying the fuel, cladding, and coolant temperatures (with the corresponding coolant density change), so that the cross sections can later be interpolated as a function of the local temperature and density fields returned by FFN's TH module during the coupled calculation. The perturbed values, summarised in Table 6, were chosen to bracket the operating temperature range obtained in the HF coupled simulation (peak coolant 325.5 K, peak cladding 360.1 K, peak fuel 360.5 K).

Table 6. Perturbed states used for the two-group cross-section generation, in addition to the isothermal 318 K reference state.

Quantity	Symbol	Perturbed values
Fuel temperature	$\mathrm{T_{fuel}}$	$320 - 340 - 360\ K$
Cladding temperature	$\mathrm{T_{clad}}$	$320 - 340 - 360\ K$
Coolant temperature (+ density)	$\mathrm{T_{cool}}$	$318 - 321 - 325\ K$

Funded by the European Union

Funded by the European Union. Views and opinions expressed are however those of the author(s) only and do not necessarily reflect those of the European Union or the European Atomic Energy Community ('EC-Euratom'). Neither the European Union nor the granting authority can be held responsible for them.

The neutronics solve is performed with the FFN steady-state two-group diffusion solver, using a fission-source (power) iteration scheme to converge k_{eff} and the flux shape. A "black" (zero re-entrant current, i.e. vacuum-equivalent) boundary condition is applied on the outer surface of the mesh, consistent with the vacuum boundary condition used in the Serpent full-core model. The solver is normalised to the same target thermal power of 10 MW used throughout this study.

The multiplication factor obtained with FFN deviates from the Serpent reference by 303 pcm, consistent with the accuracy expected from a two-group diffusion approximation relative to a continuous-energy Monte Carlo reference.

Figure 16 compares the assembly-wise power distribution obtained from the FFN diffusion solve with the Serpent detector tallies, together with the corresponding relative difference map.

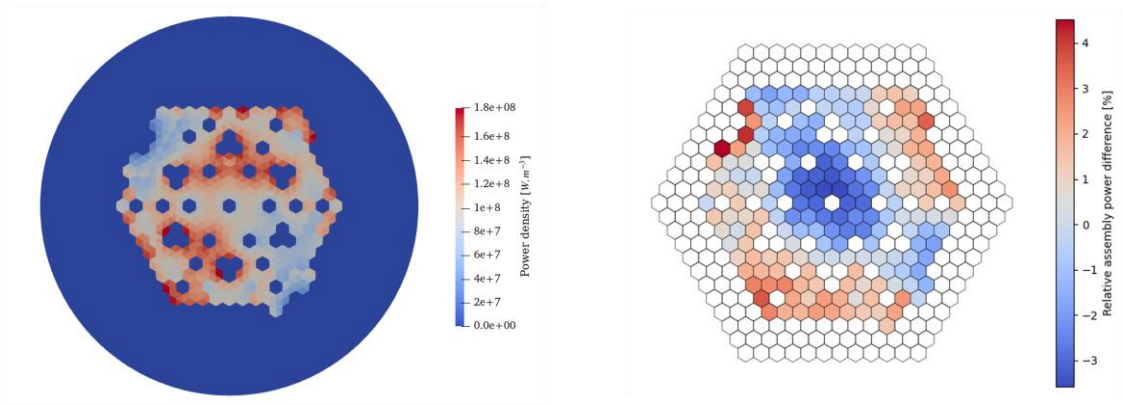


Figure 16: Assembly-wise power distribution from the FFN diffusion solver (left) and the Serpent reference (centre), and the corresponding relative difference (right).

These results demonstrate the overall good agreement in power prediction for FFN. The relative error remains below $\pm\, 4\%$. The largest error between the FFN diffusion solver and Serpent is observed in the vicinity of the strong absorber region; at the center next to the inserted central control rod and at the core periphery next to the petal-shaped absorber.

The thermal-hydraulic fields obtained from the pure FFN coupled calculation, i.e. FFN's TH module driven by its own diffusion-based power distribution, were compared to those of the coupled Serpent–FFN simulation. Figure 17 shows the resulting outlet coolant temperature field. The agreement is excellent: the coolant temperature differs by no more than 0.1 K, and the fuel temperature by no more than 0.3 K, across the full core.

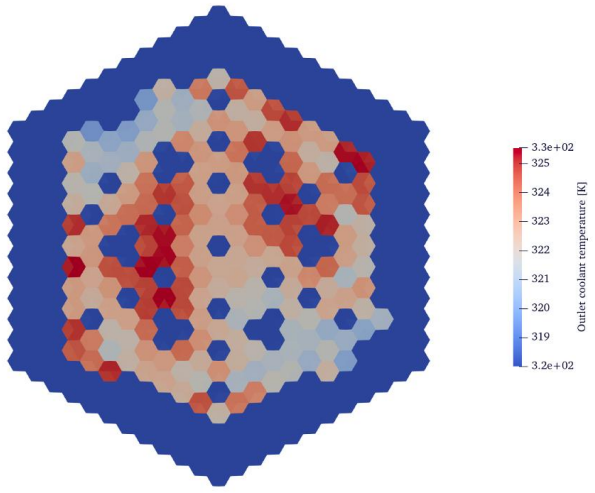


Figure 17: Outlet coolant temperature fields obtained with the LF (FFN-driven) coupled simulation.

Funded by the European Union

Funded by the European Union. Views and opinions expressed are however those of the author(s) only and do not necessarily reflect those of the European Union or the European Atomic Energy Community ('EC-Euratom'). Neither the European Union nor the granting authority can be held responsible for them.

2.3.1.6. Outlook

The Serpent–FFN coupling presented here offers an efficient path to simulate the BRR core under normal operating conditions at a high level of fidelity. On the neutronics side, Serpent provides an explicit representation of the full core with detailed material compositions for each fuel assembly according to its burnup level, and its detector routines give direct access to assembly-wise flux and power distributions. On the thermal-hydraulic side, FFN's porous-media solver delivers assembly-resolved temperatures and coolant density fields at a computational cost that is compatible with iterative coupling, while matching the accuracy of the explicit chtMultiRegionFoam solver at the assembly level. The coupling between the two codes is seamless thanks to the shared polyMesh files.

The coupled steady state is reached after a single iteration: the temperature and density fields jump from the isothermal 318 K reference to their realistic operating values, and all subsequent iterations fluctuate only within Monte Carlo statistical noise. The associated reactivity feedback amounts to -483 pcm relative to the isothermal k_{eff}, driven by the Doppler broadening in the fuel and the reduction in coolant density. The redistribution of assembly power induced by the coupling is small, with individual changes below $\pm 2.3\%$, confirming that the temperature feedback does not significantly reshape the neutron flux distribution at this operating point.

Finally another model relying solely on FFN is produced. Assembly-wise flux and power agree with the Serpent reference to within 5%, k_{eff} to within 300 pcm, and the resulting coolant and fuel temperatures to within 0.1 K and 0.3 K of the reference coupled solution for a fraction of the computational cost.

2.3.2. nTRACER/CTF

The fuel elements of the BRR EK reactor are, as described above, the VVR-M2 hexagonal assemblies consisting of three concentric fuel tubes containing a uranium--aluminum alloy meat enriched to approximately 20% U-235. Furthermore, the core also includes several types of non-fuel elements of irregular geometry. For these reasons, the BRR EK reactor is very difficult for modeling with regular lattice geometry codes, and a natural choice for such reactor modeling is a Monte Carlo method, e.g., with a constructive solid geometry capabilities. The nTRACER MOC code of SNU [8], which is in use in the EVEREST project by PSI, is designed for a structured pin-resolved core representation and thus does not provide the geometrical flexibility which is required for such complex and non-standard for commercial VVERs geometry as takes place for the BRR reactor. Nevertheless, it was initially proposed to employ the nTRACER code for simulation of the BRR experiments, in order to validate the code against the foreseen high-resolution measurements.

Thus, a general assessment of applicability of the nTRACER/CTF system of codes for analysis of the BRR reactor has been done at PSI at the initial stage of the EVEREST project. In order to represent the BRR geometry, one would need to employ a very fine-mesh regular cells with a dedicated materials homogenization approach. Unfortunately, such materials homogenization would impose a noticeable approximation diminishing the value of the direct whole-core nTRACER solver. Furthermore, development and implementation of the dedicated homogenization procedure would require significant verification efforts, which have been finally assessed as requiring too many resources to be reasonable. Another complication for the nTRACER usage is the lack of the appropriate thermal-mechanical models for determination of the fuel temperature profiles. An adaptation of the CTF models to the BRR core irregularities would also need to be addressed for a multi-physics modeling of the BRR reactor. Based on the performed assessment, it became obvious that an adequate modeling of BRR EK reactor with nTRACER/CTF is not feasible within the WP2 timeline.

Finally, the nTRACER code version available at PSI was obtained with a pre-generated cross-sections library, which cannot be modified without involvement of the code developer. This library was optimized and validated for conventual LWR UO_2 fuel, i.e. for U-235 enrichment up to 5wt%.

Funded by the European Union

Funded by the European Union. Views and opinions expressed are however those of the author(s) only and do not necessarily reflect those of the European Union or the European Atomic Energy Community ('EC-Euratom'). Neither the European Union nor the granting authority can be held responsible for them.

Application of this library for uranium--aluminum alloy with enrichment up to 20wt% of U-235 obviously should require a dedicated verification and validation activity. Thus, additional considerations have been given to this point, since producing results with nTRACER/CTF (if this was doable) without their proper qualification would not be of real value for the project objectives.

For this combination of reasons, the advanced modelling of the BRR reactor with nTRACER won't be pursued further during the EVEREST project.

Funded by the European Union

Funded by the European Union. Views and opinions expressed are however those of the author(s) only and do not necessarily reflect those of the European Union or the European Atomic Energy Community ('EC-Euratom'). Neither the European Union nor the granting authority can be held responsible for them.

3. BME Training Reactor

This chapter presents the conventional and advanced multi-physics models developed for the BME Training Reactor. Section 3.1 introduces the BME facility, its core configuration and fuel design, and summarises the experimental campaign against which the models presented in this chapter are ultimately intended to be validated. Section 3.2 describes the conventional modelling scheme, based on the nodal code PARCS coupled to the TRACE system code. Section 3.3 then presents the advanced multi-physics approaches investigated within EVEREST, namely a FENNECS/ CTF coupling developed at GRS and a foamForNuclear coupling developed at EPFL. Together, these models establish the computational basis needed to interpret the BME measurements reported in D2.1 and to inform the design of the high-resolution experiments planned in WP3.

3.1. Facility overview

The BME Training Reactor is an open-pool, light-water moderated and cooled research and training reactor operated by the Institute of Nuclear Techniques (NTI) of the Budapest University of Technology and Economics (BME), located on the university's Central Campus. Its nominal thermal power is 100 kW since 1980. The core comprises 24 EK-10 type fuel assemblies (369 fuel rods in total), fuelled with 10% enriched UO_2 in a metal-magnesium matrix and surrounded by a graphite reflector, yielding a maximum thermal neutron flux of approximately 2.7×10^{12} n/cm²s. The core sits at the bottom of an open aluminium tank approximately 140 cm in diameter and 600 cm in height (20 mm wall thickness), filled with demineralised water and enclosed by a 2 m thick ordinary-plus-heavy-concrete bioshield. The facility provides extensive irradiation capabilities through 20 vertical irradiation channels, 5 horizontal beam tubes, two pneumatic rabbit systems, and a large irradiation tunnel, supporting a mix of educational reactor-operation exercises and research activities in reactor physics, thermal-hydraulics, radiation shielding, radiochemistry, nuclear safeguards, and radioisotope production.

A series of experimental campaigns were carried out at the BME Training Reactor to provide high-fidelity validation data for coupled neutron transport and thermal-hydraulic modelling. Reactivity worth measurements used the ex-core CFUL08 fission-chamber detector chains to determine integral and differential control rod worths, fuel and graphite reflector assembly worths, and critical control rod positions via the rod-drop method and inverse kinetics analysis. Relative axial reaction rate profiles were measured at various core and reflector positions using activation wires. Then in-core and above-core coolant temperature fields across various transients spanning 1–100 kW power levels were acquired. Finally, a multi-physics campaign was carried out, recording 16 thermocouples time series with simultaneous ex-core neutronic measurements across 11 transients. Details can be found in [1]. This experimental data constitutes the primary experimental reference for the low and high-fidelity models presented in Sections 3.2 and 3.3.

3.2. Conventional model

The conventional model of the BME Training Reactor was developed using the PARCS nodal diffusion code and the U.S. NRC thermal-hydraulics system code TRACE. This section first presents the PARCS and TRACE models and then describes the implemented coupling between them. More detailed description of the models as well as corresponding simulations and measurements can be found in [16].

3.2.1. PARCS model

The detailed Monte Carlo reactor physics modelling of BME TR was carried out with the Serpent 2 continuous energy Monte Carlo code (model developed in version 2.1.31, for each simulation, the ENDF/B-VII.0 libraries were used, the unresolved resonance probability table was turned on, and S(α,β) treatment was applied to the water and graphite materials at 300 K temperature). The Serpent model

Funded by the European Union

Funded by the European Union. Views and opinions expressed are however those of the author(s) only and do not necessarily reflect those of the European Union or the European Atomic Energy Community ('EC-Euratom'). Neither the European Union nor the granting authority can be held responsible for them.

of the reactor served two purposes: it provided reference values for reactor physics code-to-code comparison where feedback was not present and it was used for group constant, as well as effective kinetic parameter generation. The coupled calculations necessitated to have a parameterised group constant library of several branches, for which the traditional two-step approach was used. In total, 17 different assembly-sized homogenised material regions were identified (see Figure 18 and Figure 19). Each geometry was taken out from the full-core reactor model with reflective boundary condition applied on all sides.

Four branches were used for the parameterised group constant library that are summarised in Table 7. Based on Serpent 2 calculations, the reactivity-fuel temperature function is linear between 300 K and 600 K. Unfortunately, the reactivity-coolant density function is rather quadratic, therefore, the applied linear approximation introduces bias to the calculations. Reference and coolant density branches were generated for all regions, while fuel temperature and control rod branches were only computed for those, which contained fuel and control rod, respectively. Group constants were generated with Serpent in 2 and 70 groups (CASMO-2 and CASMO-70 group structures). Outputs in 70 groups were necessary to calculate flux-limited and reference-current-weighted transport cross-sections. The Serpent outputs were first processed with an in-house script that computed flux-limited and reference-current-weighted transport cross-sections, then the modified outputs were further processed to PARCS PMAX cross-section files by the GenPMAXS code (version 6.2).

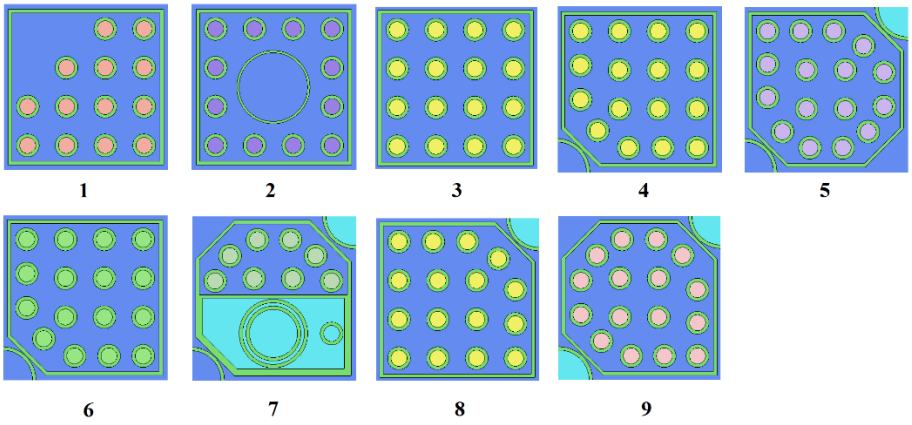


Figure 18: Homogenised fuel regions (1: position B3, 2: position F3, 3: regular fuel assembly, 4: irregular fuel around rod AUT, 5: position D4, 6: irregular fuel around rod MAN, 7: position D5, 8: irregular fuel around the safety rods, 9: position E5)

Funded by the European Union

Funded by the European Union. Views and opinions expressed are however those of the author(s) only and do not necessarily reflect those of the European Union or the European Atomic Energy Community ('EC-Euratom'). Neither the European Union nor the granting authority can be held responsible for them.

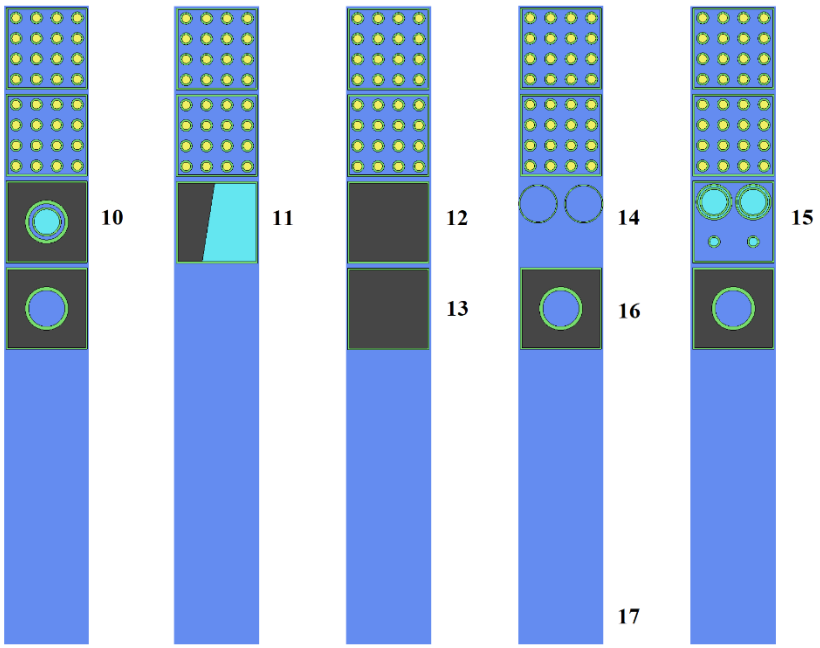


Figure 19: Homogenised reflector regions (10: neutron source, 11: graphite with irradiation channel, 12-13: double layer of graphite blocks, 14: vertical irradiation channel in water, 15: thermal sample-delivery rabbit system, 16: vertical irradiation channel in)

Table 7: Branches used for the parameterised group constant library

Branch name	T_{fuel} (K)	ρ_{cool} (kg/m^3)	Control rod position (mm)
Reference	300	996.56	z_{AUT}= 600, z_{MAN} = 600
Coolant density	300	958.37	z_{AUT}= 600, z_{MAN} = 600
Fuel temperature	600	996.56	z_{AUT}= 600, z_{MAN} = 600
Control rod	300	996.56	z_{AUT}= 0, z_{MAN} = 0

The PARCS core model consisted of an 8 × 9 Cartesian lattice (pitch: 72 mm). The total core height was 500 mm, which consisted of 10 axial subdivisions. Radially 7-7 nodes of water reflector blocks were defined in all lateral directions, while 500-500 mm of the same reflector was defined below and above the core with 10-10 subdivisions. Thus, the total dimensions of the reactor core model were 1584 mm × 1656 mm × 1500 mm. Figure 20 shows the radial cross-section of the geometry at the height of the core. The fuel regions are recommended to be supplied with group constant libraries containing flux-limited diffusion coefficients, while the reflector regions with those containing reference-current-weighted coefficients.

Funded by the European Union

Funded by the European Union. Views and opinions expressed are however those of the author(s) only and do not necessarily reflect those of the European Union or the European Atomic Energy Community ('EC-Euratom'). Neither the European Union nor the granting authority can be held responsible for them.

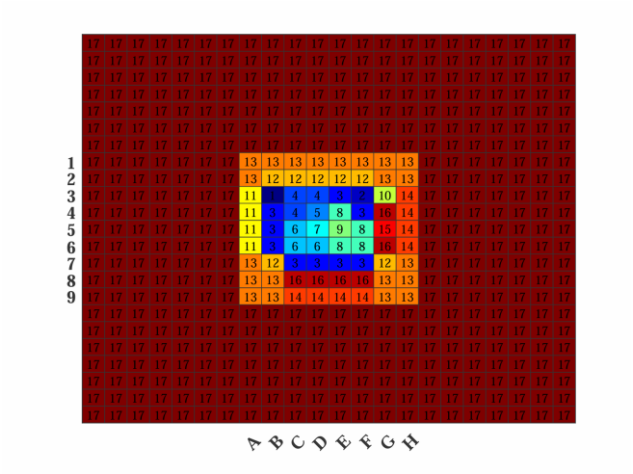


Figure 20: Radial cross-section of the PARCS model in core height. The numbers in the nodes refer to the homogenised regions of Figure 18 and Figure 19.

The transients performed in BME TR are usually initiated by control rod manoeuvres; therefore, it is important for the PARCS model to be able to reproduce measured or Serpent simulated integral and differential control rod worth results. Thus, the following modifications were introduced to the model:

- According to the differential control rod worth measurements, the z = 0 mm position of the automatic control rod is about 319 mm, while that of the manual rod is about 336 mm below the axial centre of the core. This correction was already implemented in the Serpent model and accordingly, the axial rod positions in the PARCS model were shifted as well.
- The integral rod worth values of the control rods in PARCS were adjusted to the measured values by slightly modifying the control rod branch thermal absorption cross-sections of the related materials (in the case of the manual control rod, the values had to be increased by 6%, while for the automatic rod, they had to be decreased by 2%). Instead of using the static k-eigenvalue method, the integral rod worth values were calculated by performing rod drop transients with PARCS that were evaluated by an in-house inverse kinetics script.
- Previously, when the integral control rod worth measurements were evaluated; unexpected and non-physical results were obtained while using the ENDF/B-VII.0 based effective point kinetics parameters. It was found that when parameters based on the JEFF-3.1.1 libraries were used for the same evaluations, the produced inverse kinetics results improved and were comparable to earlier reported measurement results. This effect was highlighted and investigated more thoroughly in [17]. Therefore, for the calculations of this model, also, the JEFF-3.1.1 based effective point kinetic parameters were used.

The described modelling was carried out with the PARCS code version 3.3.1.

3.2.2. TRACE model

The thermal-hydraulic part of the modelling was carried out with the U.S. NRC thermal hydraulics system code TRACE (the model was developed in version 5.1262). The graphical model interface was realised in the Symbolic Nuclear Analysis Package (SNAP) Model Editor (version 3.0.2).

The TRACE model of BME TR primarily comprises of a three-dimensional VESSEL component that represents the reactor vessel and 24 connecting CHANNEL units, each simulating a specific fuel assembly. The model is supplemented by three other units: a HEAT STRUCTURE component connected to the vessel represents the vessel wall, while a BREAK component that joins the vessel through a SINGLE JUNCTION unit simulates the spillway (see Figure 21).

Funded by the European Union

Funded by the European Union. Views and opinions expressed are however those of the author(s) only and do not necessarily reflect those of the European Union or the European Atomic Energy Community ('EC-Euratom'). Neither the European Union nor the granting authority can be held responsible for them.

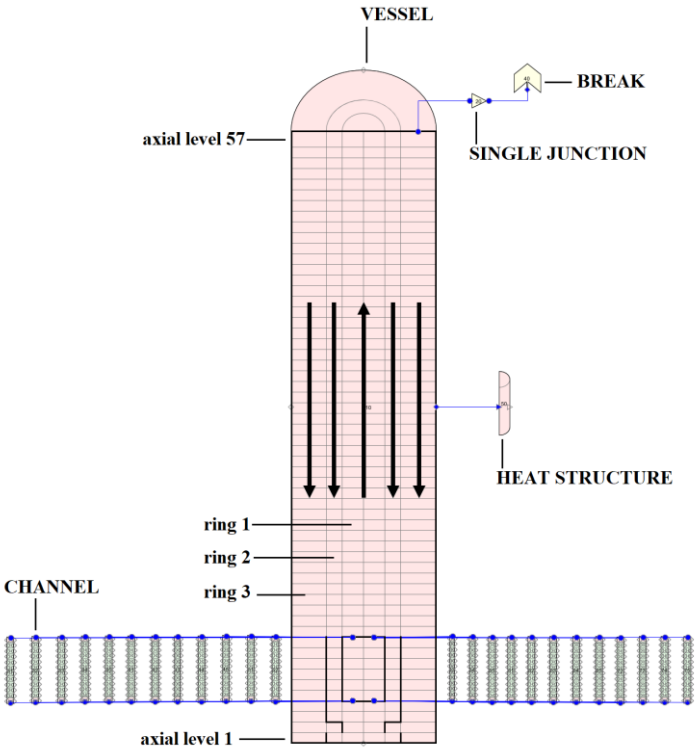


Figure 21: TRACE model of BME TR

During the modelling, special attention was given to (1) include all the flow paths, (2) preserve the heat capacity, (3) the structure volumes and (4) the key flow areas of the system.

The height of the applied VESSEL component was kept the same as that of the actual vessel, but its radius was slightly reduced to match the water volume. The vessel model was divided into 3 radial, 1 azimuthal and 57 axial nodes. The diameters of the radial nodalisation were chosen so that the first, second and third nodes (ring 1, ring 2 and ring 3) represent the core, the reflector and the coolant around the core, respectively. Ring 1-2, axial levels 1-4 represent the structures below the core; ring 1, axial level 5-10 correspond to the core area; while ring 2, axial levels 5-10 represent the reflector area including the vertical irradiation channels. The rest of the unlisted nodes correspond to water around and above the reactor core. Vessel hydraulic diameters were set for each axial level by computing the quantity of the corresponding radial cross-sections.

The core barrel structure and the relevant flow paths were modelled by setting flow area and cell volume fractions to preserve the related volumes, flow areas and heat capacities (flow area fractions that were set to zero are marked in Figure 21; for detailed description). Due to these settings, the recirculated coolant enters the core barrel structure in ring 2, axial level 2 and flows downwards to ring 2, level 1; then to ring 1, axial levels 1-4, where it may enter the CHANNEL components in ring 1, axial level 5 or flow through the reflector region in ring 2, axial levels 5-10.

The fuel assembly, canister, rod and spacer dimensions, hydraulic diameters and loss coefficients were set separately for each CHANNEL component based on the geometry specifications and empirical relations.

The vessel wall thickness was set 10 mm according to the reactor specifications. During the measurements, the primary and secondary circulating systems were not used. Therefore, the only sources of heat loss were radiation heat transfer to the environment, heat conduction through the vessel wall and water evaporation at the of the vessel. Several attempts were made to accurately

Funded by the European Union

Funded by the European Union. Views and opinions expressed are however those of the author(s) only and do not necessarily reflect those of the European Union or the European Atomic Energy Community ('EC-Euratom'). Neither the European Union nor the granting authority can be held responsible for them.

reproduce the cooling of the modelled system. Finally, historical cooling curves were studied and a single heat transfer coefficient was defined between the outer surface of the vessel wall and a constant temperature (293 K) heat sink. The value of the coefficient (12 W/m^2/K) was fitted from the slope of the cooling part of a long irradiation transient at 100 kW nominal power.

Although TRACE could simulate explicitly the water-vapour-air interface at the top of the vessel, to save computation time, ring 3, axial level 57 of the fully fluid-filled VESSEL component was connected to a BREAK unit through a SINGLE JUNCTION component. The BREAK unit was set to keep atmospheric pressure and maintain fluid conditions. During the sensitivity studies it was shown that only a negligible amount of coolant passes through the SINGLE JUNCTION component, therefore, the applied simplifications do not alter the thermal hydraulics of the system.

3.2.3. Coupling

The TRACE and PARCS calculations can be coupled internally by changing a few necessary flags in both inputs and by defining a so-called MAPTAB input file that specifies which nodes of PARCS correspond to which node of TRACE in what weight. For the calculations of this paper, due to the simplicity and the regular geometry of the problem, the so-called automated weight method was used to generate the input file of the mapping. Each of the 24 fuel assemblies of PARCS (24 radial nodes and 10 axial levels) was mapped to the corresponding TRACE channel components (24 CHANNELs, 5 heated axial levels).

The calculation of the Doppler fuel temperature (T_D), which must be specified in the MAPTAB input file, was left as default, i.e.:

$$T_D = 0.3 \cdot T_c + 0.7 \cdot T_s \,,$$

where T_c and T_s are the fuel centreline and surface temperatures, respectively. According to the sensitivity calculations, the output temperature and power curves are not sensitive to the choice of the coefficients.

The coupled calculations were carried out according to the following scheme, according to the guidelines of the developers:

- Step 1: Run steady-state, stand-alone TRACE calculation
- Step 2: Run steady-state, coupled TRACE/PARCS calculation (TRACE restart file of Step 1 is utilised)
- Step 3: Run transient, coupled TRACE/PARCS calculation (TRACE and PARCS restart files of Step 2 are utilised)

3.3. Advanced models

This section presents the advanced multi-physics models developed for the BME TR within EVEREST. Two independent routes were investigated. The first route, described in Section 3.3.1, involves the coupling done at GRS between the FENNECS deterministic neutron transport code and the CTF subchannel code. The second, detailed in Section 3.3.2 relies on the foamForNuclear (FFN) platform developed at EPFL. These models provide the assembly-wise and axial neutron flux, power, and temperature distributions required both for comparison with the D2.1 experimental campaign and for the design of the high-resolution instrumentation to be deployed in WP3.

3.3.1. FENNECS/CTF

GRS aims at modelling the BME Training Reactor in a coupled approach applying the subchannel code CTF for the thermal hydraulic and the finite-element based code FENNECS for the neutronics solution. A newly developed coupling using the codes build-in interfaces is applied. In the following, the individual models as well as initial coupled results are described.

Funded by the European Union

Funded by the European Union. Views and opinions expressed are however those of the author(s) only and do not necessarily reflect those of the European Union or the European Atomic Energy Community ('EC-Euratom'). Neither the European Union nor the granting authority can be held responsible for them.

3.3.1.1. Description of the neutronics model with FENNECS

The chosen workflow for the modelling is a two-stage deterministic scheme, i.e. lattice transport followed by a full-core finite-element solution, in which the condensation is performed on a 2D full-core geometry rather than on assemblies extracted under reflective boundary conditions. Ványi [16] used full-core and two-step to distinguish constants generated from the 3D full-core Monte Carlo model from constants generated on extracted 2D assemblies with reflective boundaries. In that vocabulary the present scheme is full-core condensation obtained deterministically: it retains the true neighbourhood of every pin cell without taking constants from the reference.

HELIOS-2 is used for the 2D lattice calculation, a 56-group transport (MoC) solution on two-dimensional pin-cell geometry, condensed to seven energy groups and homogenised region by region (pin-wise and assembly-wise). Its advantage for this modelling is besides its computational speed that its geometry is built from explicitly defined structures and connections rather than from a Cartesian or hexagonal pin grid, so a homogenisation region may be an arbitrary polygon. Hence, the condensation can be performed directly on the distorted pin cells rather than on a regularised approximation of them. FENNECS is applied for the full-core simulation: a finite-element solver on upright triangular prisms with linear basis functions, developed by GRS and distributed with the AC² code package [18], [19], originally continuous-Galerkin diffusion and since extended with an SP_3 transport solver [20]. It reads cross sections in a NEMTAB-like format parametrised against thermal-hydraulic feedback variables, which is what makes the coupling with CTF possible. Its mesh comes from a dedicated tool, PEMTY, whose ability to handle arbitrary polygons is likewise necessary for the distorted pin cell modelling described below. The SERPENT 2 model of the BME TR [16] supplies the continuous-energy reference in two and three dimensions (see Figure 22).

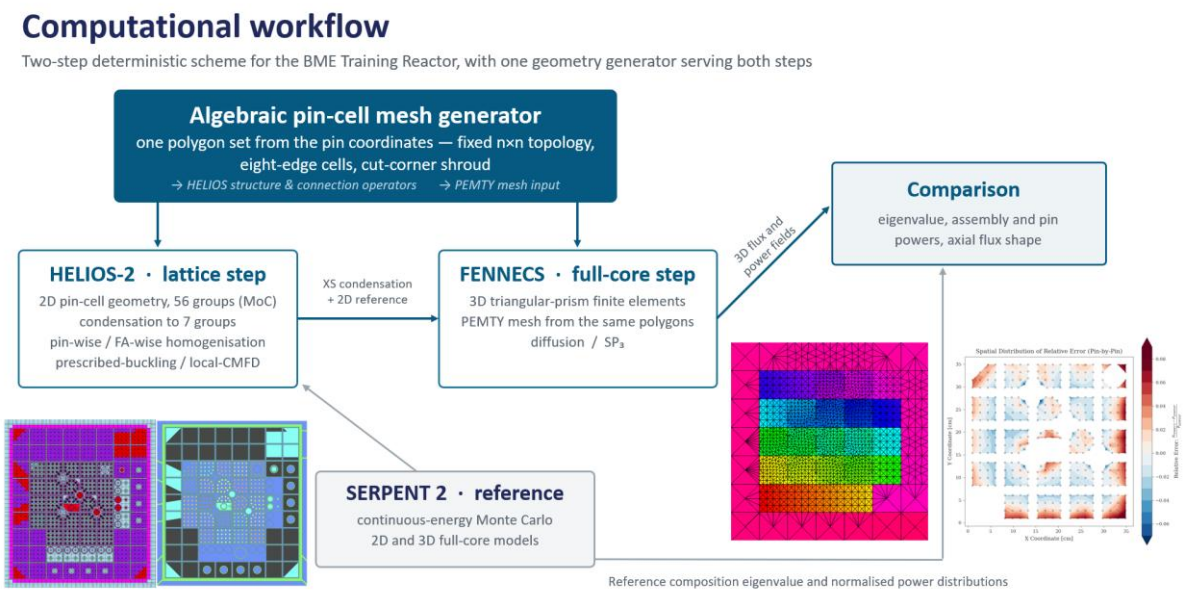


Figure 22: Computational workflow of FENNECS pin-wise modelling: conventional two-step deterministic scheme using a SERPENT reference calculation.

A dedicated Python script for generating the polygon-set of the BME TR geometry was developed, producing both the HELIOS structure, the connection operators and consistently the PEMTY input. The condensation regions and the full-core homogenization regions are therefore the same polygon regions, not two independent reconstructions, eliminating the geometry-transfer error. This is relevant, since the lattices in question have pins displaced from the regular grid by up to roughly the pin diameter itself, with nearest-neighbor distances spanning 11.9 to 18.0 mm where the nominal is 17 mm (see Figure 23). Moreover, the assembly shroud is itself cut to make space for the guide tubes of the safety and control rods, so no rectangular grid conforms to the pin positions and the assembly

Funded by the European Union

Funded by the European Union. Views and opinions expressed are however those of the author(s) only and do not necessarily reflect those of the European Union or the European Atomic Energy Community ('EC-Euratom'). Neither the European Union nor the granting authority can be held responsible for them.

boundary simultaneously. Hence, the following methodology was developed for pin-wise homogenization using a non-Cartesian mesh.

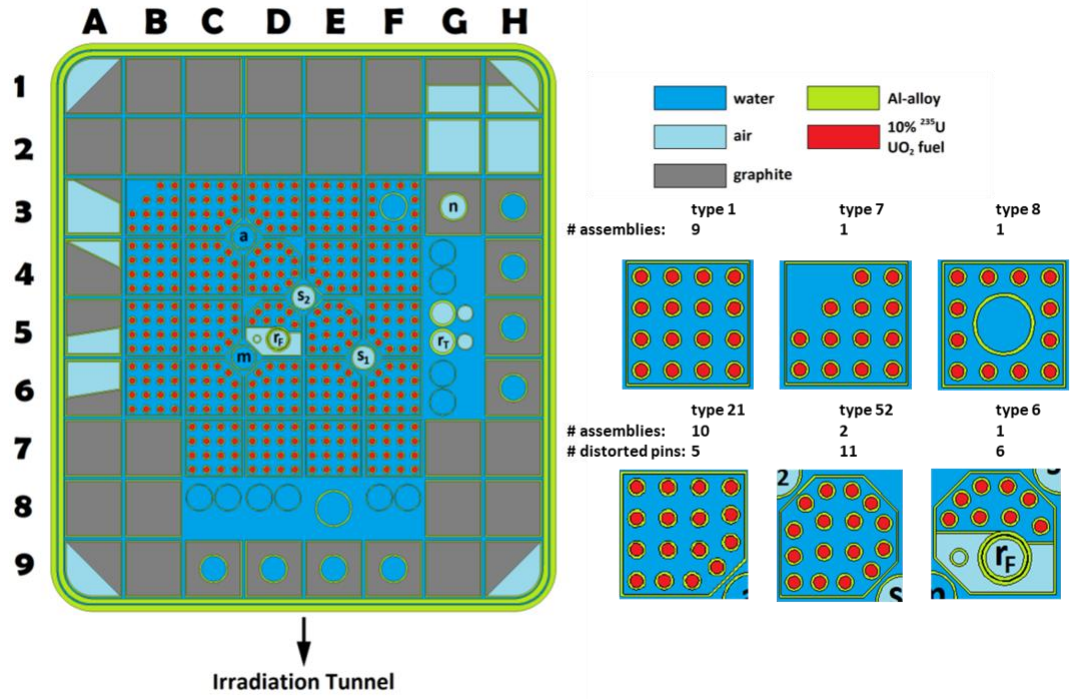


Figure 23: BME TR core midplane layout with the six FA types, showing the distorted pin arrangements near the control-rod positions.

A Voronoi tessellation is the natural partition of an irregular point set and comes with positive attributes such as guaranteed convexity and the pin as the coordinate center, but edge counts and orderings vary cell to cell, which makes the HELIOS modelling difficult, since it requires every structure (e.g. pin-cell) to be explicitly connected by its edges to its neighbors.

The construction developed here separates topology from geometry and in a closed- and non-iterative-form. Pins retain the logical indices and neighbor relations of the undistorted nxn lattice, so cell count and adjacency graph are fixed constants of the assembly type; only the vertex coordinates move. Each interface vertex is the midpoint of the vector between two logically adjacent pin centers, assigned to both cells. Each 2x2 group contributes one junction, chosen between the two diagonal midpoints by maximizing the distance between the polygon edge and the nearest pin of that group, since the shorter diagonal's midpoint can fall inside a pin for the modelled distorted lattices. In the implemented geometries the longer diagonal is selected everywhere and no intersection occurs. Four midpoints and four junctions give eight interface vertices for an interior cell; boundary nodes of the assembly shroud complete the side and corner pincell-polygons, positioned at cut corners to model the shroud contour in HELIOS (see Figure 24).

Funded by the European Union

Funded by the European Union. Views and opinions expressed are however those of the author(s) only and do not necessarily reflect those of the European Union or the European Atomic Energy Community ('EC-Euratom'). Neither the European Union nor the granting authority can be held responsible for them.

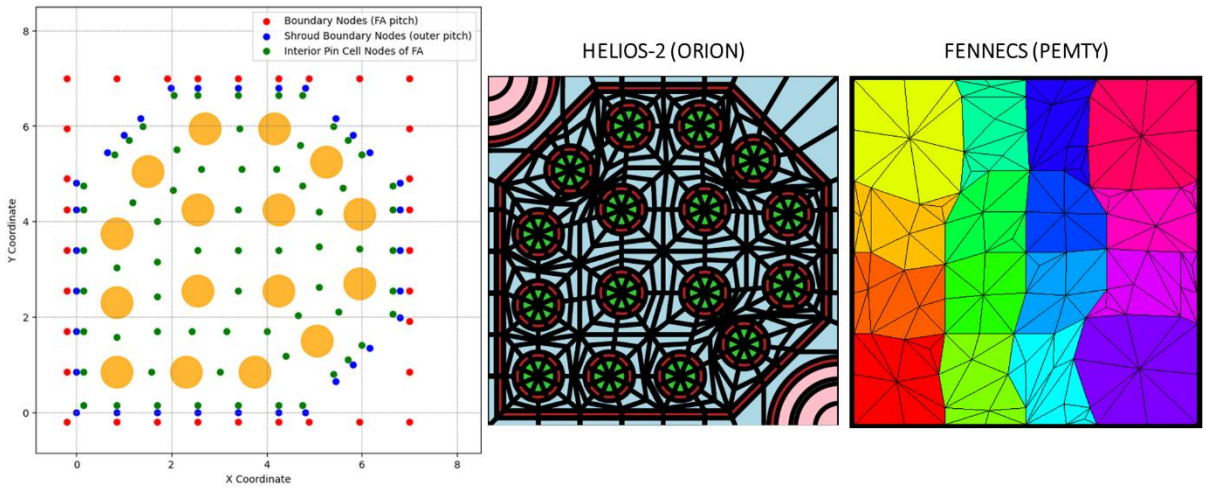


Figure 24: Mesh generation for FA Type 6: (a) algebraic construction of the pin-cell, shroud and FA boundaries; (b) the HELIOS structure representation with internal mesh refinement; (c) the FENNECS triangulation derived from the same boundaries.

The resulting polygons are associated with a pin but not centered on it: at each control-rod position the guide tube is divided among the four surrounding assemblies, a quarter homogenized into each corner cell, so that cell's material centroid sits off the pin. Recentering would either change the volume assignment or force the guide tube into an additional region, breaking the fixed topology. It also eases post-processing, since polygon coordinates are defined by their pin coordinates. The polygon-pin-cells are further meshed internally - Delaunay triangulation for FENNECS, an eight-direction subdivision around the pin boundary for HELIOS.

Four 2D HELIOS models [21] are used for the cross-section generation: two uncontrolled slices, with and without the horizontal beam tubes, and two models with the automatic and the manual control rod inserted respectively. The beam-tube model was verified against a dedicated 2D SERPENT model and reproduces it to Δk = +104 pcm, with a pin-power RMS error of 1.19 %, a maximum of 3.69 %, and a power-peaking factor of 1.373 against 1.342 (see Figure 25). The beam-tube-free model is used for the uncontrolled pin-wise cross-section generation.

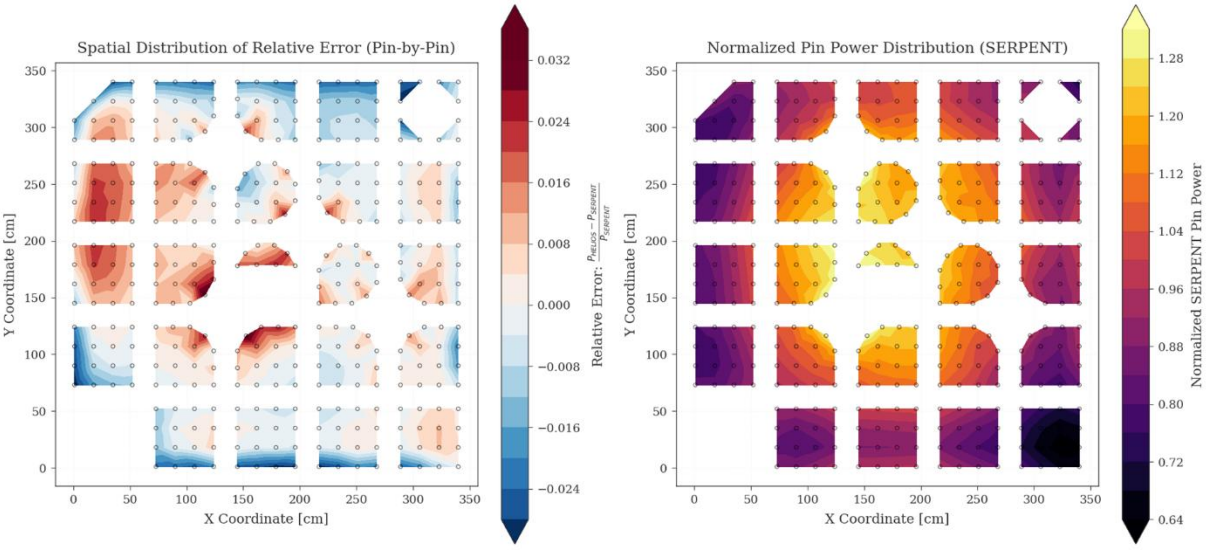


Figure 25: Spatial distribution of relative pin-power error of HELIOS model (left), normalised SERPENT pin-power distribution (right).

Funded by the European Union

Funded by the European Union. Views and opinions expressed are however those of the author(s) only and do not necessarily reflect those of the European Union or the European Atomic Energy Community ('EC-Euratom'). Neither the European Union nor the granting authority can be held responsible for them.

Several calculation options were compared, e.g. collision probabilities (CP) and the method of characteristics (MoC), flat against linear source, and the two available transport-coefficient definitions. The production setup uses MoC (three polar and 24 azimuthal angles, flat source), which is the more accurate of the two flux solvers at lattice level (pin-power RMS 1.19 % against 1.37 % for CP) and gives the better full-core power agreement using FENNECS. Axial leakage during condensation is treated by a local CMFD diffusion model at a prescribed geometric buckling rather than by a critical-buckling search.

In HELIOS the control-rod material is assigned only to the four geometrically intersected corner regions holding the guide tube, while the cross-section update used for FENNECS is broader: the unrodded pin-wise set of each adjacent assembly is replaced by its rodded counterpart, 64 regions in total, representing the rod-induced spectral redistribution computed by HELIOS. Two rodded states were computed against dedicated SERPENT references, with the automatic and the manual rod at their deepest evaluated insertion. The power distribution stays accurate with a rod inserted. One local degradation is visible for the strong absorber: with MAN inserted the pin peaking factor is under-predicted by 5.1 % (1.293 against 1.363) and the largest single assembly error, +4.09 %, occurs at the central position adjacent to the absorber.

For the uncontrolled steady state calculation at identical solver, leakage treatment and cross-section source, the assembly-wise SP_3 model gives a fuel-assembly power Mean Absolute Relative Error (MARE) of 1.39 %, RMS 1.92 % and maximum 5.72 %; the corresponding pin-wise model gives 0.75 %, 0.86 % and 1.84 %, with an integral fuel-rod MARE of 1.63 % and an eigenvalue difference of +280 pcm. The same ordering holds for diffusion, where the assembly-wise model gives 1.78 %, 2.10 % and 4.52 % against 0.91 %, 1.05 % and 2.52 % pin-wise, and in two dimensions for both solvers. Resolving the geometry therefore approximately halves the mean and RMS assembly-power error and reduces the maximum by 44 to 68 %, at unchanged solver and leakage treatment.

Separately, explicit pin-cell geometry reduces the eigenvalue sensitivity to the condensation spectrum by roughly an order of magnitude: introducing the prescribed buckling moves the pin-wise eigenvalue by -60 pcm (diffusion) and -30 pcm (SP_3), against +294 and -331 pcm for the corresponding assembly-wise models. This aspect matters because the input buckling is the one parameter supplied from outside the lattice calculation

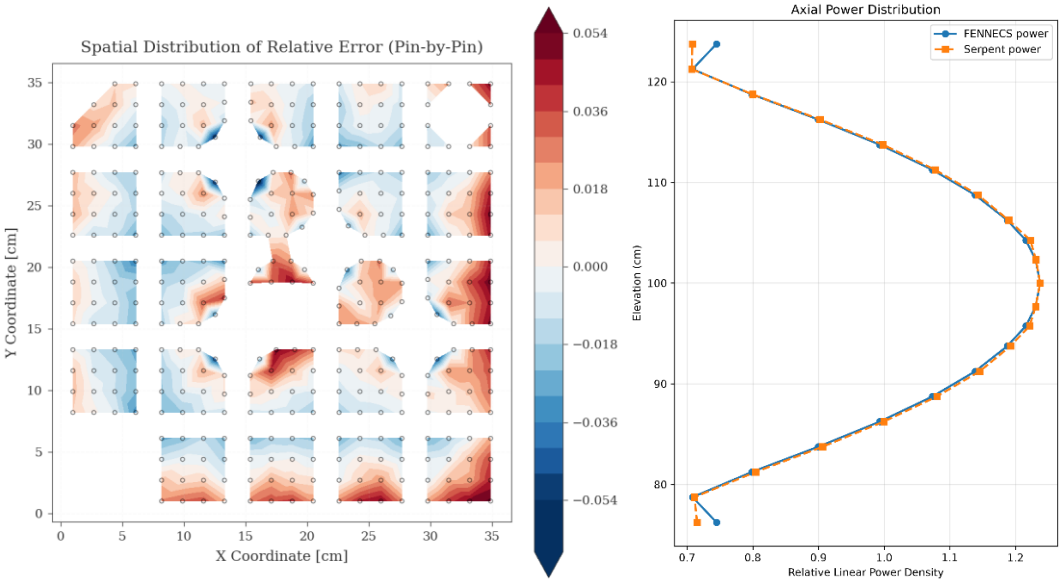


Figure 26: Spatial distribution of relative pin-power error (left) and relative linear power density (right), FENNECS against SERPENT, with the normalised SERPENT pin-power distribution alongside.

Funded by the European Union

Funded by the European Union. Views and opinions expressed are however those of the author(s) only and do not necessarily reflect those of the European Union or the European Atomic Energy Community ('EC-Euratom'). Neither the European Union nor the granting authority can be held responsible for them.

Compared to the published assembly-wise-homogenized models of this core [22], the improvement of using the pin-wise-homogenization is smaller but obtained on unfavorable terms. That earlier set spans four solvers and four group structures and saturates near 1 % mean absolute assembly-power error, the best result being 1.04 % mean and 3.81 % maximum (forty-group discrete ordinate). The FENNECS pin-wise model achieves 0.75 % and 1.84 %. The earlier results were generated by SERPENT from the full-core model itself, so that chain carries no lattice-physics error, no library discrepancy and no geometry transfer; a floor for any chain that generates its own constants at that homogenization level, and the present chain falls below it while carrying all of those error sources.

3.3.1.2. Description of the thermal-hydraulics subchannel model with CTF

The thermal-hydraulics model with the subchannel code CTF focuses on the core (open-core representation). The rest of the reactor pool is not modelled. Instead, the inlet massflow and temperatures are given as boundary conditions which are provided in Table 8.

Table 8: BME TR core TH boundary conditions

Inlet massflow	Inlet temperature	Exit pressure
1.2 kg/s	20 °C	1.5 bar

The modelling uses a channel-centered approach as illustrated in Figure 27. In standard fuel assemblies, three channel types are used: corner channels, side channels and central channels. For bundles with irregular geometries, the standard channel types are also used but with additional side and central types. The input deck is generated using the preprocessor python library SubKit.

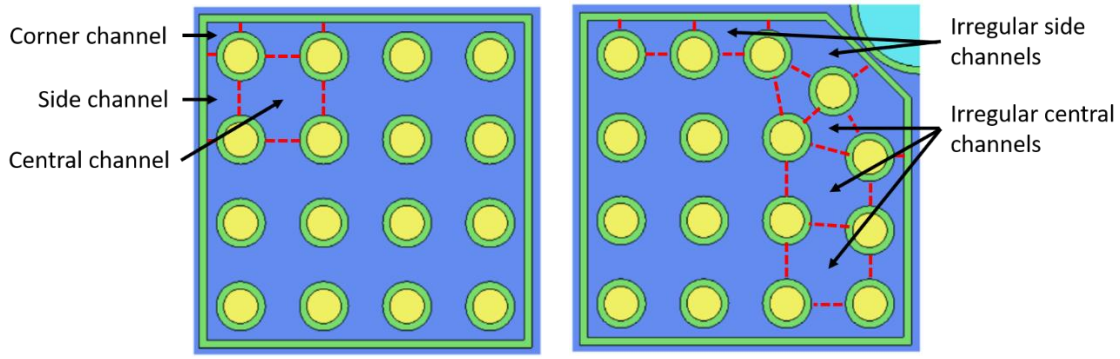


Figure 27: Channel-centered modelling with CTF of two fuel bundle types.

Overall, the model is composed of 600 thermal-hydraulics channels surrounding 384 fuel rod objects. The walls and interstitial water are not modelled in the current model.

In the axial direction, the same nodalisation as in the FENNECS model is used to simplify data exchange and remove the need for interpolation.

3.3.1.3. Coupling FENNECS/CTF

A newly developed coupling using the codes build-in interfaces is applied. As mentioned, in CTF, the coolant-centered modelling approach is applied. On the other hand, the neutronics codes usually use a fuel-centered model. Therefore, in the CTF coupling interface, an automatic remapping of the coolant-related parameter (e.g. temperature, density and boron concentration) is performed around each fuel pin model. Each FENNECS finite element containing fuel is thus coupled to a CTF pin object. This is achieved using the meshing tool PEMTY.

Preliminary steady-state results for the BME TR have been obtained using the models described above. The core power is set at 100 kW. The results show that the thermal-hydraulic feedback have a limited influence on the reactivity and the power (/flux) distribution. The delta keff between the first FENNECS

Funded by the European Union

Funded by the European Union. Views and opinions expressed are however those of the author(s) only and do not necessarily reflect those of the European Union or the European Atomic Energy Community ('EC-Euratom'). Neither the European Union nor the granting authority can be held responsible for them.

iteration (0.98270) without TH feedback (using uniform inlet conditions) and the final converged keff (0.98191) is 80 pcm. For the power distribution (see Figure 28), the maximum relative pin power difference is 1.37% between FENNECS stand-alone and FENNECS/CTF.

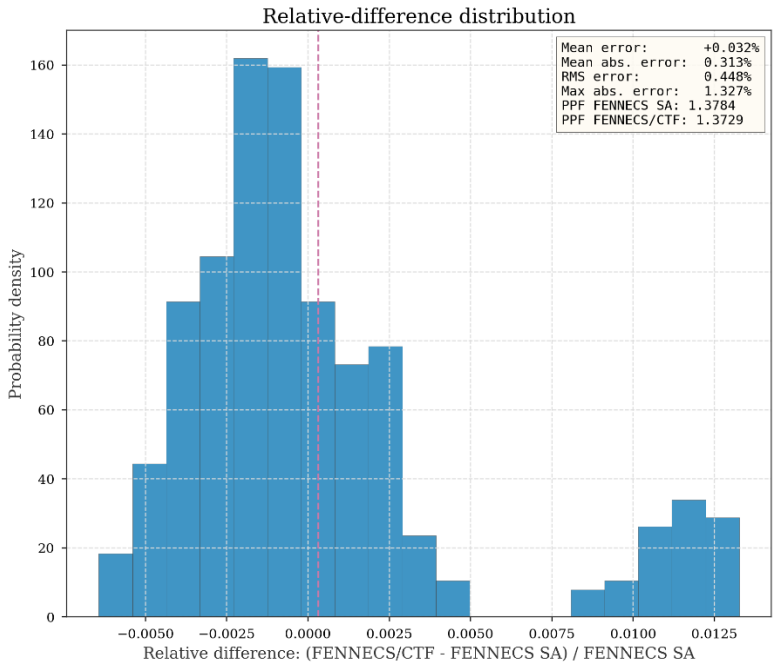


Figure 28: Probability distribution of the relative difference of the pin power between (FENNECS/CTF - FENNECS) / FENNECS

The preliminary results show that the neutronics and the thermal-hydraulics models are running (stand-alone or coupled) and that they deliver physically plausible results. The coupled model will now be validated on the power transient selected. If necessary, the model may be improved and/or extended. For example, the CTF open-core model may be coupled to a system code.

3.3.2. foamForNuclear

The present section describes a model of the BME TR reactor using the FFN platform [7]. FFN is designed as separate modules that solve individual governing equations. This design permits the coupling of arbitrary physics in several domains via the multiRegion approach. In this context, each region acts as a logical subdivision of the simulation, containing its own dedicated mesh, fields, and associated dictionaries. In the BME TR model described here, two modules are considered:

- the thermal-Hydraulics module includes both single-phase RANS and two-phase Euler–Euler (six-equation) models for water flow. In order to optimize computational resources, a porous-medium capability allows for "coarse-mesh" modeling by homogenizing complex structures like fuel assemblies.
- the Neutronics module features a series of different neutronics solvers, including point kinetics, multi-group diffusion and higher-order SP_3 and S_n transport approximations. The nuclear data management is based on a Radial Basis Functions (RBF) based interpolation scheme to accurately map cross-sections across various perturbed states, for example fluctuations in coolant density or fuel temperature.

The part of the model associated with each module mentioned above is further elaborated in the following sections.

Funded by the European Union

Funded by the European Union. Views and opinions expressed are however those of the author(s) only and do not necessarily reflect those of the European Union or the European Atomic Energy Community ('EC-Euratom'). Neither the European Union nor the granting authority can be held responsible for them.

3.3.2.1. Thermal-Hydraulic Model and Mesh Topology

To balance computational efficiency with accurate physical resolution, the thermal-hydraulic model of the BME Training Reactor adopts a hybrid spatial approach. The large, open fluid regions of the reactor pool are simulated using standard Computational Fluid Dynamics (CFD) techniques. Conversely, the dense and complex internal structure of the reactor core is modelled via a porous medium approach. Rather than discretizing every single fuel rod and narrow cooling channel—which would be computationally prohibitive—this method treats the core as a continuous, homogenized region. The presence of the solid structures is accounted for by introducing volume porosity, flow resistance parameters, and distributed heat sources into the governing fluid equations. This allows each fuel assembly to be represented as a single macroscopic mesh block, significantly reducing computational costs while accurately preserving the global mass, momentum, and energy balances.

Within this framework, the thermodynamic and transport properties of the coolant (light water) are governed by the icoPolynomial thermophysical model. Instead of using a constant value or a complex non-linear equation of state, this approach utilizes temperature-dependent polynomial functions to calculate fluid density, dynamic viscosity, and thermal conductivity. These polynomials are derived from high-precision NIST reference data[15] within the reactor's specific operating temperature range (293 K to 340 K). This implementation is crucial for capturing the buoyancy-driven flows and local density gradients that govern the natural circulation loops of the reactor.

To keep the global model computationally manageable, several geometric simplifications are systematically applied:

- Reflector Blocks: Removed from the fluid domain and treated as zero-flow zones with constant temperature.
- Control and Safety Rods: Excluded from the thermal-hydraulic domain and modelled exclusively within the neutronic phase.
- Auxiliary Components: Vertical guiding tubes, irradiation tunnels, and horizontal beam tubes were omitted.
- Diffuser Area: The complex physical structure of the diffuser was replaced by numerical mapped boundary conditions. These act as a boundary interface that directly couples and transfers the fluid-dynamic properties (velocity, pressure, and temperature) from the core barrel windows to the core inlet, bypassing the need to grid the internal geometry of the diffuser itself.

The resulting global mesh topology is illustrated in Figure 29. This visual representation highlights the conformal matching between the sub-domains and the implemented geometric simplifications; specifically, the labels indicate the regions where the diffuser and reflector blocks were originally located, now represented as external boundaries or empty zones to optimize the computational domain.

The final whole geometry mesh counts 150’000 cells and the discretization is homogeneous along the core vertical direction with finer refinement in the core window area to correctly capture all the physical phenomena with respect to the closing loop of natural circulation.

It should be highlighted here that, although it might look like triangular mesh in some post-visualization processes using ParaView, the computational mesh is essentially polyhedral.

Funded by the European Union

Funded by the European Union. Views and opinions expressed are however those of the author(s) only and do not necessarily reflect those of the European Union or the European Atomic Energy Community ('EC-Euratom'). Neither the European Union nor the granting authority can be held responsible for them.

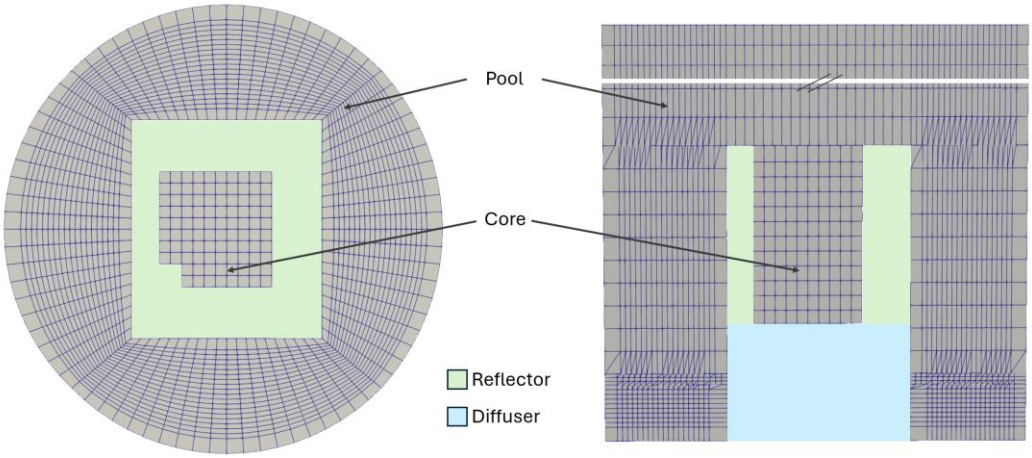


Figure 29: Global mesh topology, featuring a vertically truncated side view (right) within the pool region to highlight the core and diffuser discretization while preserving the full pool volume in the computational domain.

Due to the independent multi-block construction strategy, the reactor core and the surrounding pool geometries feature different spatial discretizations. When merged, this structural misalignment creates a non-conformal, partially overlapping interface where the mesh cells do not perfectly align. To ensure strict numerical continuity without modifying the underlying mesh, the Arbitrary Coupled Mesh Interface (ACMI) approach was implemented. This advanced boundary condition dynamically evaluates the exact geometric overlap between the contacting surfaces, allowing a conservative and physically consistent transfer of fluid-dynamic fields (such as velocity and pressure) across the "coupled" (intersecting) portion of the interface. Concurrently, the ACMI automatically treats the remaining "non-coupled" (non-overlapping) area as a solid wall boundary, effectively sealing the domain and ensuring an accurate physical transition between the core and the pool.

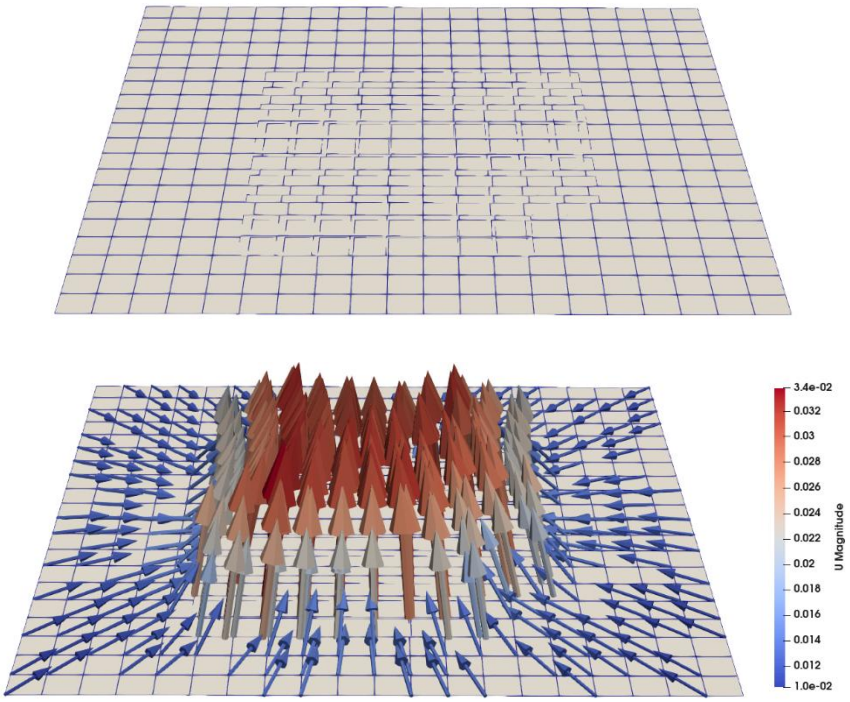


Figure 30: Core–pool interface: (top) the non-conformal mesh layout at the block boundary; (bottom) the resulting velocity field obtained through the ACMI coupling.

Funded by the European Union

Funded by the European Union. Views and opinions expressed are however those of the author(s) only and do not necessarily reflect those of the European Union or the European Atomic Energy Community ('EC-Euratom'). Neither the European Union nor the granting authority can be held responsible for them.

This spatial mapping approach across the interfaces is essential to capture the complex buoyancy-driven phenomena occurring during normal reactor operation. The coolant circulation inside the vessel is driven entirely by natural convection as the water heated by the core rises in a central thermal plume, splits at the pool surface, and flows back down along the colder outer walls. Upon reaching the lower plenum, this stream enters the core barrel through the peripheral windows where the numerical mapped bridge performs three essential functions to maintain strict physical realism.

First, it rescales the fluid velocity to account for the different surface areas and the core porosity, ensuring that the global mass flow rate remains perfectly constant without introducing artificial fluid sources or sinks.

Second, it acts as an ideal version of the physical component by forcing the incoming fluid vectors to enter perfectly perpendicular and uniform beneath the core, successfully replicating the stream-straightening and homogenizing effect of the real device on the incoming fluid before it enters the fuel elements.

Third, it spatially averages the temperature and pressure fields across the interface to filter out local numerical fluctuations, ensuring that the code handles the multi-physics coupling and natural convection in a stable manner. Finally, to account for the physical flow resistance that the real diffuser and the fuel support grid exert on the fluid, their combined hydraulic restriction is still incorporated by explicitly imposing a lumped pressure drop across the interface. This engineering compromise effectively captures the full internal natural circulation loop of the reactor while completely eliminating the heavy geometric and computational burdens of modeling the lower plenum structures.

3.3.2.2. Neutronic Model

The neutronic modelling and validation of the BME Training Reactor were executed to establish a robust, independent verification of the deterministic two-group diffusion solver within the foamForNuclear framework relying on code-to-code benchmarks against high-fidelity, continuous-energy Monte Carlo simulations from Serpent 2. To translate the highly heterogeneous physical layout of the reactor core into a computationally viable format for the diffusion solver, a rigorous spatial homogenization and energy condensation procedure was implemented. Using Serpent 2, the complex energy spectrum of the neutrons was condensed into a simplified two-group structure, distinguishing between fast and thermal neutrons. This homogenization was performed on an assembly-by-assembly basis, assigning unique sets of macroscopic nuclear constants and cross-sections to each individual fuel element and reflector block to preserve their localized spectral characteristics.

To bridge these high-fidelity Monte Carlo calculations with the deterministic solver, foamForNuclear utilizes a dedicated Python utility called nuclearData.py. This script automatically processes the output data generated by Serpent 2 and assembles the required input structures for FFN, mapping each cell of the computational mesh to its corresponding homogenized Serpent universe through predefined cellZone entities. To address the anisotropic forward-scattering behaviour typical of light water and graphite moderators, TRC transport corrections [23] were applied directly within this data processing pipeline to determine the final diffusion coefficients. Spatially, the global neutronic domain was mapped onto a Cartesian mesh consisting of seventy-three distinct homogeneous regions, dedicating seventy-two zones to the active core grid and reflectors, while the remaining volume was treated as a large surrounding water region. Black boundary conditions, representing zero incoming neutron flux, were applied at the outermost boundaries of this water domain.

The resulting standalone steady-state verification against Serpent2 highlighted several critical physical insights regarding the limitations and accuracy of the multi-group diffusion approach. The multiplication coefficient (k_{eff}) obtained by the diffusion solver exhibited a systematic underestimation of approximately 2908 pcm compared to the reference Monte Carlo solution. This large difference is a

Funded by the European Union

Funded by the European Union. Views and opinions expressed are however those of the author(s) only and do not necessarily reflect those of the European Union or the European Atomic Energy Community ('EC-Euratom'). Neither the European Union nor the granting authority can be held responsible for them.

well-known limitation inherent to two-group diffusion calculations and spatial homogenization when applied to small, highly heterogeneous cores with steep flux gradients, yet it does not compromise the transient capability of the tool since this systematic difference mathematically cancels out when assessing differential reactivity changes.

In terms of spatial power distribution (see Figure 31), the radial assembly-by-assembly power profile demonstrated excellent agreement within the central region of the core, yielding discrepancies below two percent. The maximum local error reached nearly ten percent at the outermost corners of the core perimeter, where the diffusion model slightly overpredicts the flux near the graphite interfaces due to thermalization gradients and underpredicts it near the water reflector due to the steep absorption gradients that diffusion theory struggles to resolve perfectly.

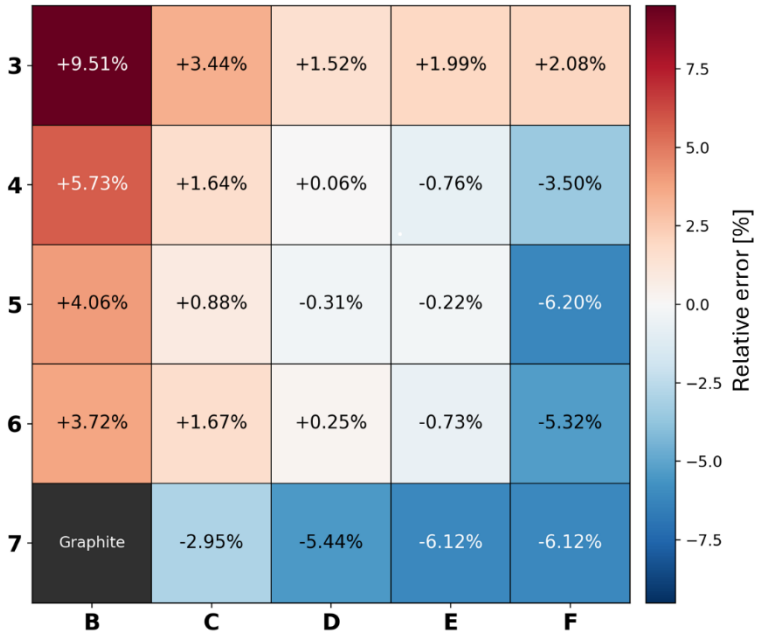


Figure 31: FFN vs. Serpent 2 relative error in radial power distribution

The axial power distributions (Figure 32) followed the expected cosine shape with remarkable fidelity, showing minor deviations confined strictly to the fuel ends due to local transport edge effects.

Funded by the European Union

Funded by the European Union. Views and opinions expressed are however those of the author(s) only and do not necessarily reflect those of the European Union or the European Atomic Energy Community ('EC-Euratom'). Neither the European Union nor the granting authority can be held responsible for them.

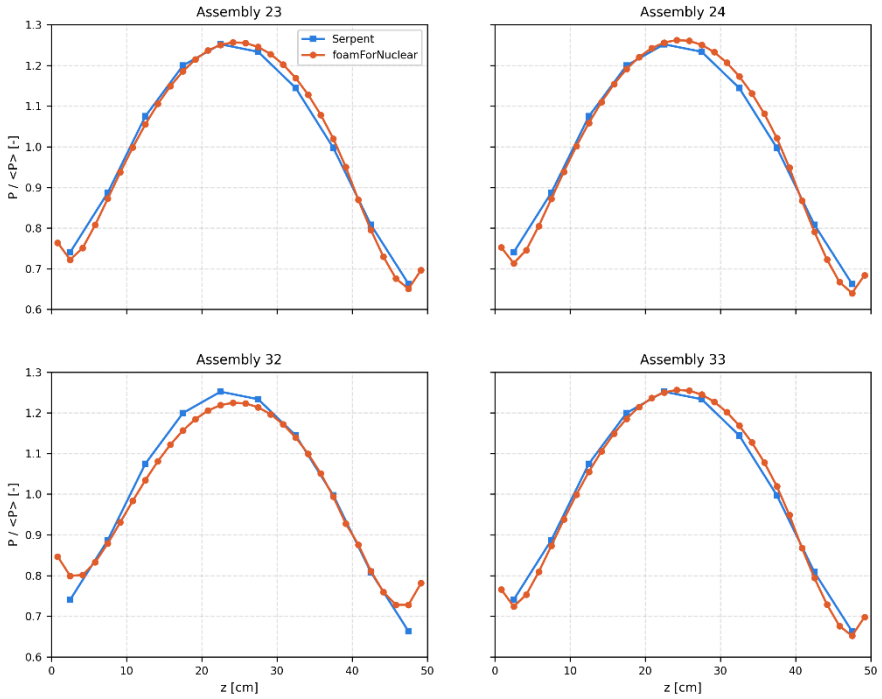


Figure 32: Axial power density profiles: FFN vs. Serpent 2, for the assemblies surrounding the AUT control rod

Because the deterministic solver ultimately needs cross sections as a function of operating conditions the reference calculation is repeated across a set of perturbed states. For the Doppler temperature coefficient, separate calculations are performed at different fuel temperatures using an on-the-fly Doppler-broadening method in Serpent2; for the moderator temperature coefficient, an analogous sweep is performed across different moderator densities and temperatures, capturing the combined effect of thermal-scattering changes and density variation on the neutron spectrum.

Finally, the localized reactivity perturbations and material displacements induced by control and safety rod movements were integrated into the foamForNuclear framework using the CRmove utility. By generating dedicated sets of two-group constants for the fully inserted states from full-core Serpent2 reference runs, the solver can handle rod positioning dynamically to correctly reproduce the differential reactivity worth and flux shadowing effects associated with control rod insertion.

3.3.2.3. Coupling strategy

The interaction between the thermal-hydraulic and neutronic solvers is handled through a coupled, segregated. At the beginning of every time step, all inter-physics fields are exchanged simultaneously through the platform's mesh-mapping infrastructure, after which each solver is advanced once, before the simulation proceeds to the next step. This operator-split approach introduces a one-step lag in the feedback between the two physics but the resulting power field is immediately available to the thermal-hydraulics solver within the same step. For the slow feedback timescales characteristic of a pool-type research reactor operating under natural circulation, this approximation is considered acceptable.

In the coupled configuration, the point-kinetics solver governs the total reactor power as a single time-dependent quantity, while the spatial distribution of delayed-neutron precursor concentrations is still tracked on the full three-dimensional neutronics mesh. The fission power density is obtained by scaling a fixed spatial shape function, derived from the initial steady-state solution, by this instantaneous power amplitude, and the resulting field is transferred to the thermal-hydraulics mesh, where it is injected as a volumetric heat source into the fluid energy equation. Within each porous cell, a multi-

Funded by the European Union

Funded by the European Union. Views and opinions expressed are however those of the author(s) only and do not necessarily reflect those of the European Union or the European Atomic Energy Community ('EC-Euratom'). Neither the European Union nor the granting authority can be held responsible for them.

node radial thermal conduction model is solved to determine the temperature profiles of the fuel and the cladding. The resulting outer cladding surface temperature is then utilized to compute the convective energy source term injected directly into the fluid energy equation of the coolant (the pool water), using heat transfer coefficients derived from specific Nusselt correlations [24].

The thermal-hydraulics solver then advances the temperature and velocity fields over the current time step under the influence of this heat source. The resulting temperature distribution is fed back to the point-kinetics solver as a single volume-averaged quantity, computed by weighting the local temperature field with the one-group neutron flux distribution; this flux-weighting is performed zone by zone, ensuring that the feedback temperature is representative of the neutronically active fuel regions alone and preventing the much larger volume of the reflector and open pool from artificially diluting the average and suppressing the computed reactivity feedback. The resulting reactivity contributions from fuel temperature (Doppler effect) and from coolant temperature and density are evaluated from these zone-averaged quantities through feedback coefficients determined using the Serpent2 code (see section 3.3.2.2 for details) and supplied back into the point kinetic solver for the following time step.

3.3.2.4. Application to the modelling of the FB#2 Transient Case

To demonstrate the validity of this coupled multi-physics model and establish its ability to produce results comparable to the experimental data, the FB#2 transient case of D2.1 [1] is analysed. This specific transient provides a validation case for coupled code platforms, focusing on a long-term, buoyancy-driven natural circulation transient initiated by a time-dependent external reactivity insertion from an initial critical low-power state. In this section, the analysis of the FB#2 transient focuses on the prediction of the temperature field within the pool as well as reproducing the temperature timeseries of thermocouples positioned at the exit of specific fuel assemblies.

To ensure reasonable accuracy in the core heat deposition rates during the simulation, the numerical setup incorporates an input power correction that was established during the same experimental campaign to resolve discrepancies between nominal instrumentation readings and high-fidelity Monte Carlo simulations. The true physical reactor power is equal to 1.44 times the nominal reading displayed by the legacy instrumentation of the reactor ($P_{reactor} = 1.44 \cdot P_{nom}$).

The evolution of the temperature field during the transient in the reactor pool is shown in Figure 32. The development of natural circulation is clearly visible, with a buoyant upward jet peaking at 0.15 $m.s^{-1}$ and a peripheral downward flow. This confirms qualitatively that the mass flow rate is correctly established by the balance between thermal head and flow resistance.

Funded by the European Union

Funded by the European Union. Views and opinions expressed are however those of the author(s) only and do not necessarily reflect those of the European Union or the European Atomic Energy Community ('EC-Euratom'). Neither the European Union nor the granting authority can be held responsible for them.

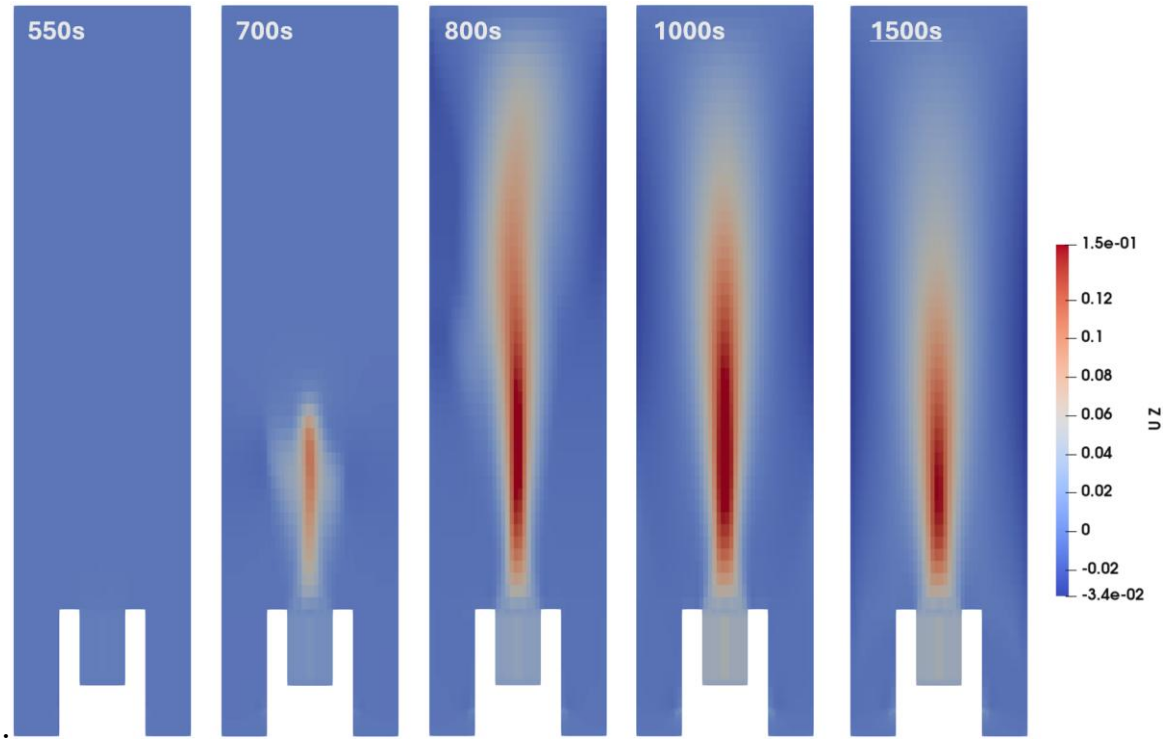


Figure 33: Development of the vertical velocity component uz in a core cross- section at successive instants, illustrating the establishment of natural circulation in the reactor pool

Then, the time series of thermocouples are considered, and the computed quantities together with the experimental data are illustrated in Figure 34. The simulated temperature response for assemblies E3, B3, C7, and F7 shows good agreement with experimental data, with minor discrepancies. The model effectively reproduces the observed thermal dynamics, including the heating onset, system inertia, and the relaxation phase.

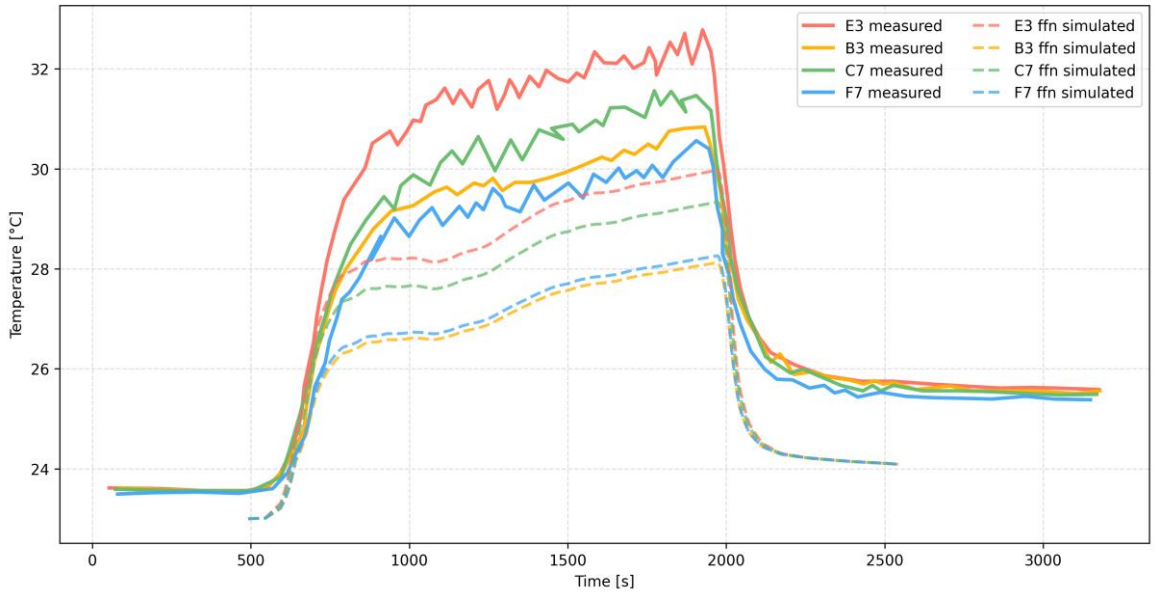


Figure 34: Comparison of measured and simulated temperature profiles for four fuel assemblies (E3, B3, C7, F7) under the forced power history. Data are extracted from the FFN solution at the top of the active fuel length.

Concerning assembly ranking, the simulation correctly identifies E3 and C7 as the hottest. The observed inversion between F7 and B3 is investigated further: the model's discrepancy arises from its simplified geometry. Specifically, the simulation represents B3 with a wider coolant flow area due to a lower rod count (13 instead of 16), which leads to lower flow resistance and a higher mass flow rate, resulting in

Funded by the European Union

Funded by the European Union. Views and opinions expressed are however those of the author(s) only and do not necessarily reflect those of the European Union or the European Atomic Energy Community ('EC-Euratom'). Neither the European Union nor the granting authority can be held responsible for them.

a lower temperature rise that offsets the power margin. Furthermore, the omission of the surrounding reflector and adjacent cooler water blocks, which would otherwise influence the thermal balance of these specific assemblies, is the most likely reason for this ranking shift.

These results demonstrate that the FFN model of the BME TR is ready for the validation exercise envisioned in the later part of the project.

Funded by the European Union

Funded by the European Union. Views and opinions expressed are however those of the author(s) only and do not necessarily reflect those of the European Union or the European Atomic Energy Community ('EC-Euratom'). Neither the European Union nor the granting authority can be held responsible for them.

4. JSI TRIGA reactor

This chapter presents the conventional and advanced multi-physics models developed for the TRIGA Mark II Reactor of JSI. Section4.1cintroduces the JSI facility, its core configuration and fuel design, and summarises the experimental campaign against which the models presented in this chapter are ultimately intended to be validated. Section 4.2 describes the conventional modelling schemes available at JSI to model the reactor. Section 4.3 then presents the advanced multi-physics approaches investigated within EVEREST, namely a Serpent to OpenFOAM coupling developed at VTT and a FENNECS/ CTF coupling developed at GRS. Together, these models establish the computational basis needed to interpret the TRIGA measurements reported in D2.1 and to inform the design of the high-resolution experiments planned in WP3.

4.1. Facility overview

The JSI TRIGA Mark II reactor is a pool-type research and training reactor operated by the Jožef Stefan Institute (JSI) in Ljubljana, Slovenia, with a maximum steady-state power of 250 kW (natural convection cooled) and pulse operation reaching peak powers of up to 1 GW for millisecond durations. The core is submerged roughly 4.9 m below the water surface in a 6.25 m high, 1.98 m diameter aluminium-lined open tank, surrounded by a graphite reflector housing a 40-position rotary Carousel irradiation facility. The 91 in-core positions are arranged in concentric rings (A–F) and can hold 20% LEU fuel elements, a neutron source, or irradiation channels; four positions house control rods, three with U-ZrH fuel-followers and one (the Transient rod) equipped with a pneumatic rapid-ejection system for pulsing. Heavy concrete biological shielding surrounds the tank and provides access to several ex-core irradiation facilities: four horizontal ports (tangential, thermal, radial beam, radial piercing), a Thermalizing Column, and a Dry Chamber facility.

A broad range of experimental campaigns have been carried out at the JSI TRIGA and reported in D2.1 [1]to provide validation data for coupled neutronics and thermal-hydraulics modelling. Absolute axial thermal-neutron flux profiles were measured at four in-core measuring positions (MP15, MP16, MP17, MP21) using ^{197}Au(n,γ)^{198}Au activation wire probes, scaled to absolute reaction rates via reactor power calibration. Benchmark-quality absolute fission-rate axial profiles were obtained at nine radial/axial positions using CEA-calibrated ^{235}U and ^{238}U fission chambers moved by a pneumatic positioning system. Pool-wide water temperature measurements were performed with up to 60 K-thermocouples across steady-state (with and without external cooling) and transient natural-convection regimes, enabling estimation of bulk coolant velocities and characterization of the 500 s transition to stable natural convection. In-core coolant temperature profiles were further measured with a dedicated 10-thermocouple vertical probe at multiple MP positions and orientations during full-power steady-state operation, revealing significant azimuthal mixing effects along the active fuel length. Finally, the JSI TRIGA Pulse Database compiles 26 years of pulse-operation data (289 pulses since the 1991 reactor reconstruction), archiving raw 20 kHz power and temperature waveforms, control rod calibration curves and displacements, peak power (60 MW–829 MW), energy release (~2.1–11.2 MJ), FWHM (12.8–57.9 ms), and core isotopic/burnup and Xenon state for each event. This experimental data constitutes the primary experimental reference for the low- and high-fidelity models presented later in this chapter.

4.2. Conventional model

Initial conventional modelling of JSI TRIGA neutronics was performed with the deterministic code TRIGLAV [25] where WIMS [26] is used to calculate the calculate the group constants in fueled and non-fueled regions, followed by a subsequent 2D diffusion transport. The aim of the code was primarily for fuel management and core loading calculations, but also allowed for the calculation of neutron spectra and fluxes in particular areas within the reactor core. With the increasing availability of

Funded by the European Union

Funded by the European Union. Views and opinions expressed are however those of the author(s) only and do not necessarily reflect those of the European Union or the European Atomic Energy Community ('EC-Euratom'). Neither the European Union nor the granting authority can be held responsible for them.

computer power, neutron transport calculations have since been moved to Monte Carlo particle transport methods. The initial model was made for the MCNP particle transport code, which was validated by several experimental campaigns on neutron and gamma profile measurements [27]–[30] and nuclear heating [31]. This served as a basis to develop models for other particle transport codes such as Serpent 2 [32]–[34], TRIPOLI-4 [35] and OpenMC [36], [37] with varying degrees of modelling accuracy, from completely fresh fuel, to each fuel element having calculated the exact isotopic inventory over 15 axial layers.

In the sense of the thermal-hydraulic modelling, efforts have been done in the part to assess the effect of temperature changes in both the fuel and the surrounding water, by coupling the OpenFoam solver to the TRIPOLI-4 calculation scheme [38], which was not developed further beyond the published work.

4.3. Advanced models

This section presents the advanced multi-physics models developed for the TRIGA Mark II reactor within EVEREST. Two independent routes were investigated. The first route, detailed in Section 4.3.1 relies on a model developed at VTT, coupling Serpent2 with OpenFOAM. The second one, described in Section 4.3.2, involves the coupling done at GRS between the FENNECS deterministic neutron transport code and the CTF subchannel code. These models provide the assembly-wise and axial neutron flux, power, and temperature distributions required both for comparison with the D2.1 experimental campaign and for the design of the high-resolution instrumentation to be deployed in WP3.

4.3.1. Serpent/OpenFOAM

VTT aims to develop a toolchain for modelling the JSI TRIGA reactor in a coupled approach utilizing OpenFOAM for the thermal hydraulic and Serpent2 for the neutronics solution. The coupling is done using the Cerberus multiphysics driver of the Kraken platform [39]. In the following, the toolchain is described.

4.3.1.1. OpenFOAM model

A multi-region CFD model for the TRIGA reactor is constructed in OpenFOAM consisting of separate regions for solid and fluid domains. This approach makes it possible to resolve the temperature distributions in the fluid and in the different solid structures in high fidelity. Currently, the CFD model and needed in-house tools are based on version 13 of the standard OpenFOAM release from the OpenFOAM Foundation (OpenFOAM Foundation, ei pvm).

The thermal hydraulic solution consists of two regions: fluid and solid. Conservation equations for mass, momentum and energy are solved for single-phase fluid in the fluid region, while energy balance with heat conduction is solved in the solid. The regions are coupled through temperature boundary conditions. The cells in the solid region are split to several cell zones which represent different structural materials and for which material properties can be defined independently. In principle, the current multi-region modular solver structure in the OpenFOAM release makes it possible to simulate a case with any number of regions and combination of physics solvers. For example, it would be possible to simulate two-phase flow with phase change with thermal coupling to resolved solid structures, although single-phase flow is sufficient for the current application.

The CFD geometry and mesh are based on a 3D CAD model of the reactor by JSI [40]. For purposes of demonstrating the toolchain in a simplified setup, the current CFD model only includes the core region of the reactor pool limited by the surrounding radial reflector. In addition, some simplifications were made to the support structures connecting the rods to the upper and lower support plates. In the future, a CFD model including the whole reactor pool will be constructed to calculate a steady-state inlet condition for the core region model.

Funded by the European Union

Funded by the European Union. Views and opinions expressed are however those of the author(s) only and do not necessarily reflect those of the European Union or the European Atomic Energy Community ('EC-Euratom'). Neither the European Union nor the granting authority can be held responsible for them.

It is likely, that also in the future, the coupled simulations will include only the core region on the CFD side to reduce computational effort. It is expected that the thermal response and time scales in the core are much faster than the resulting changes in the pool flow in transient pulse cases, making the inlet condition nearly stationary.

A polyhedral mesh was prepared for the reactor core in Ansys Fluent Meshing after geometry clean-up in Ansys CAD products. The aim was to construct a coarse mesh for initial testing and demonstrating the toolchain. The mesh had 0.85M and 1.78M cells in the fluid and solid regions, respectively. The mesh was prepared such that the faces in the interface between the solid and fluid are conformal.

The different regions of the core are shown in Figure 35. The solid region is split to four zones by material: fuel, steel cladding and support structures, graphite reflectors, and zirconium rods inside the fuel elements. For each, constant material properties are used with same values used by [35]. The density of the coolant water is represented by a polynomial function of temperature, while other fluid properties are taken as constant for now. Following previous work of [35], the gas gap is not included as separate thermal resistance although this is technically possible.

As the goal is to calculate both the reactor steady state and transient pulses, both steady and transient versions of the CFD model have been prepared. The differences between the models are related to numerical aspects, while the physical parameters of the model are same in both.

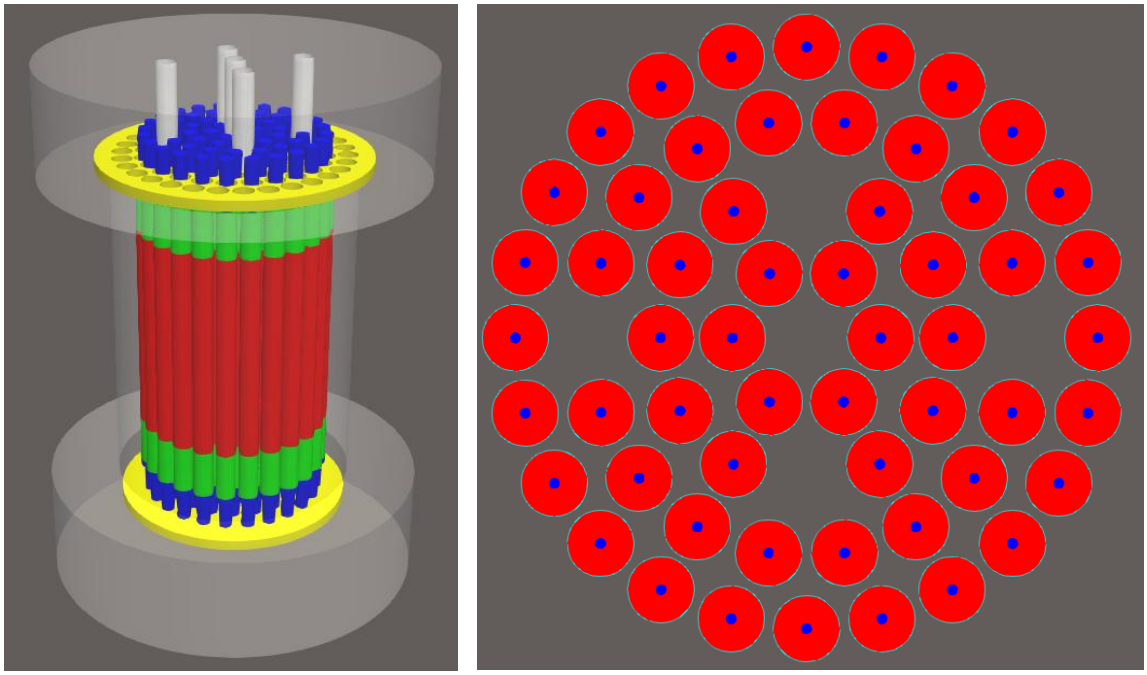


Figure 35: On left: Different geometric zones of the TRIGA CFD model. The colours indicate steel support structures (blue and yellow), graphite reflectors (green), and fuel (red). The outer boundary of the fluid domain is shown with opaque grey, while the cladding is not shown. On right: Cross-section of different solid structures including cladding (cyan), fuel (red), and zirconium rods (blue). The control rod/special channels are not included in the current CFD model.

4.3.1.2. Serpent model

As a starting point for the neutronics modelling three Serpent models corresponding to core configurations 190, 218 and 253 were received from JSI. The core 190 model is presented in Figure 36 and in Figure 37. For the modelled pulse transient, the Serpent model needs to be modified to include the exact core configuration used in the experiment. The depleted fuel compositions corresponding to the point of the operating history of the reactor in which the pulse experiment was conducted must

Funded by the European Union

Funded by the European Union. Views and opinions expressed are however those of the author(s) only and do not necessarily reflect those of the European Union or the European Atomic Energy Community ('EC-Euratom'). Neither the European Union nor the granting authority can be held responsible for them.

be also included in the Serpent model. These compositions are calculated by JSI [33], [34] using the Serpent 2 code. The temperature and density distributions of the coolant and fuel calculated by OpenFOAM are taken into account in Serpent2 using multi-physics interfaces. A separate interface is defined for the coolant region and for the fuel region. The temperature and density distributions are represented in Serpent directly using the OpenFOAM mesh without approximations to the fidelity of the distributions. The fission power is also tallied directly in the mesh for the fuel region.

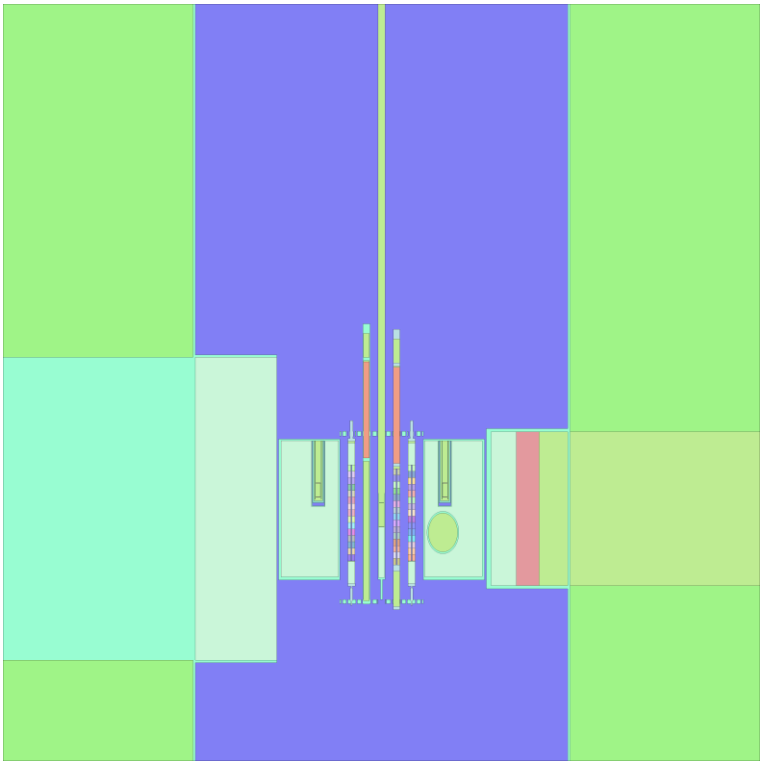


Figure 36: YZ plot of the Serpent model for core configuration 190.

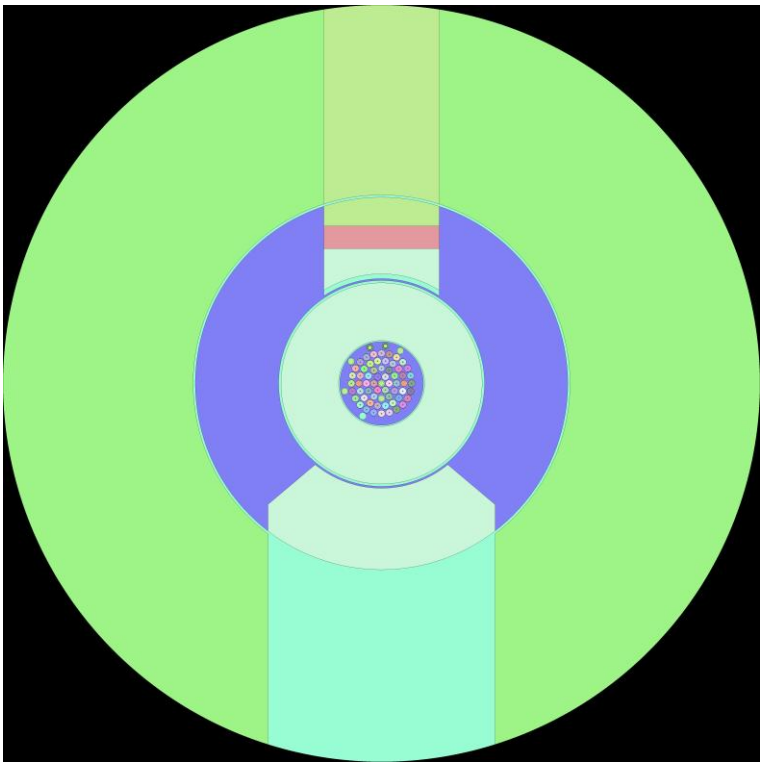


Figure 37: XY plot of the Serpent model for core configuration 190.

Funded by the European Union

Funded by the European Union. Views and opinions expressed are however those of the author(s) only and do not necessarily reflect those of the European Union or the European Atomic Energy Community ('EC-Euratom'). Neither the European Union nor the granting authority can be held responsible for them.

4.3.1.3. Coupled simulation

The coupled simulation is managed by the Python based multi-physics driver Cerberus which communicates with the solvers using sockets. The solution flow of the coupled calculation is set up with a simple Python script.

In steady state the coupling is based on Picard iteration. On each coupled iteration a new power distribution is first calculated by Serpent and transferred to OpenFOAM. Next, OpenFOAM solves the temperature and density distributions which are transferred to Serpent. The iteration is continued until a converged solution is reached. The convergence is assessed based on the differences in the temperature and density distribution of two subsequent iterations.

In transients explicit coupling is used i.e. there is no iteration between the two solvers inside a time step. The transient Serpent simulation requires a lot of computational resources in order to achieve a sufficiently low statistical uncertainty and, therefore, iteration of the time step with Serpent is not a viable option. However, the explicit approach will not cause issues if the time step size is kept small. In contrast to deterministic codes, the computational time required by Serpent does not depend on the time step size. Serpent must track the neutrons through the same time period regardless of how the time period is divided into time steps.

Regarding the implementation of the coupling, as an in-house code Serpent supports the Cerberus coupling natively. On the OpenFOAM side, the communication interface between Cerberus and OpenFOAM has been implemented in the in-house krakenIO library. The library contains the communication logic used by Cerberus (e.g. for time stepping the solver) and the actual data transfer routines based on socket communication. In addition, the in-house tools include the modified main programs krakenRun/krakenMultiRun which replace the standard foamRun/foamMultiRun in coupled simulation use. The modified versions add the creation of the krakenIO object and hooks for communication and solution control in the main solver loop. The modular solver structure in the OpenFOAM release (Foundation branch) then makes it possible to flexibly use all the standard solvers available in OpenFOAM without further modifications.

The krakenIO library also includes a set of submodels that implement the actual physics coupling between the coupled solvers. For the TRIGA simulations, an OpenFOAM fvModel called krakenScalarFieldSource is used which applies a source term in the energy equation based on the power field from Serpent and collects the density and temperature fields to be sent back to Serpent. At the beginning of the simulation, the fvModel defines and subscribes these input/output fields such that they are visible to Cerberus. As there are separate meshes and solver modules for the fluid and solid regions, a separate fvModel is defined for each. Currently, the fvModel only supports use of the same mesh on both Serpent and OpenFOAM and no interpolation of the fields is done.

4.3.1.4. Steady-state demonstration and development needs

Serpent does the final material temperature/density search in a tetrahedral mesh which is automatically generated by splitting other polyhedra to tetrahedra when Serpent is initialized. Each surface of a tetrahedron is defined by three points and this is the number of points required to uniquely define a plane. During the neutron tracking Serpent can then use these planes to check inside which tetrahedron the neutron is and which temperature/density should be used.

During initial testing it was noticed that the simple splitting algorithm used in Serpent requires that the original polyhedral cells must be convex. The OpenFOAM simulation does not have the same limitation, and it proved to be non-trivial to generate a mesh without any non-convex cells. Generating directly a tetrahedral mesh was tried to remedy to problem but even then, non-tetrahedral cells need to be used to model the boundary layer in the fluid-solid interface and some of these cells were non-convex. The next steps are to check if the splitting algorithm can be updated to allow the use of non-convex cells

Funded by the European Union

Funded by the European Union. Views and opinions expressed are however those of the author(s) only and do not necessarily reflect those of the European Union or the European Atomic Energy Community ('EC-Euratom'). Neither the European Union nor the granting authority can be held responsible for them.

and try to generate the mesh using a different toolchain to get rid of non-convex cells. If the problem cannot be solved with those two approaches, an option will be implemented to Serpent to remove the non-convex cells and simply use a default temperature/density in the regions covered by these cells. Based on the initial mesh generation, it is possible to generate a mesh with very low amount of non-convex cells so this sort of approximation will have a negligible effect on the accuracy of the Serpent solution.

Due to the issues with Serpent, the status of the modelling pipeline was tested with a simulation case including only the OpenFOAM solution. The test case was a steady-state operation at the nominal 250 kW power level. Due to the lack of the neutronics coupling, a uniform heat source was added to the fuel. The velocity and temperature distributions in the core are shown in Figure 38. Due to buoyant flow caused by the heating from the fuel, the flow is accelerated near the center of the core. As the simulation domain is restricted to only the core vicinity, there is some backflow from the outlet plane. The backflow would most likely be absent in a simulation including the whole pool which allows alternate routes for the natural circulation.

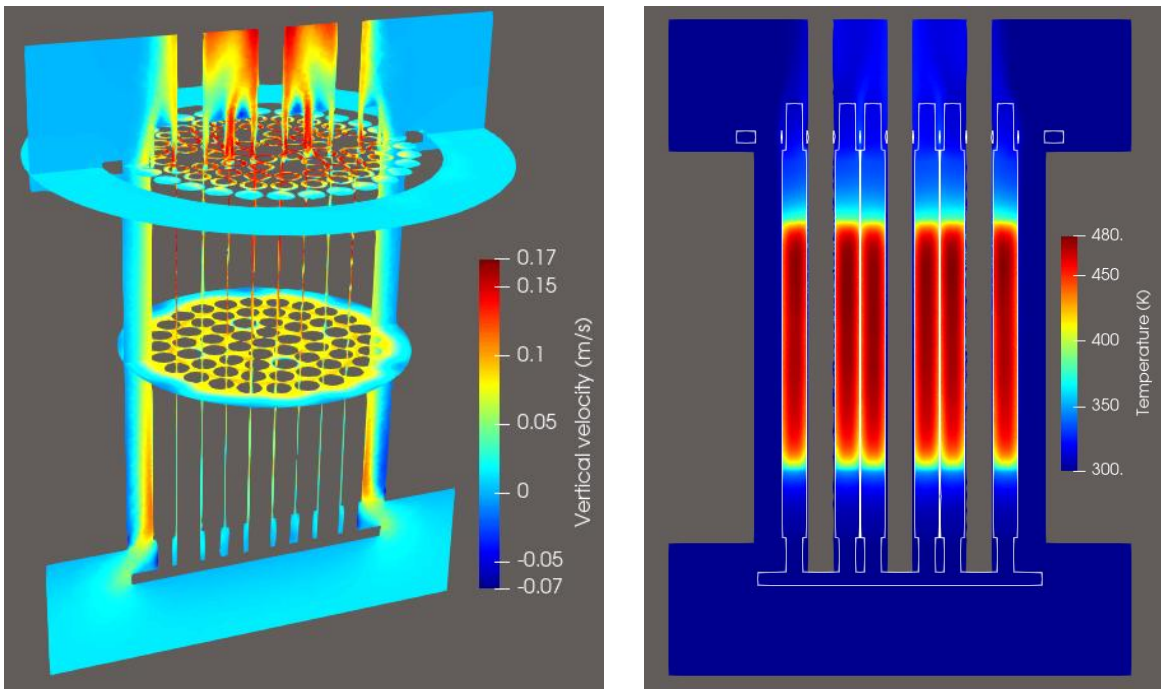


Figure 38: Results from a stand-alone CFD simulation of the TRIGA core. On left: Vertical component of the velocity in the fluid region. On right: Temperature distribution in both the fluid and solid regions.

4.3.2. FENNECS/CTF

GRS aims at modelling the JSI TRIGA reactor in a coupled approach applying the subchannel code CTF for the thermal hydraulic and the finite-element based code FENNECS for the neutronics solution. A newly developed coupling using the codes build-in interfaces is applied. In the following, the individual models as well as initial coupled results are described.

4.3.2.1. Description of the neutronics model using FENNECS

To describe the neutronic behaviour of the JSI TRIGA reactor, cross-section libraries in two energy groups were first generated using the Serpent model provided by JSI [33], [34], which was modified to generate all the required cross-section libraries. A total of 915 libraries were produced and subsequently converted into the NEMTAB format using PEMTY (Python External Meshing Tool for YAML Input), a tool developed in conjunction with the FENNECS code.

PEMTY was also used to define the reactor geometry and generate the corresponding mesh. The geometry was derived from the provided Serpent model. The reactor core comprises 64 pin-slot types

Funded by the European Union

Funded by the European Union. Views and opinions expressed are however those of the author(s) only and do not necessarily reflect those of the European Union or the European Atomic Energy Community ('EC-Euratom'). Neither the European Union nor the granting authority can be held responsible for them.

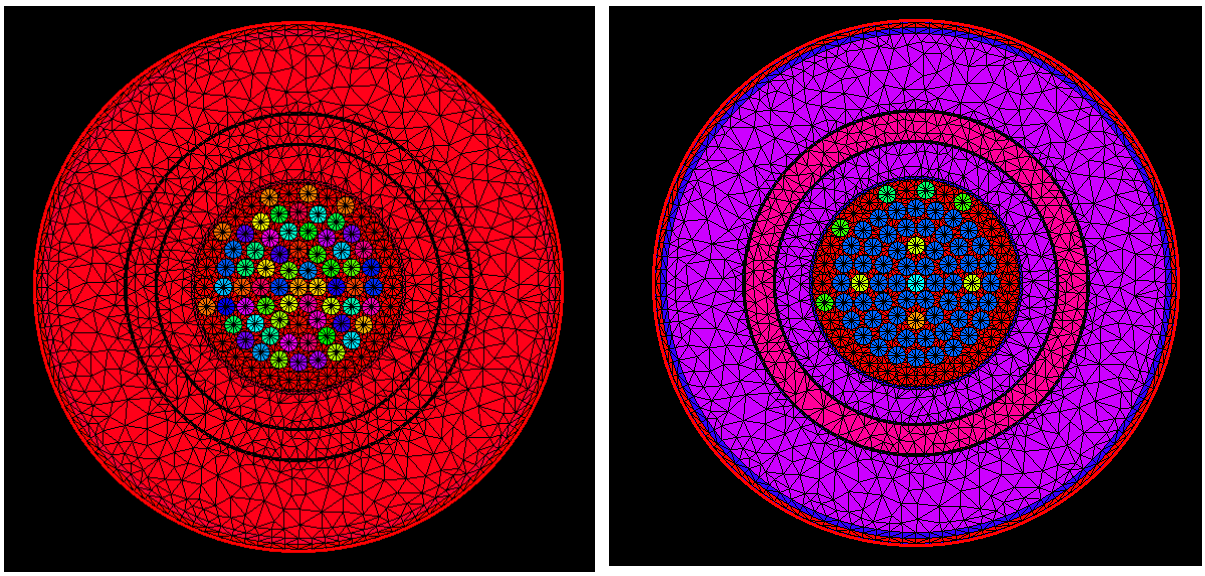
and a total of and a total of 91 pin positions. Depending on the assigned slot type, these positions can accommodate fuel elements, irradiation channels, structural components, or control rods. The core has a height of 3 m. The lower 61.69 cm and upper 165.07 cm sections of the fuel elements consist of water, while the active fuel region is located between them. The axial composition of the fuel was described using more than 20 cross-section libraries, with a dedicated set of libraries assigned to each fuel type. Similarly, multiple cross-section libraries were employed to represent the axial heterogeneity of the remaining pin types. In the computational model, the pins are represented as regular dodecagons. To compensate for the use of dodecagonal rather than circular geometries, the polygon radius was adjusted to preserve the original cross-sectional area of the pins. Since the core layout is not geometrically symmetric, the pin locations were defined explicitly. A reference pin position was first placed at the core centre. Five concentric rings centred on this position were then generated. The rings contain 6, 12, 18, 24, and 30 equally spaced pin locations, respectively. Each pin location was subsequently assigned a specific pin-slot type according to the reactor configuration.

The pins are immersed in a water moderator. The water tank is represented by a 120-sided polygon, to better reproduce the shape of a circle. Unlike the fuel pins, no geometrical correction was applied to preserve the original area of the tank. The moderator was assumed to be axially homogeneous throughout the model. A single cross-section library was generated and used to represent all water regions in the model.

Structures surrounding the moderator were also included in the model. Due to limitations of PEMTY, it was not possible to assign material properties to individual angular sectors of a region. Consequently, material distributions originally represented as partial annular segments in the Serpent model were approximated by continuous concentric rings. The original Serpent model contains 14 concentric cylindrical regions with radii ranging from 22.098 cm to 57.900 cm. These regions were reproduced in PEMTY using concentric 120-sided polygons. Seven distinct axial material distributions were employed to represent the rings. In all configurations, the upper and lower axial sections are filled with water, while the central region contains the structural materials specific to each ring type. The first ring consists primarily of aluminium, and the same axial configuration is also adopted for the ninth ring. The eleventh ring is characterized by the same material composition, although the aluminium region extends over a larger axial length. The second and eighth rings contain a central graphite region bounded by thin aluminium layers, which separate the graphite from the upper and lower water regions. The third and seventh rings feature the same materials but the upper aluminium section is much thicker. Similarly, the fourth and sixth rings share an identical composition; however, part of the aluminium is replaced by water in the central region. The fifth ring has a composition comparable to that of the fourth and sixth rings, with the difference that part of the central water region is replaced by an AlMg cladding material. Finally, the tenth ring is composed entirely of water. To generate the mesh, PEMTY used as axial and radial maximum discretisation 5 cm and 2 cm, respectively. With these specifications, the mesh has 567600 elements. The resulting mesh at various heights is illustrated in Figure 39.

Funded by the European Union

Funded by the European Union. Views and opinions expressed are however those of the author(s) only and do not necessarily reflect those of the European Union or the European Atomic Energy Community ('EC-Euratom'). Neither the European Union nor the granting authority can be held responsible for them.



Meshing of the geometry at 80.95 cm from the bottom

Meshing of the geometry at 126.0594 cm from the bottom

Figure 39 FENNECS mesh for the TRIGA Mark II model.

4.3.2.2. Description of the thermal-hydraulics subchannel model with CTF

The thermal-hydraulics model with the subchannel code CTF focuses on the core (open-core representation). The rest of the reactor pool is not modelled. Instead, the inlet massflow and temperatures are given as boundary conditions which are provided in Table 9.

Table 9: TRIGA core TH boundary conditions

Inlet massflow	Inlet temperature	Exit pressure
4.5 kg/s	20 °C	1.5 bar

The modelling uses a channel-centered approach. Standard channels between fuel pins are triangles as illustrated in Figure 40. At the core periphery, trapezoids are used. Overall, the model is composed of 126 thermal-hydraulics channels surrounding 61 fuel rod objects. The input deck was generated with Python scripts using the CTF preprocessor Python library SubKit.

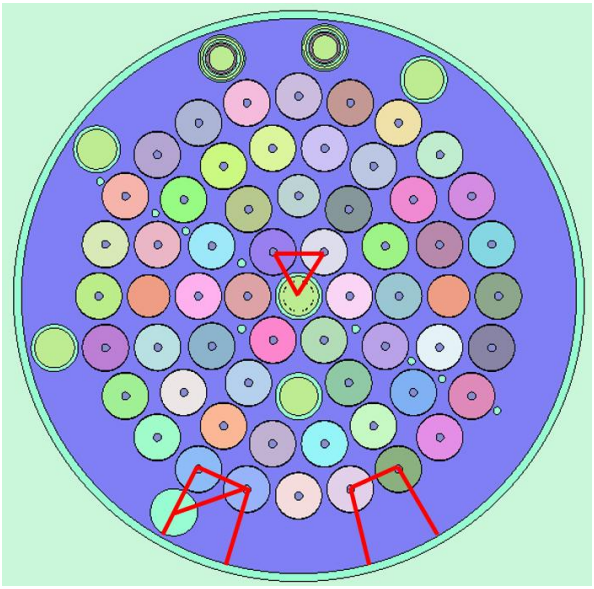


Figure 40: Representation of CTF thermal-hydraulics channels in the TRIGA core

Funded by the European Union

Funded by the European Union. Views and opinions expressed are however those of the author(s) only and do not necessarily reflect those of the European Union or the European Atomic Energy Community ('EC-Euratom'). Neither the European Union nor the granting authority can be held responsible for them.

In the axial direction, a coarser nodalization is used in CTF than in FENNECS to facilitate convergence (see Table 10). Indeed, in CTF, smaller axial nodes impose smaller timestep sizes due to the Courant limit and therefore can hinder convergence.

Table 10: Axial nodalization of the TRIGA core in CTF

Axial node (From bottom)	Node Size (m)
1	8.79E-02
2	8.79E-02
3	7.62E-02
4	7.62E-02
5	7.62E-02
6	7.62E-02
7	7.62E-02
8	8.78E-02
9	8.78E-02

The model converges to a steady-state without issues and the computation time remains low (a few seconds) given the comparatively small size of the model (less than half a single PWR fuel assembly at the pin level).

4.3.2.3. Coupling FENNECS/CTF

A newly developed coupling using the codes build-in interfaces is applied. As mentioned, in CTF, the coolant-centered modelling approach is applied. On the other hand, the neutronics codes usually use a fuel-centered model. Therefore, in the CTF coupling interface, an automatic remapping of the coolant-related parameter (e.g. temperature, density and boron concentration) is performed around each fuel pin model. Each FENNECS finite element containing fuel is thus coupled to a CTF pin object. This is achieved using the meshing tool PEMTY.

Preliminary steady-state results for the TRIGA reactor have been obtained using the models described above. The core power is set at 250 kW (nominal power). Currently the cross-section libraries for FENNECS were generated for a single thermal-hydraulics state. Therefore, in the coupled calculation, the TH feedback doesn't influence the neutronics model. However, the effect of the power distribution from FENNECS on the TH results can be clearly seen in Figure 41 and Figure 42, which show a comparison of the axial distribution of coolant temperature in two core channels (one toward the center and one in the between the last two rings of pins).

Funded by the European Union

Funded by the European Union. Views and opinions expressed are however those of the author(s) only and do not necessarily reflect those of the European Union or the European Atomic Energy Community ('EC-Euratom'). Neither the European Union nor the granting authority can be held responsible for them.

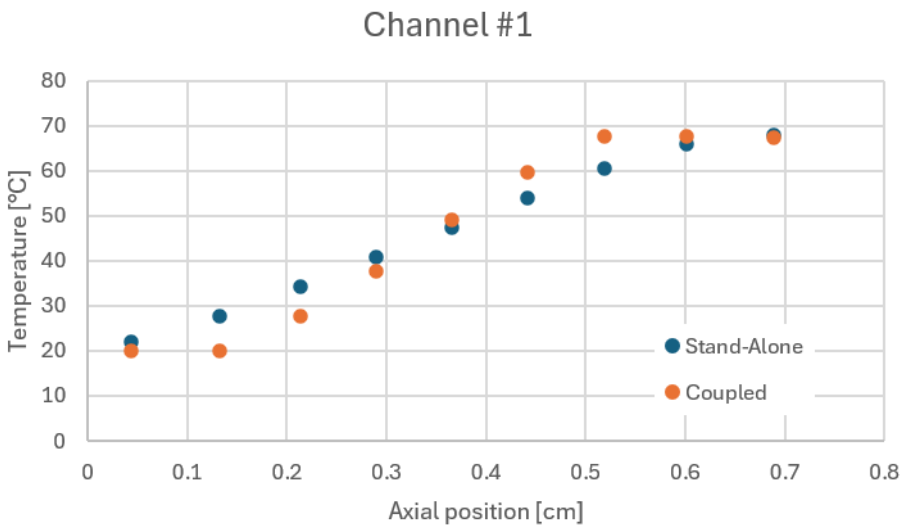


Figure 41: Axial distribution of coolant temperature in CTF a core central channel (#1) – Comparison of Stand-Alone and Coupled simulations

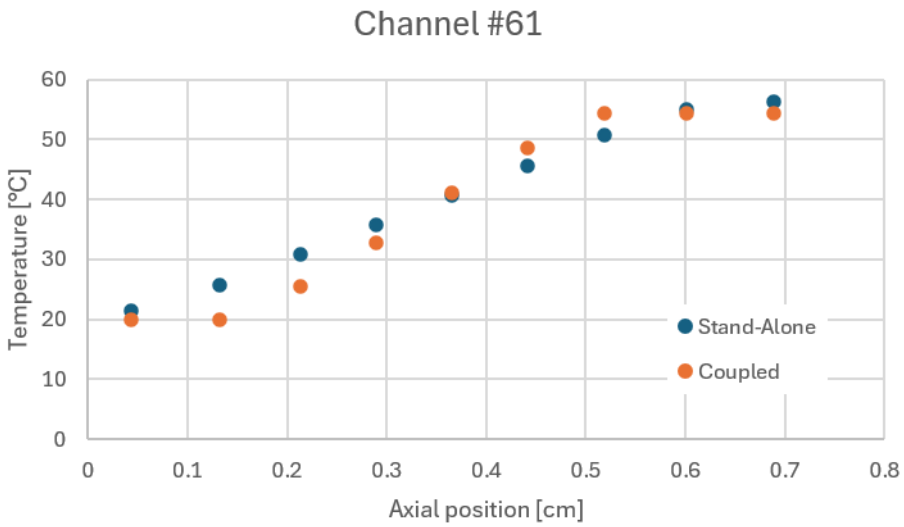


Figure 42: Axial distribution of coolant temperature in CTF a core channel in the third ring of pins (#61) – Comparison of Stand-Alone and Coupled simulations

The preliminary results show that the neutronics and the thermal-hydraulics models are running stand-alone as they deliver physically plausible results and that the data exchange works in the coupled case. Macroscopic cross-sections dependent on TH state will now be generated to enable fully coupled physics. The coupled model will then be validated on the power transient selected. If necessary, the model may be improved and/or extended. For example, the CTF open-core model may be coupled to a system code.

Funded by the European Union

Funded by the European Union. Views and opinions expressed are however those of the author(s) only and do not necessarily reflect those of the European Union or the European Atomic Energy Community ('EC-Euratom'). Neither the European Union nor the granting authority can be held responsible for them.

5. Conclusions and future work

This deliverable has documented the conventional and advanced multi-physics models developed within Work Package 2 of the EVEREST project for the three consortium research reactors: the Budapest Research Reactor, the BME Training Reactor, and the JSI TRIGA Mark II reactor. For each facility, a conventional model (KIKO3D/ATHLET for the BRR, PARCS/TRACE for the BME TR, and the deterministic TRIGLAV/MCNP-based schemes for the JSI TRIGA) was presented alongside at least one advanced, higher-resolution multi-physics coupling built around continuous-energy Monte Carlo neutronics (Serpent 2) or deterministic pin-resolved transport (HELIOS-2/FENNECS), coupled to CFD or subchannel thermal-hydraulics (foamForNuclear, CTF, or OpenFOAM).

Across the three reactors, the advanced modelling routes converge on a common picture. The Serpent/foamForNuclear coupling developed for the BRR demonstrates that a full-core, geometry-faithful Monte Carlo neutronics model can be coupled to a computationally efficient porous-media thermal-hydraulic representation, reaching a converged steady state after a single fixed-point iteration and reproducing the explicit chtMultiRegionFoam reference temperatures to within a fraction of a kelvin. The lower-fidelity FFN diffusion variant, driven by pre-generated two-group cross-section libraries, was shown to reproduce the Serpent-referenced assembly power distribution to within about four percent and the coupled temperature fields to within 0.1 to 0.3 K, at a small fraction of the computational cost, making it an attractive candidate for transient and parametric studies. For the BRR, the deterministic nTRACER/CTF route was assessed but found impractical within the project timeline owing to the irregular VVR-M2 geometry and the lack of a qualified cross-section library at the fuel enrichment used in the reactor.

For the BME Training Reactor, the FENNECS/CTF pin-wise deterministic scheme, built on an algebraic mesh-generation methodology that preserves the true distorted-pin topology of the EK-10 assemblies, was shown to approximately halve the mean and RMS assembly-power error relative to a conventional assembly-homogenised model, while remaining self-consistent from lattice transport (HELIOS-2) through full-core condensation (FENNECS) without recourse to externally supplied reference constants. In parallel, the foamForNuclear model of the BME TR, combining a porous-medium core representation with a two-group diffusion solver and a point-kinetics/thermal-hydraulics coupling, performed qualitatively well when modelling the FB#2 natural-circulation transient from the D2.1 experimental campaign and correctly reproduced the observed heating onset, system inertia, and relaxation behaviour.

For the JSI TRIGA Mark II reactor, two complementary advanced routes were established: a Serpent2/OpenFOAM coupling using the Cerberus/Kraken multi-physics driver, and a FENNECS/CTF deterministic scheme analogous to that developed for the BME TR. The Serpent/OpenFOAM toolchain was demonstrated in a simplified, core-only configuration, reproducing the expected buoyancy-driven flow pattern in a stand-alone thermal-hydraulic simulation; full two-way coupling remains contingent on resolving the treatment of non-convex mesh cells in Serpent's tetrahedral temperature/density search. The FENNECS neutronics model, built from a dedicated pin-slot mesh generator driven by more than nine hundred two-group cross-section libraries, provides the geometric and material fidelity needed to represent the TRIGA's irregular core layout ahead of the planned CTF thermal-hydraulic coupling.

5.1.1. Outlook

Taken together, the models presented in this deliverable establish the computational basis required to interpret the experimental data reported in D2.1 and to design the further instrumentation planned in WP3. Several items remain open for the next phase of the project:

Funded by the European Union

Funded by the European Union. Views and opinions expressed are however those of the author(s) only and do not necessarily reflect those of the European Union or the European Atomic Energy Community ('EC-Euratom'). Neither the European Union nor the granting authority can be held responsible for them.

- Resolution of the non-convex mesh limitation in the Serpent/OpenFOAM (Cerberus/Kraken) toolchain for the JSI TRIGA, and extension of the CFD domain to the full reactor pool to remove the artificial backflow observed in the core-only model.
- Extension of the coupled schemes to transient and pulse conditions where relevant (in particular for the JSI TRIGA pulse database), building on the explicit and point-kinetics coupling strategies already implemented for the BRR and BME TR.

Beyond these improvements, the models described in this deliverable will be applied to a validation exercise based on the experimental data reported in EVEREST D2.1, using the computational uncertainty quantification estimates reported in D2.3 (to be published concurrently with the present deliverable). The goal of this exercise is to demonstrate the trustworthiness of the advanced multi-physics models against multi-physics experimental data and to showcase the added spatial resolution they provide relative to the conventional models. The validated models will also be used to support the design of the new experiments expected within WP3 of the EVEREST project.

These next steps will allow the multi-physics platforms described here to be carried from demonstration to validated, production-ready tools, fulfilling the WP2 objective of quantifying the added value of advanced multi-physics modelling for long-term operation and reactor-pressure-vessel fluence assessment applications.

Funded by the European Union

Funded by the European Union. Views and opinions expressed are however those of the author(s) only and do not necessarily reflect those of the European Union or the European Atomic Energy Community ('EC-Euratom'). Neither the European Union nor the granting authority can be held responsible for them.

Bibliography

[1] S. Czifrus, Y. Perin, M. Hursin, A. Vanyi, K. Ambrožič, and T. Belgya, “D2 . 1 - Report describing the experiments performed at each reactor and associated data uncertainties,” *EVEREST Delivr.*, no. 2.1, pp. 1–100, 2026.

[2] A. Keresztúri, “Validation Report of KIKO3D,” *KFKI Rep.*, no. AEKI/PH208/R6, 1998.

[3] A. Keresztúri *et al.*, “Development and Validation of the Three-Dimensional Dynamic Code KIKO3D,” *Ann. Nucl. Energy*, vol. 30, pp. 93–120, 2003.

[4] A. Keresztúri, G. Hegyi, M. Telbisz, and C. Maráczy, “Handbook of the KIKO3D Program for Campaign-Planning and Reactor-Kinetics Calculations of the Budapest Research Reactor,” *KFKI Rep.*, no. AEKI-RAL-2006-136/01/M0, 2009.

[5] “Input Handbook of the ATHLET mod 2.0 -- cycle A Program for the Safety Analyses of the Budapest Research Reactor,” *KFKI Rep.*, no. AEKI-2006-136/02/M0, 2006.

[6] J. Leppänen, M. Pusa, T. Viitanen, V. Valtavirta, and T. Kaltiaisenaho, “The Serpent Monte Carlo code: Status, development and applications in 2013,” *Ann. Nucl. Energy*, vol. 82, pp. 142–150, 2015, doi: 10.1016/j.anucene.2014.08.024.

[7] G. Nervi, T. Guilbaud, C. Fiorina, M. Hursin, and A. Scolaro, “foamForNuclear : A unified OpenFOAM multi-physics platform for nuclear applications,” *Prog. Nucl. Energy*, vol. 193, no. January, 2026, doi: 10.1016/j.pnucene.2026.106250.

[8] M. Ryu, Y. S. Jung, H. H. Cho, and H. G. Joo, “Solution of the BEAVRS benchmark using the nTRACER direct whole core calculation code,” *J. Nucl. Sci. Technol.*, vol. 52, no. 7–8, pp. 961–969, 2015, doi: 10.1080/00223131.2015.1038664.

[9] V. Gnielinski, “New Equations for Heat and Mass Transfer in the Turbulent Flow in Pipes and Channels,” *NASA STI/Recon Tech. Rep. A*, vol. 41, no. 1, pp. 8–16, 1975.

[10] J. K. Fink, “Thermophysical Properties of Uranium Dioxide,” *J. Nucl. Mater.*, vol. 279, no. 1, pp. 1–18, 2000, doi: 10.1016/S0022-3115(99)00273-1.

[11] I. K. Abdukadyrova, S. A. Alikulov, F. R. Akhmedzhanov, S. A. Baitelesov, A. F. Boltaboev, and U. S. Salikhbaev, “High-Temperature Thermal Conductivity of {SAV-1} Aluminum Alloy,” *At. Energy*, vol. 116, no. 2, pp. 100–104, 2014, doi: 10.1007/s10512-014-9825-0.

[12] G. S. Kell, “Density, Thermal Expansivity, and Compressibility of Liquid Water from 0.Deg. to 150.Deg.. Correlations and Tables for Atmospheric Pressure and Saturation Reviewed and Expressed on 1968 Temperature Scale,” *J. Chem. \& Eng. Data*, vol. 20, no. 1, pp. 97–105, 2002, doi: 10.1021/je60064a005.

[13] M. L. Huber *et al.*, “New International Formulation for the Viscosity of {H2O},” *J. Phys. Chem. Ref. Data*, vol. 38, no. 2, pp. 101–125, 2009, doi: 10.1063/1.3088050.

[14] M. L. Huber *et al.*, “New International Formulation for the Thermal Conductivity of {H2O},” Gaithersburg, MD, 2012. [Online]. Available: https://www.nist.gov/publications/new-international-formulation-thermal-conductivity-h2o.

[15] P. Linstrom, “NIST Chemistry WebBook, NIST Standard Reference Database 69,” 1997. doi: 10.18434/T4D303.

[16] A. Vanyi, “Experimental and numerical multi-physics analysis for the BME Training Reactor,” PhD thesis, Budapest University of Technology and Economics, 2023.

[17] A. Rais, “Performance Assessment of a 3-D steady state and spatial kinetics model for the CROCUS reactor,” PhD thesis, Ecole Polytechnique Federale de Lausanne, 2018.

Funded by the European Union

Funded by the European Union. Views and opinions expressed are however those of the author(s) only and do not necessarily reflect those of the European Union or the European Atomic Energy Community ('EC-Euratom'). Neither the European Union nor the granting authority can be held responsible for them.

[18] J. Bousquet, A. Seubert, and R. Henry, “New finite element neutron kinetics coupled code system FENNECS/ATHLET for safety assessment of (very) Small and Micro Reactors,” *J. Phys. Conf. Ser.*, vol. 1689, no. 1, 2020, doi: 10.1088/1742-6596/1689/1/012008.

[19] A. Seubert, “A 3-D finite-element few-group diffusion code and its application to Generation IV reactor concepts,” 2020.

[20] S. lo Muzio and A. Seubert, “Implementation of the steady-state simplified P3 (SP3) transport solver in the finite-element neutronic code FENNECS, Part 1: Theory,” *Ann. Nucl. Energy*, vol. 200, p. 110303, 2024.

[21] J. Zert, Y. Perin, and A. S. Ványi, “Pin-wise modelling of the distorted lattices of the BME Training Reactor with FENNECS and HELIOS-2,” 2026.

[22] A. S. Ványi *et al.*, “Steady-state neutronic measurements and comprehensive numerical analysis for the BME training reactor,” *Ann. Nucl. Energy*, vol. 155, 2021, doi: 10.1016/j.anucene.2021.108144.

[23] B. R. Herman, B. Forget, K. Smith, and B. N. Aviles, “IMPROVED DIFFUSION COEFFICIENTS GENERATED FROM MONTE CARLO CODES,” in *International Conference on Mathematics and Computational Methods Applied to Nuclear Science & Engineering (M&C 2013)*, 2013, pp. 2947–2961.

[24] E. N. Sieder and G. E. Tate, “Heat Transfer and Pressure Drop of Liquids in Tubes,” *Ind. \& Eng. Chem.*, vol. 28, no. 12, pp. 1429–1435, 1936, doi: 10.1021/ie50324a027.

[25] A. Peršič, T. Žagar, M. Ravnik, and L. Snoj, “TRIGLAV: A program package for TRIGA reactor calculations,” *Nucl. Eng. Des.*, 2017, doi: 10.1016/j.nucengdes.2017.04.010.

[26] B. A. Lindley, J. G. Hosking, P. J. Smith, D. J. Powney, and others, “Current status of the reactor physics code WIMS and recent developments,” *Ann. Nucl. Energy*, 2017, doi: 10.1016/j.anucene.2016.09.013.

[27] Ž. Štancar, L. Barbot, C. Destouches, D. Fourmentel, J.-F. Villard, and L. Snoj, “Computational validation of the fission rate distribution experimental benchmark at the JSI TRIGA Mark II research reactor using the Monte Carlo method,” *Ann. Nucl. Energy*, vol. 112, pp. 94–108, 2018, doi: 10.1016/j.anucene.2017.09.039.

[28] V. Radulović, Ž. Štancar, L. Snoj, and A. Trkov, “Validation of absolute axial neutron flux distribution calculations with MCNP with ^{197}Au(n,$γ$)^{198}Au reaction rate distribution measurements at the JSI TRIGA Mark II reactor,” *Appl. Radiat. Isot.*, vol. 84, pp. 57–65, 2014, doi: 10.1016/j.apradiso.2013.11.027.

[29] A. Gruel, K. Ambrožič, C. Destouches, V. Radulović, A. Sardet, and L. Snoj, “Gamma-Heating and Gamma Flux Measurements in the JSI TRIGA Reactor: Results and Prospects,” *IEEE Trans. Nucl. Sci.*, vol. 67, no. 4, pp. 559–567, 2020, doi: 10.1109/TNS.2020.2974968.

[30] K. Ambrožič and L. Snoj, “JSIR2S code for delayed radiation simulations: Validation against measurements at the JSI TRIGA reactor,” *Prog. Nucl. Energy*, vol. 129, p. 103498, 2020, doi: 10.1016/j.pnucene.2020.103498.

[31] K. Ambrožič *et al.*, “Nuclear heating at the JSI TRIGA reactor : measurements and simulations,” *Nucl. Sci. Tech.*, vol. 37, no. 4, pp. 1–11, 2026, doi: 10.1007/s41365-025-01877-z.

[32] D. Ćalić, G. Žerovnik, A. Trkov, and L. Snoj, “Validation of the Serpent 2 code on TRIGA Mark II benchmark experiments,” *Appl. Radiat. Isot.*, vol. 107, pp. 165–170, 2016, doi: 10.1016/j.apradiso.2015.10.022.

[33] A. Pungerc\vic, V. Mascolino, A. Haghighat, and L. Snoj, “Verification of a novel fuel burnup algorithm in the RAPID code system based on Serpent-2 simulation of the TRIGA Mark II

Funded by the European Union

Funded by the European Union. Views and opinions expressed are however those of the author(s) only and do not necessarily reflect those of the European Union or the European Atomic Energy Community ('EC-Euratom'). Neither the European Union nor the granting authority can be held responsible for them.

research reactor," *Nucl. Eng. Technol.*, vol. 55, no. 10, pp. 3732–3753, 2023, doi: 10.1016/j.net.2023.06.040.

[34] A. Pungerc\vic, A. Haghighat, and L. Snoj, "JSI TRIGA fuel rod reactivity worth experiments for validation of Serpent-2 and RAPID fuel burnup calculations," *Nucl. Eng. Technol.*, vol. 56, no. 8, pp. 3405–3424, 2024, doi: 10.1016/j.net.2024.03.041.

[35] R. Henry, I. Tiselj, and L. Snoj, "Analysis of JSI TRIGA MARK II reactor physical parameters calculated with TRIPOLI and MCNP," *Appl. Radiat. Isot.*, vol. 97, pp. 140–148, 2015, doi: 10.1016/j.apradiso.2014.12.017.

[36] M. Sánchez, "EFFECT OF HYDROGEN DISTRIBUTION IN UZRHX ON PHYSICAL PARAMETERS OF JSI TRIGA REACTOR," Master thesis of the LUT University, 2023.

[37] D. M. Cuellar Fernandez, "Feasibility study for design and utilization of a cold neutron irradiation facility at the JSI TRIGA reactor," Master thesis, University of Ljubljana, 2023.

[38] R. Henry, "NEUTRONIC AND THERMAL-HYDRAULICS COUPLING FOR SIMULATIONS OF THE TRIGA MARK II REACTOR," PhD Thesis, University of Ljubljana, 2017.

[39] J. Leppänen *et al.*, "Current Status and On-Going Development of VTT's Kraken Core Physics Computational Framework," *Energies*, vol. 15, no. 3, 2022, doi: 10.3390/en15030876.

[40] JSI, "CAD of the JSI Mark II TRIGA reactor." https://cad.onshape.com/documents/093424542e530378735970c8/w/8c8ac1f39d7696eca83f0a8b/e/30ca88e615ef02ed04cb57f1.

Funded by the European Union

Funded by the European Union. Views and opinions expressed are however those of the author(s) only and do not necessarily reflect those of the European Union or the European Atomic Energy Community ('EC-Euratom'). Neither the European Union nor the granting authority can be held responsible for them.